HIGH-SPEED FLOW THROUGH POROUS MEDIA

Interim Technical Report No. 1

by

Eric Weger
School of Engineering
Washington University
St. Louis, Missouri

and

Edward F. Blick
School of Engineering
Oklahoma University
Norman, Oklahoma

Department of the Army
Contract No. DA-ORD-31-124-61G74
AROD Project No.: 3005-C
"Pressure Wave Interactions In Porous Media"

Research Contract Director: Eric Weger

University of Oklahoma Research Institute
Norman, Oklahoma

January, 1963

HIGH-SPEED FLOW THROUGH POROUS MEDIA

Interim Technical Report No. 1

by

Eric Weger
School of Engineering
Washington University
St. Louis, Missouri

and

Edward F. Blick
School of Engineering
Oklahoma University
Norman, Oklahoma

Department of the Army
Contract No. DA-ORD-31-124-61G74
AROD Project No.: 3005-C
"Pressure Wave Interactions In Porous Media"

Research Contract Director: Eric Weger

University of Oklahoma Research Institute
Norman, Oklahoma

January, 1963

ASTIA AVAILABILITY NOTICE

Requests for additional copies by agencies of the Department of Defense, their contractors, and other Government agencies should be directed to:

Armed Services Technical Information Agency
Arlington Hall Station
Arlington 12, Virginia

Department of Defense contractors must be established for ASTIA services or have their "need-to-know" certified by the cognizant military agency of their project or contract.

All other persons and organizations should apply to the:

U. S. Department of Commerce
Office of Technical Services
Washington 25, D. C.

ABSTRACT

A new model called the capillary-orifice model for flow of fluids through a porous media is presented. A comparison between the capillary-orifice model theory and experimental data on pressure drop through porous media shows a close correlation.

A computer program is developed to study the effects of temperature dependant flow geometry on steady flow of a gas through porous media taking into account variable viscosity, viscous dissipation and a first order, temperature dependent irreversible catalytic reaction.

An experimental and theoretical analysis is made of two interacting planar pressure waves. The waves are generated by application of pressure step functions to the opposite faces of a porous core. An unsteady state computer program is developed to handle the associated nonlinear parabolic partial differential equations.

TABLE OF CONTENTS

LIST OF TABLES

LIST OF ILLUSTRATIONS

Figure

Page

HIGH-SPEED FLOW THROUGH POROUS MEDIA

CHAPTER I

STATEMENT OF THE PROBLEM

The question of flow behavior of gases and liquids through porous media has always attracted a considerable amount of attention. Interest in such studies has been motivated by their many fields of application: soil physics, petroleum technology, surface measurement, gas separations and more recently flow of gases through porous propellants, and transpiration cooling of porous wall reentry vehicles and rocket nozzles.

An engineer in designing or analyzing porous flow systems has to rely heavily on empirical data. For example, in determining the pressure gradient for high speed flow through a porous medium the usual empirical equation is composed of the sum of two terms. One term, which contains the velocity to the first power, is analogous to the Darcy expression for viscous flow through such material. The other term is a function of the square of the velocity and has been referred to as the "turbulent" or "inertia" term. Multiplying factors for both terms have had to be obtained empirically.

$$-\text{grad}\, p = \alpha \mu V + \beta \rho V^2 \qquad (1.1)$$

where p = Fluid pressure

μ = Viscosity

ρ = Density

v = Filter velocity (volume flow per unit area)

α = Viscous resistance coefficient

β = Inertial resistance coefficient

In an attempt to arrive at a more logical understanding of flow in porous media a better model, than those currently available, is needed. The optimum model would be one that predicts all the flow properties and variables in a porous media, without resorting to experimental testing. It is doubtful if this model will ever be discovered, however, this does not rule out the possibility of formulating models that successively approach this ideal or optimum model.

Review of Previous Work

The use of models to predict flow behavior in porous media is not new. The large bulk of literature, however, has been generally restricted to low speed flow through porous media.

The simplest models that have been constructed are those that depict the porous media to be a bundle of capillary tubes. Scheidegger (1), Kawakami (2), Smith (3), Rainard (4), Henderson (5), Purcell (6), Burdine (7), and Calhoun (8) have discussed the capillary model. These men investigated the correlation of the permeability (reciprocal of the viscous resistance coefficient) with the average pore size or with the pore size distribution curve.

By using the well known law of Hagen-Poiseuille the capillary model will predict for the pressure gradient, (See (9)),

$$\text{grad}\, p = \frac{-32}{\epsilon \delta^2} \mu v \tag{1.2}$$

where ϵ = Porosity (ratio of void volume to total volume)

δ = Average pore diameter

By modifying the resulting equation with empirical tortuosity factors, they have had moderate success in predicting pressure gradients at low flow velocities. The objection to the capillary model is that the fluid is supposed to flow straight through the tubes without encountering any obstacles and without losing any momentum due to inertial effects. Hence, the theoretical pressure gradient predicted by the capillary does not include the "velocity-squared" term that is detected experimentally for high speed flows.

Attempts to explain the presence of the "velocity-square" term in Equation (1.1) have been based primarily on the turbulent flow analogy (for an excellent review of this subject see (9)). However, this analogy has produced no universal determination of the viscous or inertial resistance coefficients of Equation (1.1).

Scheidegger (9) argues that the emergence of the "velocity-square" term in Equation (1.1) is probably due not to the onset of turbulence, but rather to the emergence of inertia effects in laminar flow. So rather than call this a turbulent flow term, Scheidegger believes it should be called a non-linear laminar flow term.

Purpose of This Work

The purpose of this work can be divided into three main divisions.

1) The primary objective is to investigate the general problem of gaseous pressure wave interaction. This investigation is broken up into an experimental study and a theoretical analysis of the conservation equations for unsteady flow. The pressure wave interaction investigated is the type consisting of the interaction of two planar pressure waves (initiated by the application of pressure step functions to opposite faces of a porous core) with each other.

2) The second objective is to develop a computer program that would simulate the steady flow of a gas through a porous media taking in account temperature dependent flow geometry, variable viscosity, and viscous dissipation. The gas is considered to contain a certain concentration of reactant which undergoes a first order, irreversible catalytic reaction. The temperature dependence of the rate constant is included.

3) The third objective (which in reality must be investigated first) is to develop a mathematical model of porous flow that will improve upon existing models and enable one to calculate theoretical values of the viscous and inertial resistance coefficients for a given porous media.

CHAPTER II

DEVELOPMENT OF CAPILLARY-ORIFICE MODEL

As mentioned in the previous section many models have been proposed to describe the flow in porous media, but all fall short of completely describing flow phenomenon over the complete range from low to high velocities. The following analysis represents an attempt to partially fill this void.

In developing a new model for flow in porous media, it was felt the simplicity of the parallel capillary model in predicting viscous drag should be preserved, but somehow the inertia loss that the fluid must surely experience in winding through a porous media should be taken into account. The "capillary-orifice model" is then proposed with those thoughts in mind.

The "capillary-orifice model" is assumed to consist of a bundle of capillary tubes with orifice plates spaced along the tube a distance equal to the mean pore diameter apart. If the mean pore diameter is defined to be δ, then the number of orifices per unit length is δ^{-1}. No assumptions are made as to the exact diameter of the orifice except that it is much less than the mean pore diameter (See Figure 1).

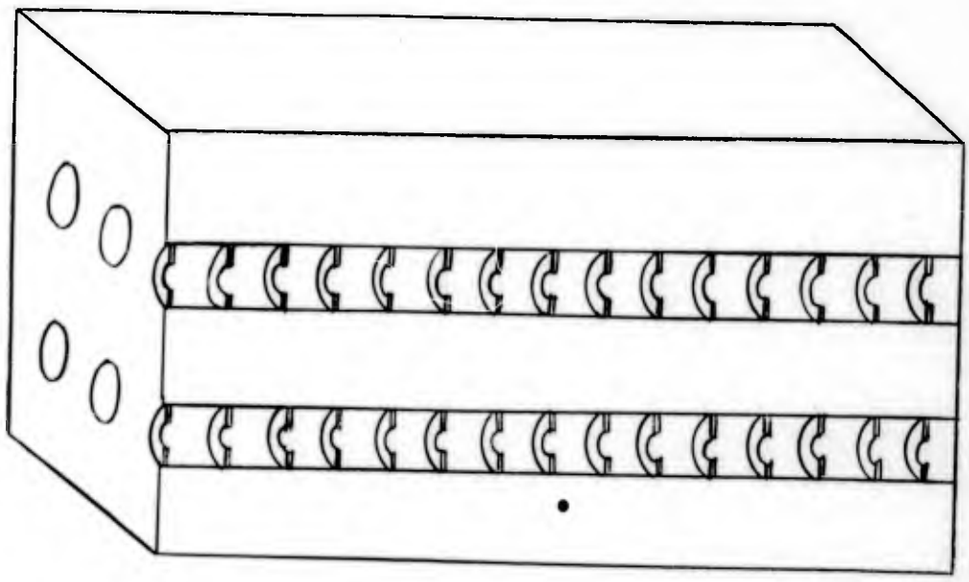

Figure 1. Capillary-Orifice Model

Momentum Balance

Figure 2 shows a section of a capillary tube and the external forces acting on the control volume. The diameter of each tube is taken as (δ) and the mean flow velocity through each tube is designated as (u) (this will sometimes be referred to as the local pore velocity). The forces acting on the control volume are pressure forces, skin friction forces, drag forces (due to the orifice plates), and body forces. Body forces act on the fluid element as a whole and are usually due to fields such as gravity, electric or magnetic.

For the momentum balance on the model element in Figure 2, the following assumptions are made.

1) Only one fluid is passing through the media.
2) The fluid is a Newtonian fluid with no slip flow at the walls.
3) Shrinking or swelling of the porous media is neglected.
4) The porous media is non-adsorbent, hence there exists no absorbed phase.
5) The mean pore diameter is much larger than the mean free path of the gas molecule (if the fluid is a gas).
6) The flow is one dimensional.
7) The thickness of the orifice plates is much smaller than the mean pore diameter.

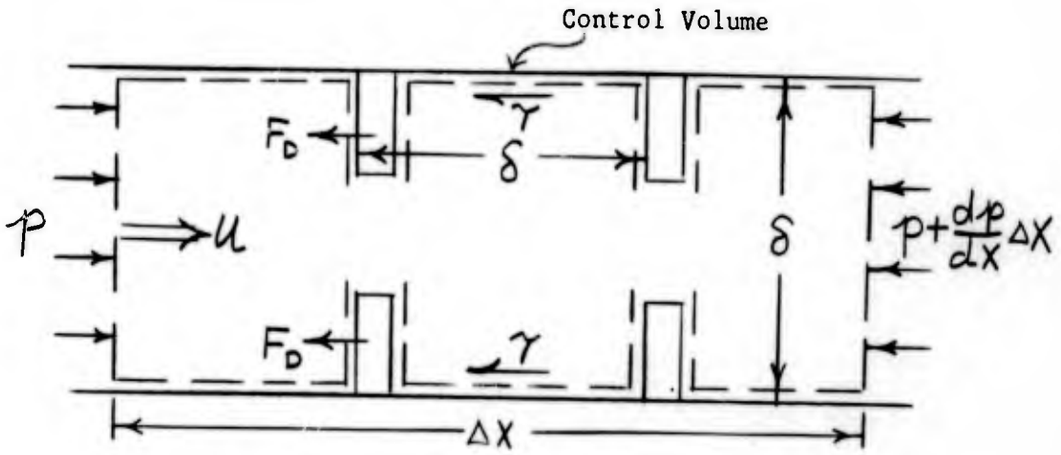

Figure 2. Capillary-Orifice Tube Section

The momentum theorem for a control volume states (10),

$$\Sigma \vec{F} = \oiint_{C.S.} \vec{V}(\rho \vec{V} \cdot d\vec{A}) + \frac{\partial}{\partial t} \iiint_{C.V.} \vec{V} \rho \, d\check{V} \qquad (2.1)$$

where $\oiint_{C.S.}$ = Closed integral over control surface

$\iiint_{C.V.}$ = Integral through control volume

$\frac{\partial}{\partial t}$ = Partial derivative with respect to time

$\Sigma \vec{F}$ = Sum of forces acting on control volume

$\vec{V}$ = Velocity of fluid (vector quantity)

ρ = Density of fluid

$d\check{V}$ = Differential volume

dA = Differential area

For the small element in Figure 2 one can write Equation (2.1) for the X direction as

$$-\frac{dp}{dx}\Delta x \frac{\pi}{4}\delta^2 - \tau \pi \delta \Delta x - C_D \tfrac{1}{2} \rho u^2 \pi/4 \delta^2 \left(\frac{\Delta x}{\delta}\right)$$

$$+ F_B \rho \pi/4 \delta^2 \Delta x = \frac{\partial(\rho u^2)}{\partial x}\Delta x \, \pi/4 \delta^2 + \frac{\partial(\rho u)}{\partial t}\frac{\pi}{4}\delta^2 \Delta x \qquad (2.2)$$

where τ = Shear stress at wall

C_D = Drag coefficient of orifice plate

F_B = Body force per unit mass

Divide Equation (2.2) by $\pi/4 \delta^2 \Delta x$

$$-\frac{dp}{dx} = \frac{4\tau}{\delta} + \frac{C_D \rho u^2}{2\delta} + \frac{\partial(\rho u^2)}{\partial x} + \frac{\partial(\rho u)}{\partial t} - \rho F_B \qquad (2.3)$$

Equation (2.3) is then the general momentum equation for non-steady flow through porous media. For steady flow and for a body force due to a gravity field only, Equation (2.3) becomes,

$$-\frac{dp}{dx} = \frac{4\tau}{\delta} + \frac{C_D \rho u^2}{2\delta} + \rho u \frac{\partial u}{\partial x} - \rho g \cos\sigma \qquad (2.4)$$

where g = Local acceleration of gravity

σ = Angle between X direction and the direction in which gravity acts

The shear stress τ can be expressed as

$$\tau = C_f \tfrac{1}{2} \rho u^2 = C_f \tfrac{1}{2} \frac{4\mu}{\delta} \left(\frac{\rho u \delta}{\mu}\right)$$

or

$$\tau = C_f \frac{1}{2} \frac{4\mu}{\delta} Re \qquad (2.5)$$

where C_f = Skin friction coefficient

R_e = Reynolds number based on mean pore diameter

Using the Dupuit-Forcheimer assumption (9),

$$v = \epsilon u \qquad (2.6)$$

where v = Filter velocity (volume flow per unit area)

ϵ = Porosity (ratio of void volume to total volume)

It should be mentioned briefly that the "pore velocity" (u) is really the imaginary mean velocity in the capillary tubes of the capillary-orifice model. The true velocity of the fluid will fluctuate grossly in a porous media.

Substituting Equations (2.5) and (2.6) into Equation (2.4) there results

$$-\frac{dp}{dx} = \frac{2C_f Re}{\delta^2 \epsilon}\mu v + \frac{C_D \rho}{2\epsilon^2 \delta} v^2 + \frac{\rho v}{\epsilon^2}\frac{\partial v}{\partial x} - \rho g \cos\sigma \qquad (2.7)$$

For flow parallel to the earth's surface σ is ninety degrees and the last term in Equation (2.7) vanishes. The term

$$\frac{\rho v}{\epsilon^2}\frac{\partial v}{\partial x}$$

was examined for porous media having mean pore diameter on the order of ten microns and porosities of thirty per cent (typical values for the sintered metal cores uses in our experiments) and its value was found to be negligible compared with that of the other terms. For horizontal flow Equation (2.7) becomes now,

$$-\frac{dp}{dx} = \frac{2C_f Re}{\delta^2 \epsilon}\mu v + \frac{C_D \rho}{2\epsilon^2 \delta} v^2 \qquad (2.8)$$

If Equation (2.8) is compared with Equation (1.1), it is obvious that

$$\alpha = \frac{2C_f Re}{\delta^2 \epsilon} \qquad (2.9)$$

and

$$\beta = \frac{C_D}{2\epsilon^2 \delta} \qquad (2.10)$$

Here then are two equations with which one can predict the empirical coefficients α and β if something is known of the variation of C_f and C_D.

The expression for α is not entirely new (a similar expression was previously derived from the Hagen-Poiseuille Law for laminar flow in a capillary-tube model (9)), however, the expression for β (Equation 2.10) seems to be unique. In the past there seemed to have been little effort to require a porous model to do more than predict values of α . This is understandable because the bulk of the research in porous fluid flow has been done in petroleum technology where the flow velocities are usually so low that inertia effects are negligible. A second reason for the scarcity of research being applied to the β term is because the complexity of porous fluid flow has discouraged work in this area and, because as yet, no one is really satisfied with the values of α predicted by the various models. To the neophyte in the field it appears to be much easier to improve upon the existing theoretical values of α (due to the different models) than to tackle the seemingly very difficult turbulent or non-linear flow term.

The success of the "capillary-orifice" model can be determined by comparing experimental and theoretical values of α and β (this is done in a later section) and by the following comparison of experimental and theoretical pressure drops.

Comparison Between Theory and Experiment for a Gas

Equation (2.8) can be put in the following form.

$$-\rho \frac{dp}{dx} = \frac{2 C_f Re}{\delta^2 \epsilon} \mu G + \frac{C_D}{2\epsilon^2 \delta} G^2 \qquad (2.11)$$

where $G = \rho v$ the mass flow/unit area

For a quasi-ideal gas,

$$\rho = \frac{p M}{Z R T} \tag{2.12}$$

where Z = Compressibility factor

M = Molecular weight

Then if Equation (2.12) is substituted in Equation (2.11), there results,

$$-\frac{M}{2ZRT}\frac{d(p^2)}{dX} = \frac{2 C_f Re}{\delta^2 \epsilon}\mu G + \frac{C_D G^2}{2\epsilon^2 \delta} \tag{2.13}$$

Integrating Equation (2.13) for p from p_1 to p_2 and X from 0 to L, and replacing Reynolds number by its equivalent, there results (for isothermal flow,)

$$\psi = 2 C_f + \frac{C_D}{2} \tag{2.14}$$

where $$\psi = \left[(p_1^2 - p_2^2) M \delta \epsilon^2\right] \Big/ \left[2 L G^2 Z R T\right] \tag{2.15}$$

From Equation (2.14) it is seen that the problem of predicting pressure drops in porous media reduces to one of determining skin friction coefficients and drag coefficients. For most engineers this puts the problem onto a more familiar plane.

For a very rough approximation laminar flow is assumed to exist below a Reynolds number of 2000 and turbulent flow above that number. For a first order approximation on the skin friction one can assume

that the skin friction coefficient in the capillary for laminar flow is given by the Hagen-Poiseuille Law,

$$C_f = \frac{16}{Re} \tag{2.16}$$

For the turbulent regime the skin friction is assumed to be given by the Von Karman-Nikuradse formula,

$$C_f^{-1/2} = 4.0 \log_{10}[Re\, C_f^{1/2}] - 0.4 \tag{2.17}$$

The drag coefficient for Equation (2.14) is for a circular disk with a hole in its center and completely bounded by the cylinder. Due to lack of experimental drag data for this type of body, it becomes advantageous to use drag data for a solid disk with no wall effects. The drag coefficient in Equation (2.14) is taken then from Rouse (11) for disks.

Equation (2.14) is plotted in Figure 3 along with experimental data. Equations (2.16) or (2.17) are used for C_f and data from (11) is used for C_D.

From Figure 3 it is seen that Equation (2.14) compares well with experimental data, even though considerable scatter of the data does exist. This scatter of the data is believed to be largely due to the way in which the mean pore diameter is defined and measured. The concept of expressing the varying shapes of flow passages by means of a fictitious tube of mean diameter δ is crude to say the least. Methods, such as mercury intrusion, can enable one to determine the

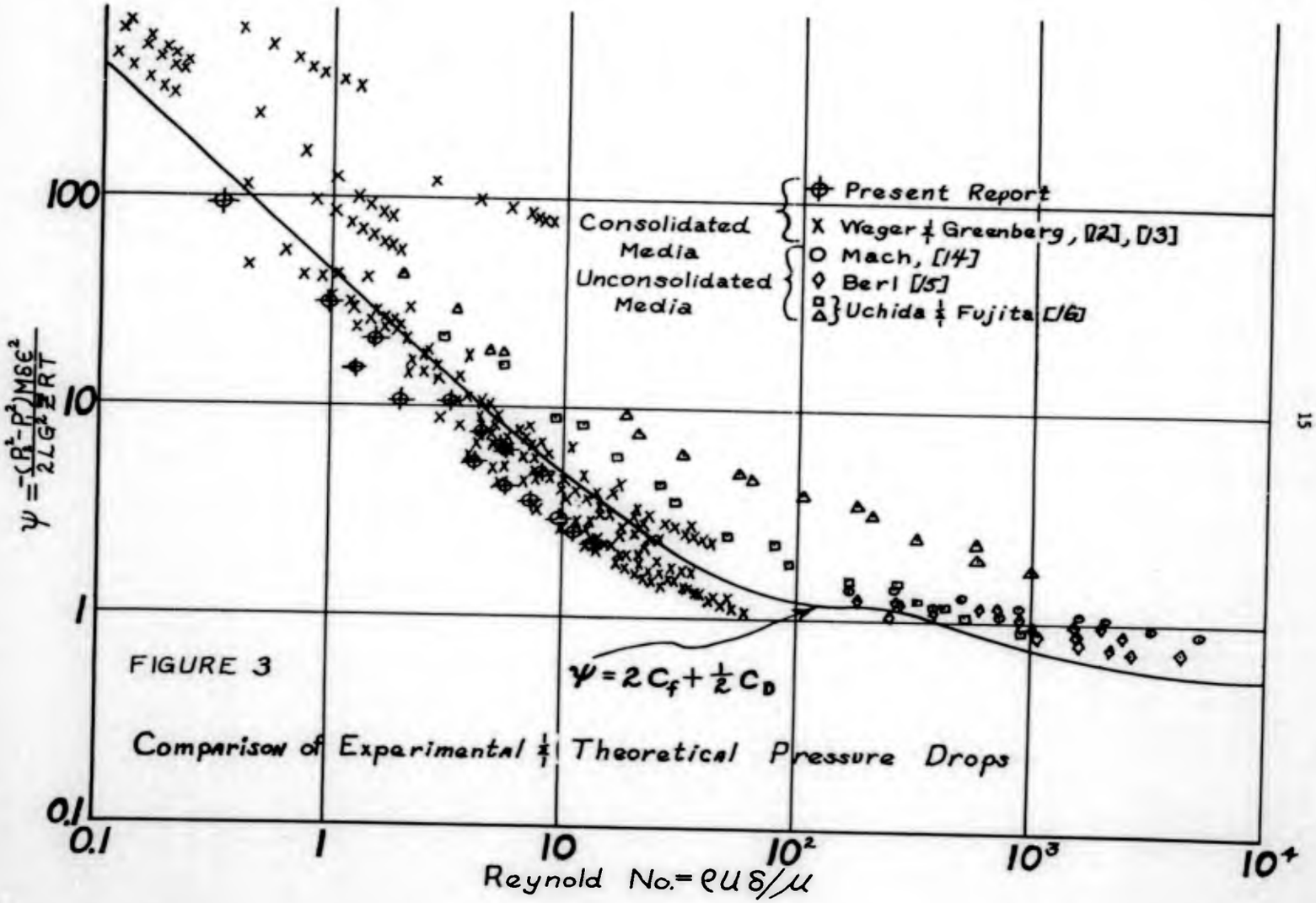

FIGURE 3

Comparison of Experimental & Theoretical Pressure Drops

distribution of pore diameters in porous media. Any improvement in the present theory might well come from using this concept of pore size distribution.

The capillary-orifice model does, however, indicate the trend that the experimental points follow, and a large percentage of the experimental data does fall very close to the theory line.

A comparison of terms indicates that at low Reynolds number the skin friction coefficient term is the dominant term in Equation (2.14) while at high Reynolds number (greater than 10) the drag coefficient term is the dominant term. Past a Reynolds number of 1000 the drag coefficient of flat disks (and most shapes) vary little with Reynolds number. Experimental data in Figure 3 seems to bear this out.

In the past the region beyond Reynolds of 10 has been spoken of as being the turbulent region, since some experimenters had envisioned the pressure drop in this regime as being primarily due to turbulent motion of the fluid (see for example (17)). However, the present analysis does not employ the concept of turbulent motion until a Reynolds number of 2000 is reached and yet the theory matches experiment fairly well. It is the author's opinion that the labeling of the region beyond Reynolds number of 10 as the turbulent region is then a misnomer. It might well be labeled better as the drag regime, since the particle drag coefficients are so predominant in this region.

It might also be mentioned that Blake (18) empirically found a dimensionless pressure loss factor

$$\psi' = \frac{\Delta P^2 \epsilon^3 M}{2 L G^2 S R T} \tag{2.18}$$

and a modified Reynolds number, $\frac{\rho u}{\mu S}$ that was useful in correlating data. S is the specific internal area, that is the internal area per unit volume of media. In equation form it is possible to show that,

$$S = \frac{4\epsilon}{\delta} \tag{2.19}$$

Hence substituting Equation (2.19) into Equation (2.18)

$$\psi' = \frac{\Delta P^2 M \delta \epsilon^2}{8 L G^2 R T} \tag{2.20}$$

This is very nearly equal to ψ in Equation (2.15) and if ΔP is very large then

$$\psi' \approx \psi/4 \tag{2.21}$$

This then is the second case (the first being Equation (2.8)) where the "capillary-orifice model" has been used to analytically determine an expression which had previously been empirically determined.

CHAPTER III

HEAT TRANSFER WITH A REACTING GAS

The use of porous sintered metallic compacts as catalytic chemical reactors is assuming an ever-increasing importance in modern technology. For instance, the hydrocarbon converters being developed for internal combustion engine exhaust make use of porous metals. Another example would be in the important field of aerodynamic cooling. Catalyst-coated porous walls in which an endothermic reaction is carried out are extremely effective heat sinks for the large thermal fluxes which are generated on nose cones, inside rocket chambers, etc.

One of the main problems encountered in the use of these materials is that their flow geometry is marked function of temperature that is, for a given pressure drop, the flow rate depends on the temperature conditions in the compact. This effect was reported in a recent paper (12), where some hypotheses were also presented which may explain the causes of this phenomenon.

This chapter presents the equations which are used for the calculation of flow rate, conversions, and temperatures as a function of reactor length, porous metal properties, rate constant, and heat of reaction. Some results were calculated by the Oklahoma University IBM 650 Computer for a typical porous metal. These results demonstrate

the large variation in flow rates and temperature gradients which may be expected for flow reactions taking place in these types of materials.

Analysis

The following assumptions are made for the energy balance analysis for a reacting fluid through a porous media.

1) Gas temperature is equal to body temperature

2) Viscous resistance coefficient is temperature dependent

$$\alpha = \eta e^{\gamma T} \tag{3.1}$$

3) Viscosity is temperature dependent

$$\mu = \mu^* \frac{T}{T^*} \tag{3.2}$$

4) Viscous dissipation is present. (See Appendix A.)

$$\Phi = -u\left[\frac{dp}{dx} + \rho u \frac{du}{dx}\right] \tag{3.3}$$

5) Conservation of mass, momentum and energy is based on the "capillary-orifice model."

6) Gas is inert containing a reactant which is undergoing a first order irreversible catalytic reaction of the type

$$M \longrightarrow N \tag{3.4}$$

where the reaction rate

$$r = kC \tag{3.5}$$

and k the reaction rate constant are temperature dependent.

$$k = A e^{-E_a/RT} \tag{3.6}$$

where C_A = Concentration of reactant A

A = Constant

E_a = Activation energy

R = Gas constant

T = Gas temperature (absolute)

7) Flow is steady.

Assumption number one is not at all obvious when one first glances at the problem. In fact when this portion of the analysis was initiated it was assumed that the gas temperature was different than the body temperature. A computer program was written and a solution was attempted using the University of Oklahoma IBM 650 Digital Computer. The program was found to produce instability. The problem was found to be in the energy equation of the solid.

$$\frac{d^2t}{dx^2} = \frac{hS}{k_s(1 - \epsilon)} (t - T) \qquad (3.7)$$

where h = Heat transfer coefficient

S = Specific area

k_s = Effective thermal conductivity of solid

ϵ = Porosity

t = Body temperature

T = Gas temperature

The constant multiplying factor $\frac{hS}{k_s (1 - \epsilon)}$ for flow through metallic porous media has an order of magnitude of 10^7. Hence a computer error of only 10^{-2} in the temperature difference would make the

second derivative of temperature in error by 10^5. This would in turn increase the temperature difference, etc. Experimentally the second derivative has been shown to be of order of magnitude less than 10^3. Therefore from Equation (3.1) it is obvious that the difference between gas and body temperature must be of the order of 10^{-4}! This is a very small difference and hence the reason for assumption number one.

Alt (20) expressed the paradox of instability quite well when he wrote "Quite frequently, instability is introduced by improvident attempts to improve the accuracy or elequence of a method."

The following conservation equations are used to solve for the mass flow, pressure and temperature distribution for one-dimensional flow through a porous core. (See Figure 4.)

Conservation of Reactant Mass

$$u \frac{dC_A}{dx} = -k C_A \tag{3.8}$$

Conservation of Total Mass

$$\rho v = \text{Constant} \tag{3.9}$$

Conservation of Momentum

$$-\frac{dp}{dx} = \alpha \mu v + \beta \rho v^2 \tag{3.10}$$

Conservation of Energy of Gas

$$\rho C_p u \frac{dT}{dx} = k H C_A + u \frac{dp}{dx} + k_g \frac{d^2T}{dx^2} + \Phi \tag{3.11}$$

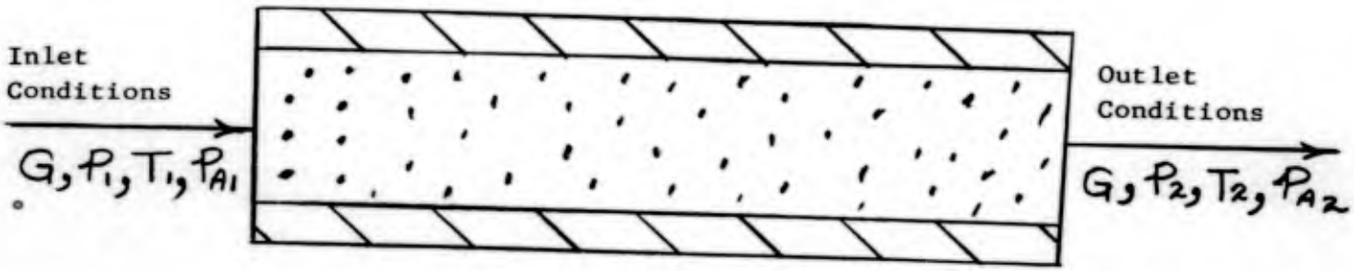

Figure 4. Porous Core

Conservation of Energy of Solid

$$k_s \frac{d^2T}{dX^2} = 0 \qquad (3.12)$$

where H = Heat of reaction

k_g = Gas Thermal conductivity

k_s = Effective solid thermal conductivity

These equations can be solved for fixed values of the inlet pressure and temperature, fixed core length and fixed outlet pressure. Equations (3.8) through (3.11) were solved by use of the Runge Kutta Numerical Method on the IBM 650 Computer. (See Appendix B for program details.)

The following terms were held constant for all runs.

ϵ = Porosity = .3

P_{final} = 1 Atmosphere

$T_{initial}$ = $530^{\circ}F$

L = Core length = 1/4 ft.

M = Molecular weight of gas = 30 lbm/mole

μ = Viscosity = $4X10^{-7}$ $\left(\frac{T}{530}\right)$ lb_f sec/ft^2

α = $e^{\gamma T}$ = $2180e^{0.0349T}$ ft^{-2}

β = $1.7X10^{7}$ ft^{-1}

The following terms were variable input constants.

P initial: 2, 10, 100, 1000 atmospheres

P partial initial: 0.01, 0.05, 0.1 atmospheres

H : -45000, 0, +45000 Btu/lbMole

A : $4.8X10^{11}$, $4.8X10^{12}$ sec^{-1}

Ea : 17000, 34,000 cal/Mole

Figures 5 through 22 graphically present the results of this computer analysis.

Discussion of Results

The computer analysis demonstrates the significant degree to which the flow rate of a reacting gas in a porous metallic element is affected by the rate and heat of reaction. As can be seen from Figure 5 the flow rate will decrease more rapidly for a rise in heat of reaction (hence rise in temperature) than it will decrease due to a corresponding decrease in heat of reaction. The decrease in flow rate will, in turn, lead to a longer residence time causing yet larger conversions and temperature increases. This is the reason for the lower flow rates and higher exit temperatures (See Figure 8 or Figure 20) for the exothermic reactions at a given rate constant.

Corroborating this conclusion are Figures 6 and 7 which show that for an endothermic reaction, any effects which tend to decrease the temperature (such as increased reaction rate constant, increased amount of reactant or decreased activation energy) tend to increase the mass flow rate.

It is evident also from Figures 5 through 7 that the mass flow seems to be practically independent of reaction rate constants, heats of reactions, activation energy and initial partial pressure when the initial pressure is much greater than 10 atmospheres. The reason for

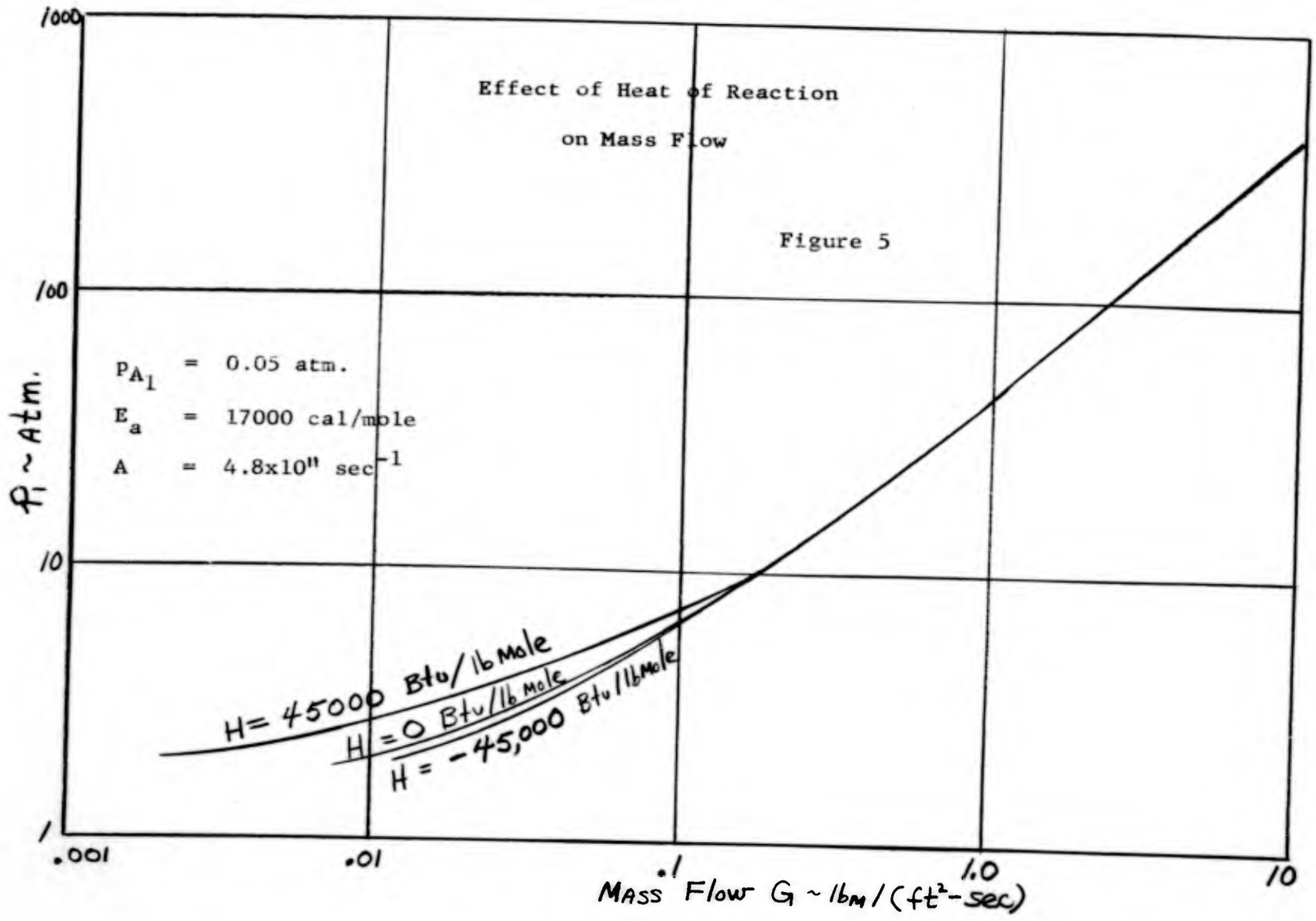
Effect of Heat of Reaction
on Mass Flow
Figure 5
P_{A_1} = 0.05 atm.
E_a = 17000 cal/mole
A = 4.8x10¹¹ sec⁻¹
H= 45000 Btu/lb Mole
H = 0 Btu/lb Mole
H = -45,000 Btu/lbMole
P₁ ~ Atm.
1000
100
10
1
.001
.01
.1
1.0
10
Mass Flow G ~ lbM/(ft²-sec)

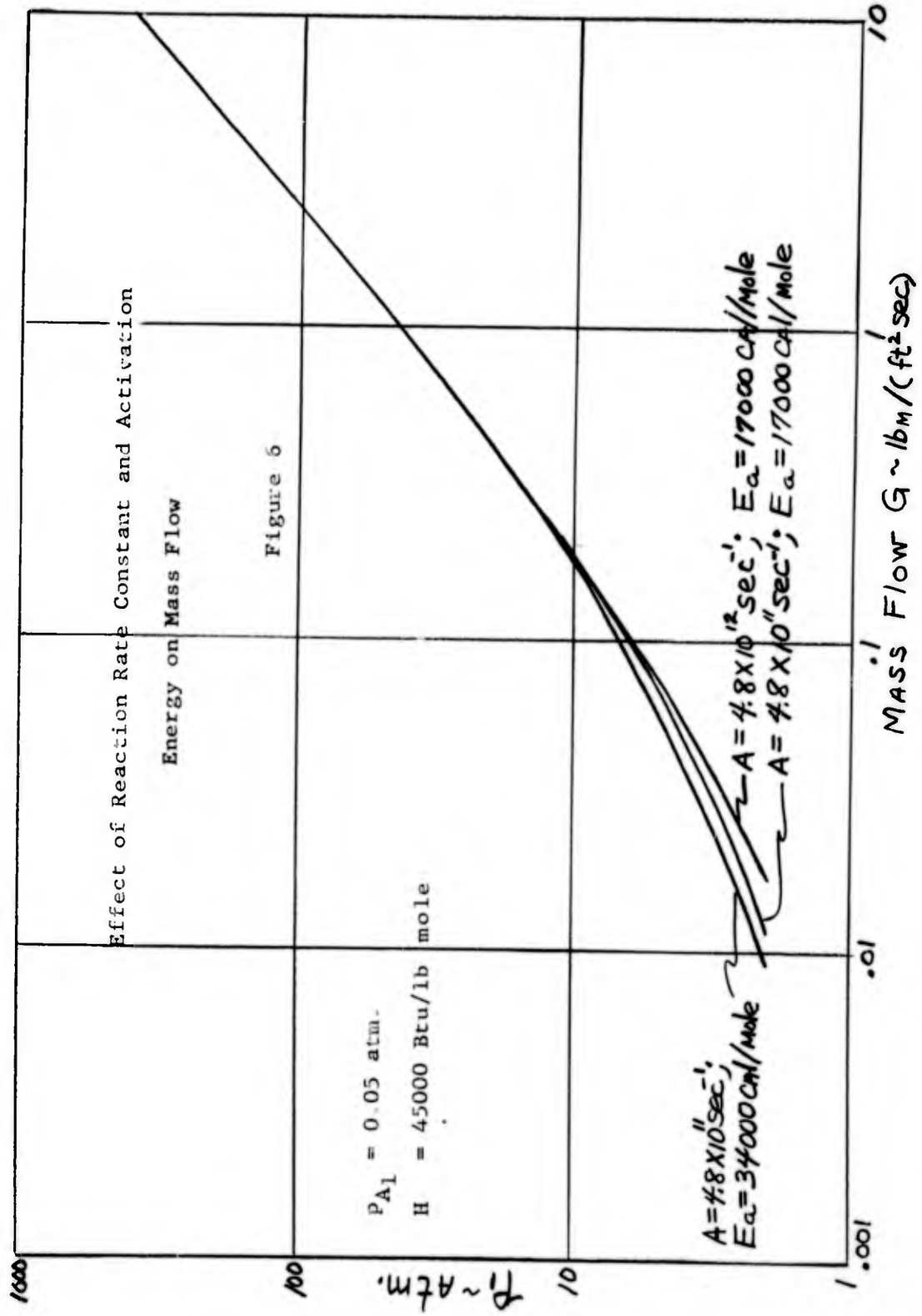
Effect of Reaction Rate Constant and Activation Energy on Mass Flow
Figure 6
P_{A_1} = 0.05 atm.
H = 45000 Btu/lb mole
P ~ atm.
1000
100
10
1
.001
.01
.1
1
10
Mass Flow G ~ lbM/(ft² sec)
A=4.8X10¹² sec⁻¹; Ea=17000 cal/Mole
A=4.8X10¹¹ sec⁻¹; Ea=17000 cal/Mole
A=4.8X10¹⁰ sec⁻¹; Ea=34000 cal/Mole

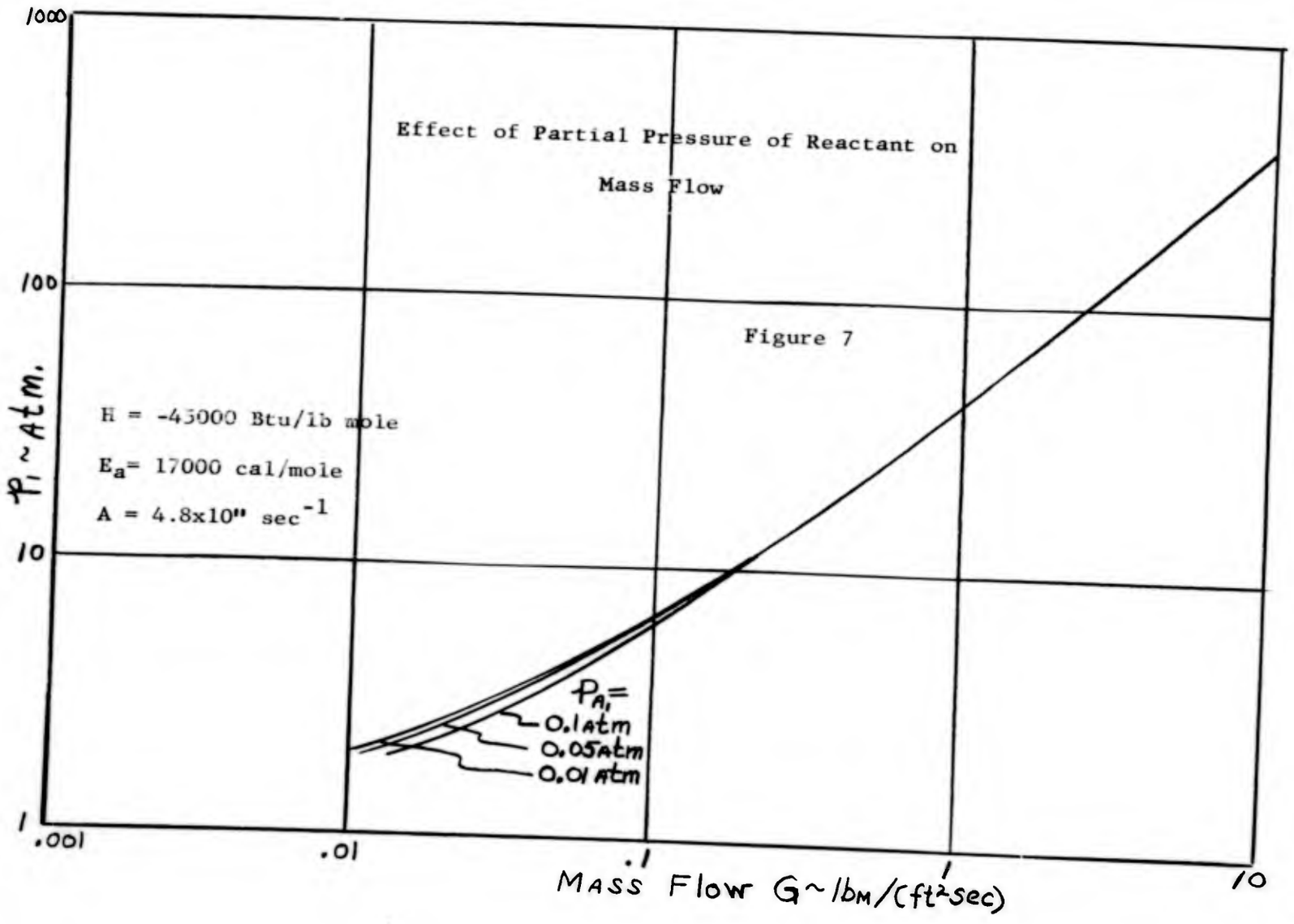
Effect of Partial Pressure of Reactant on Mass Flow
Figure 7
H = -45000 Btu/lb mole
E_a= 17000 cal/mole
A = 4.8x10" sec^{-1}
P_t ~ Atm.
1000
100
10
1
.001
.01
.1
1
10
P_{A_1}=
0.1 atm
0.05 atm
0.01 atm
Mass Flow G ~ lbm/(ft²sec)

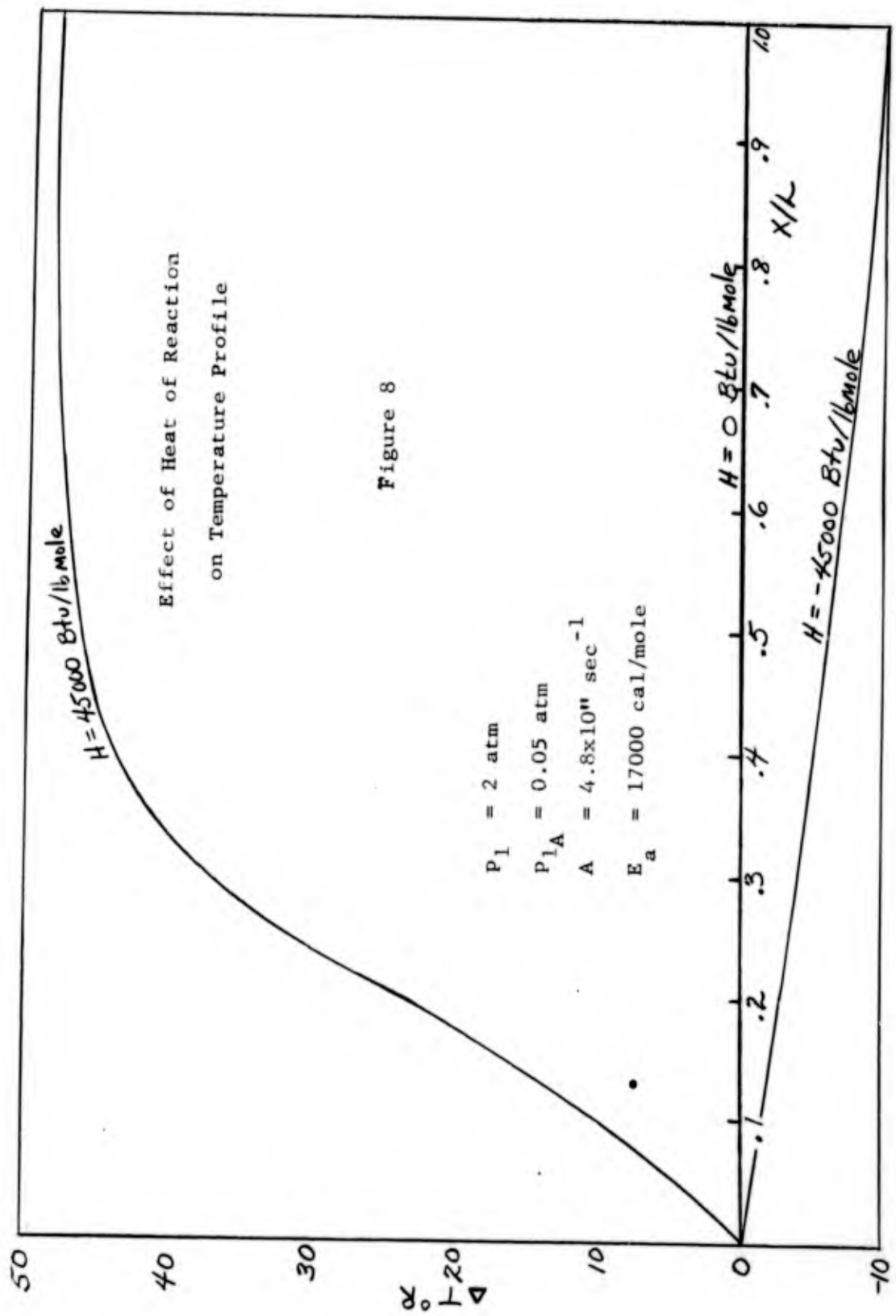

Effect of Heat of Reaction on Temperature Profile

Figure 8

P_1 = 2 atm

P_{1_A} = 0.05 atm

A = 4.8×10^{11} sec^{-1}

E_a = 17000 cal/mole

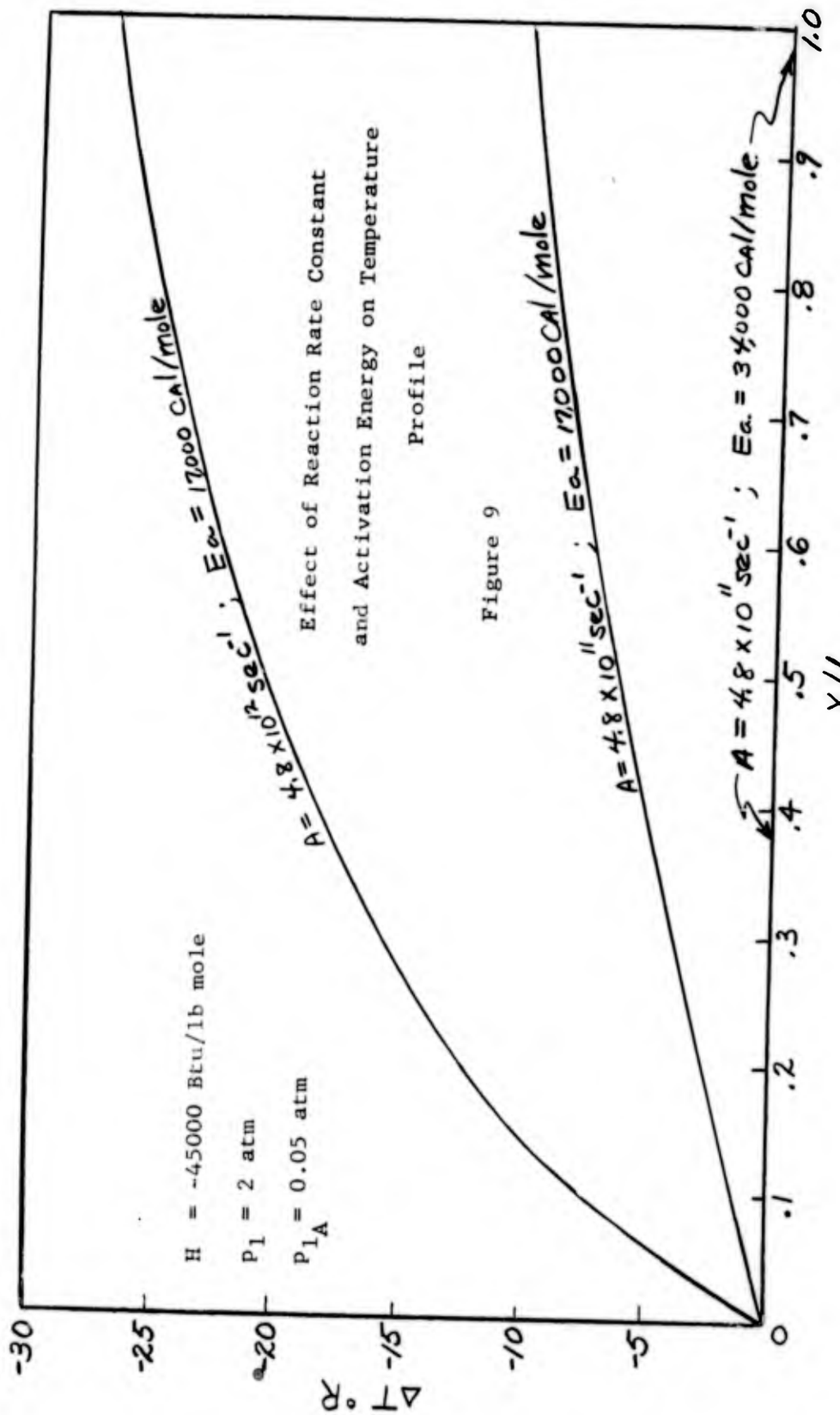

Effect of Reaction Rate Constant and Activation Energy on Temperature Profile

Figure 9

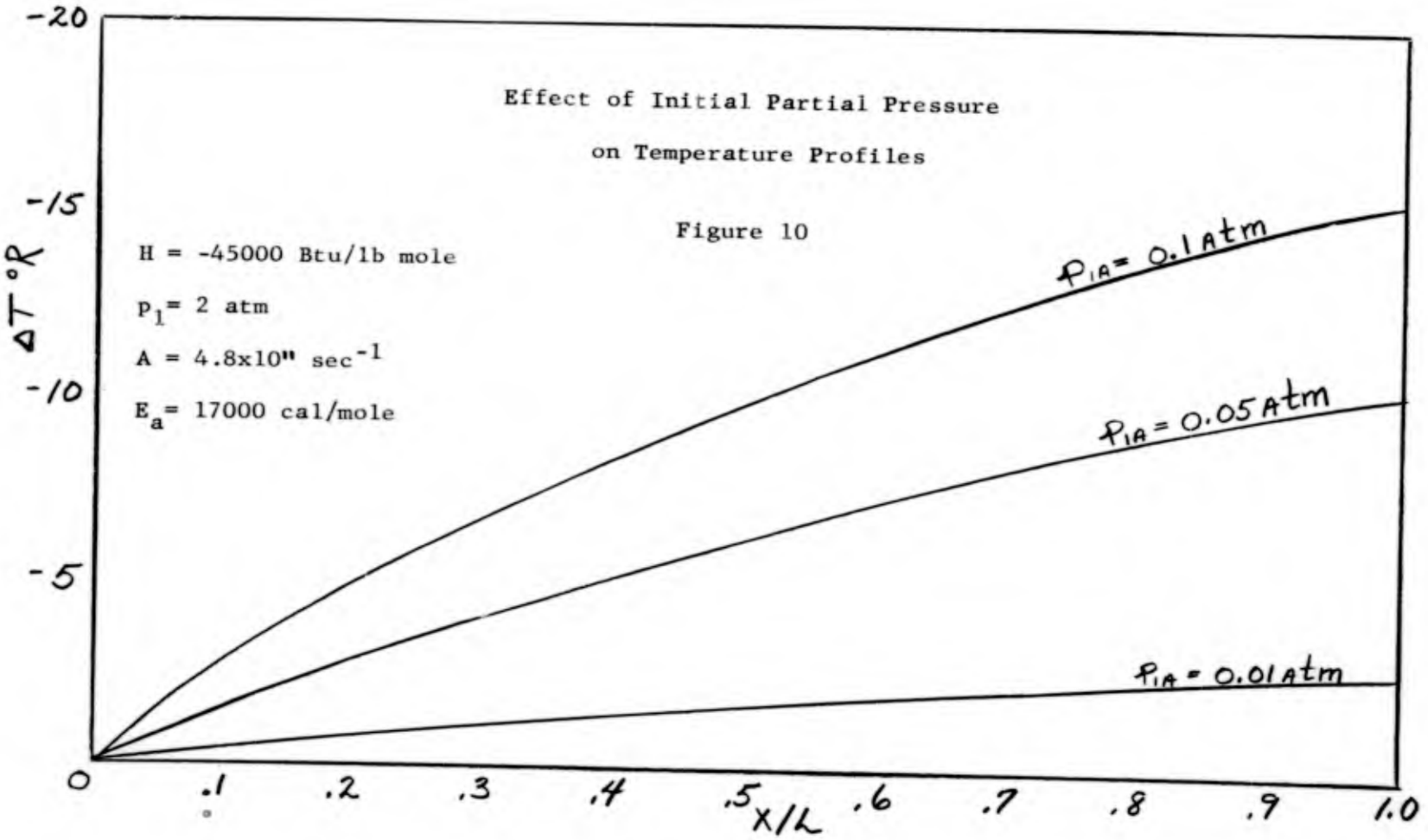
Effect of Initial Partial Pressure
on Temperature Profiles
Figure 10
H = -45000 Btu/lb mole
P_1 = 2 atm
A = 4.8x10" sec^{-1}
E_a = 17000 cal/mole
P_{1A} = 0.1 Atm
P_{1A} = 0.05 Atm
P_{1A} = 0.01 Atm
ΔT °R
-20
-15
-10
-5
0
.1
.2
.3
.4
.5
X/L
.6
.7
.8
.9
1.0

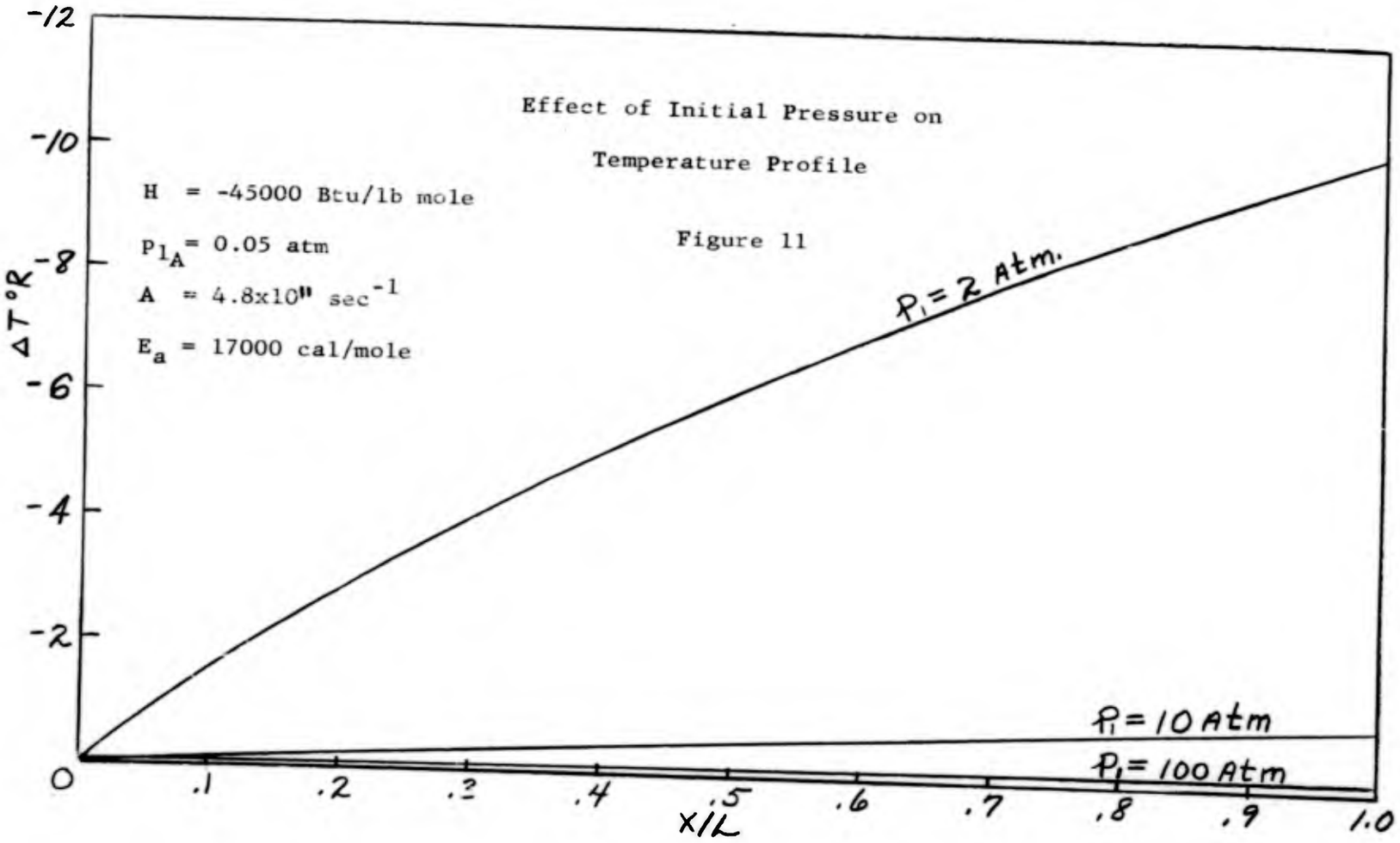
Effect of Initial Pressure on
Temperature Profile
H = -45000 Btu/lb mole
P_{1_A} = 0.05 atm
A = 4.8x10^{11} sec^{-1}
E_a = 17000 cal/mole
Figure 11
P_i = 2 Atm.
P_i = 10 Atm
P_i = 100 Atm
ΔT°R
X/L
-12
-10
-8
-6
-4
-2
0
.1
.2
.3
.4
.5
.6
.7
.8
.9
1.0

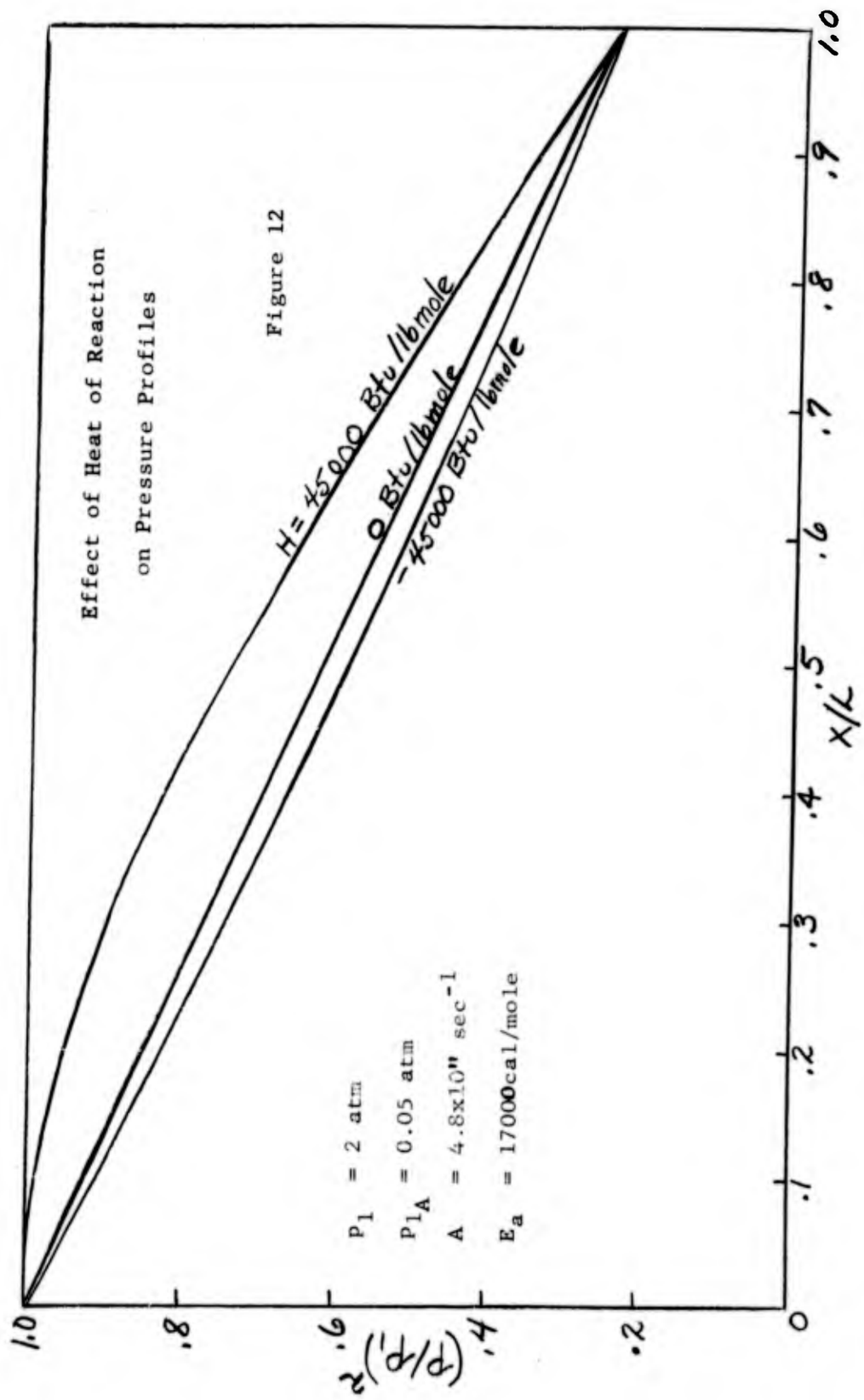
Effect of Heat of Reaction
on Pressure Profiles
Figure 12
H= 45000 Btu/lb mole
0 Btu/lbmole
-45000 Btu/lbmole
P1 = 2 atm
P1A = 0.05 atm
A = 4.8x10" sec-1
Ea = 17000cal/mole
(P/P1)2
X/L
1.0
.8
.6
.4
.2
0
.1
.2
.3
.4
.5
.6
.7
.8
.9
1.0

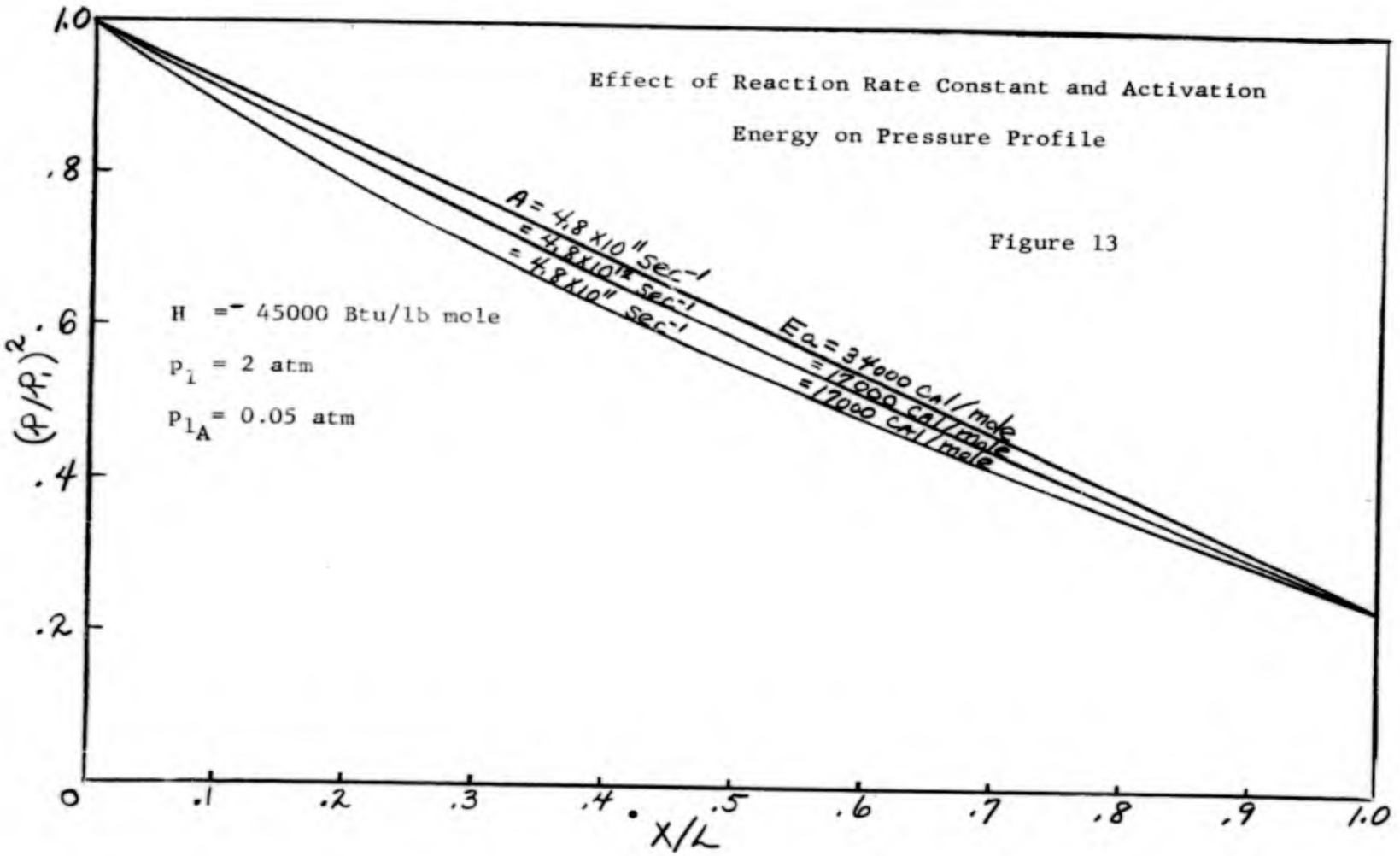
Effect of Reaction Rate Constant and Activation
Energy on Pressure Profile
Figure 13
H = - 45000 Btu/lb mole
p_i = 2 atm
p_{1_A} = 0.05 atm
A = 4.8 x 10^11 sec^-1
= 4.8 x 10^12 sec^-1
= 4.8 x 10^11 sec^-1
Ea = 34000 Cal/mole
= 17000 Cal/mole
= 17000 Cal/mole
$(P/P_i)^2$
X/L
1.0
.8
.6
.4
.2
0
.1
.2
.3
.4
.5
.6
.7
.8
.9
1.0

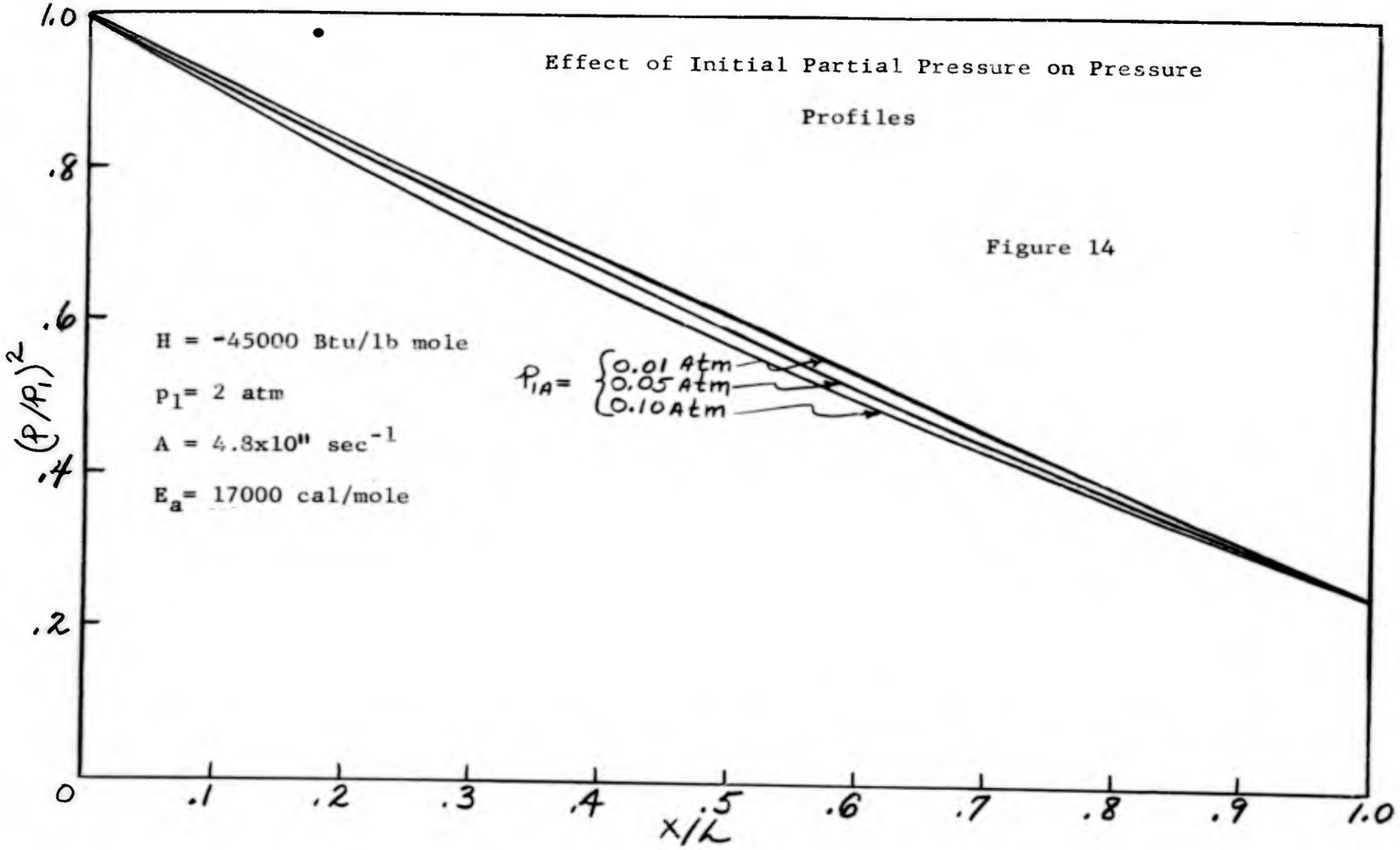
Effect of Initial Partial Pressure on Pressure Profiles
Figure 14
H = -45000 Btu/lb mole
p_1= 2 atm
A = 4.8x10^{11} sec^{-1}
E_a= 17000 cal/mole
P_{1A}= 0.01 Atm, 0.05 Atm, 0.10 Atm
$(P/P_1)^2$
1.0
.8
.6
.4
.2
0
.1
.2
.3
.4
.5
.6
.7
.8
.9
1.0
x/L

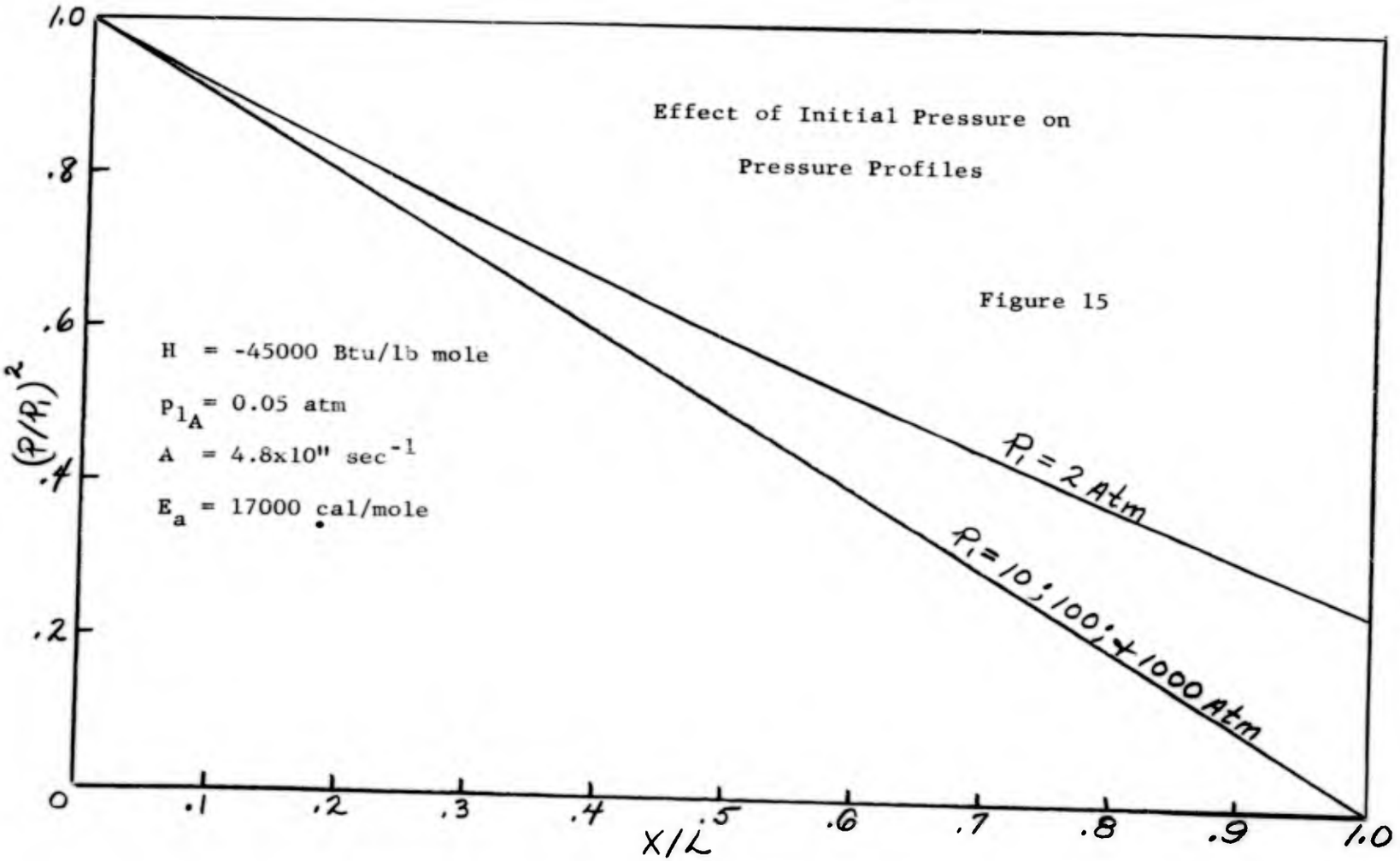
Effect of Initial Pressure on
Pressure Profiles
Figure 15
H = -45000 Btu/lb mole
P_{1_A} = 0.05 atm
A = 4.8x10" sec^{-1}
E_a = 17000 cal/mole
P_1 = 2 Atm
P_1 = 10, 100, & 1000 Atm
$(P/P_1)^2$
X/L
1.0
.8
.6
.4
.2
0
.1
.2
.3
.4
.5
.6
.7
.8
.9
1.0

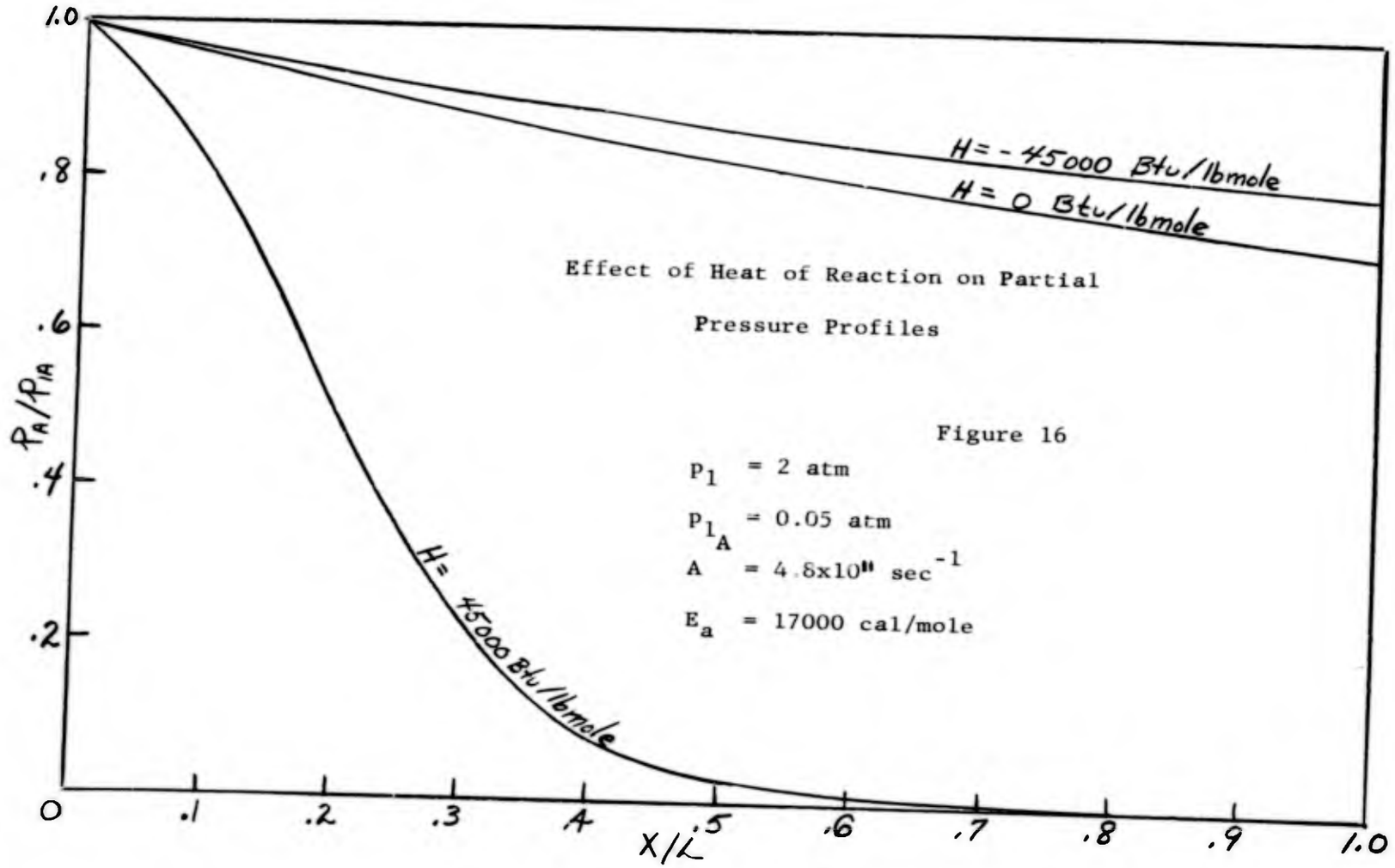

Effect of Heat of Reaction on Partial Pressure Profiles

Figure 16

P_1 = 2 atm

P_{1_A} = 0.05 atm

A = 4.8×10^{11} sec^{-1}

E_a = 17000 cal/mole

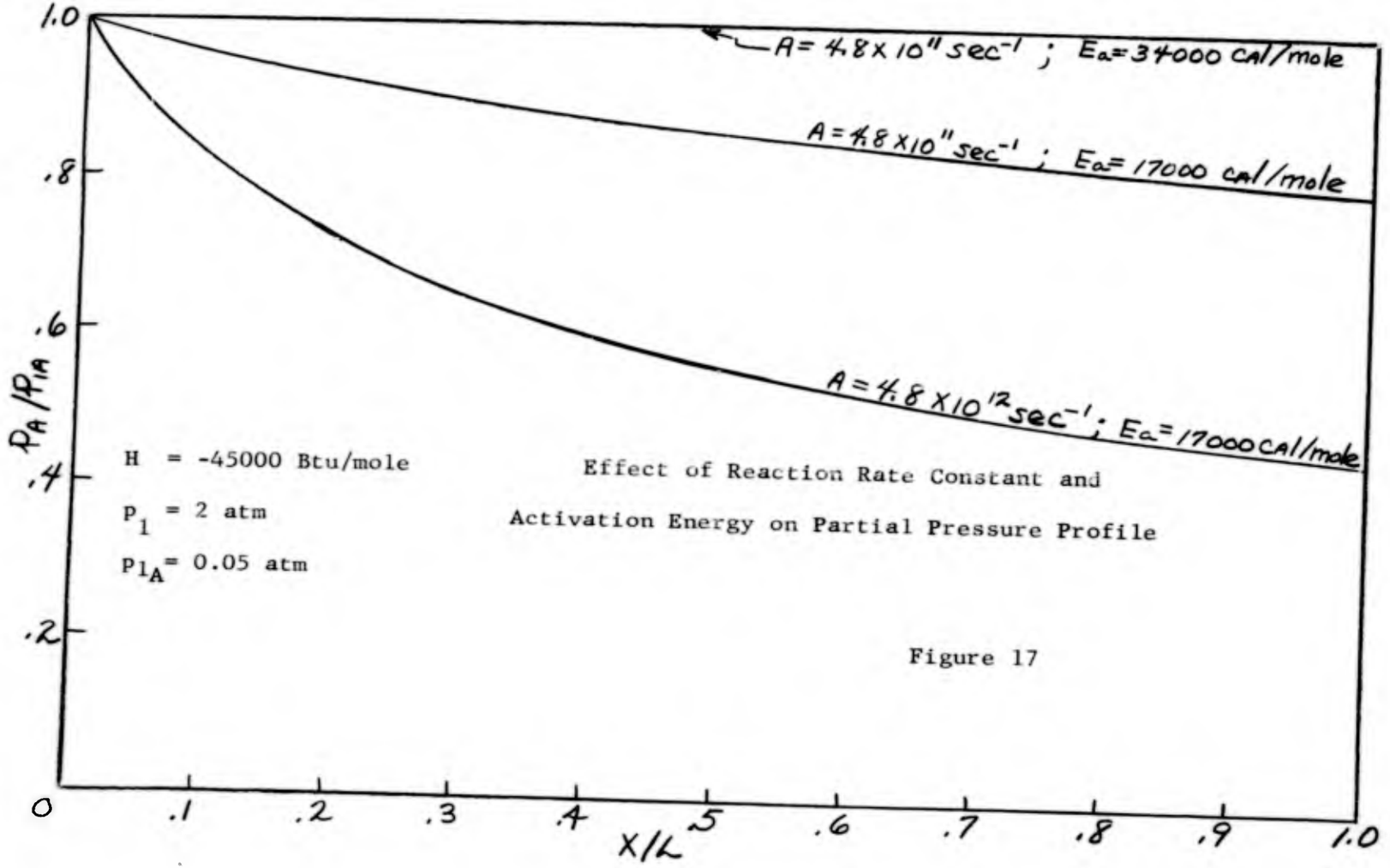

H = -45000 Btu/mole

P_1 = 2 atm

P_{1A} = 0.05 atm

Effect of Reaction Rate Constant and Activation Energy on Partial Pressure Profile

Figure 17

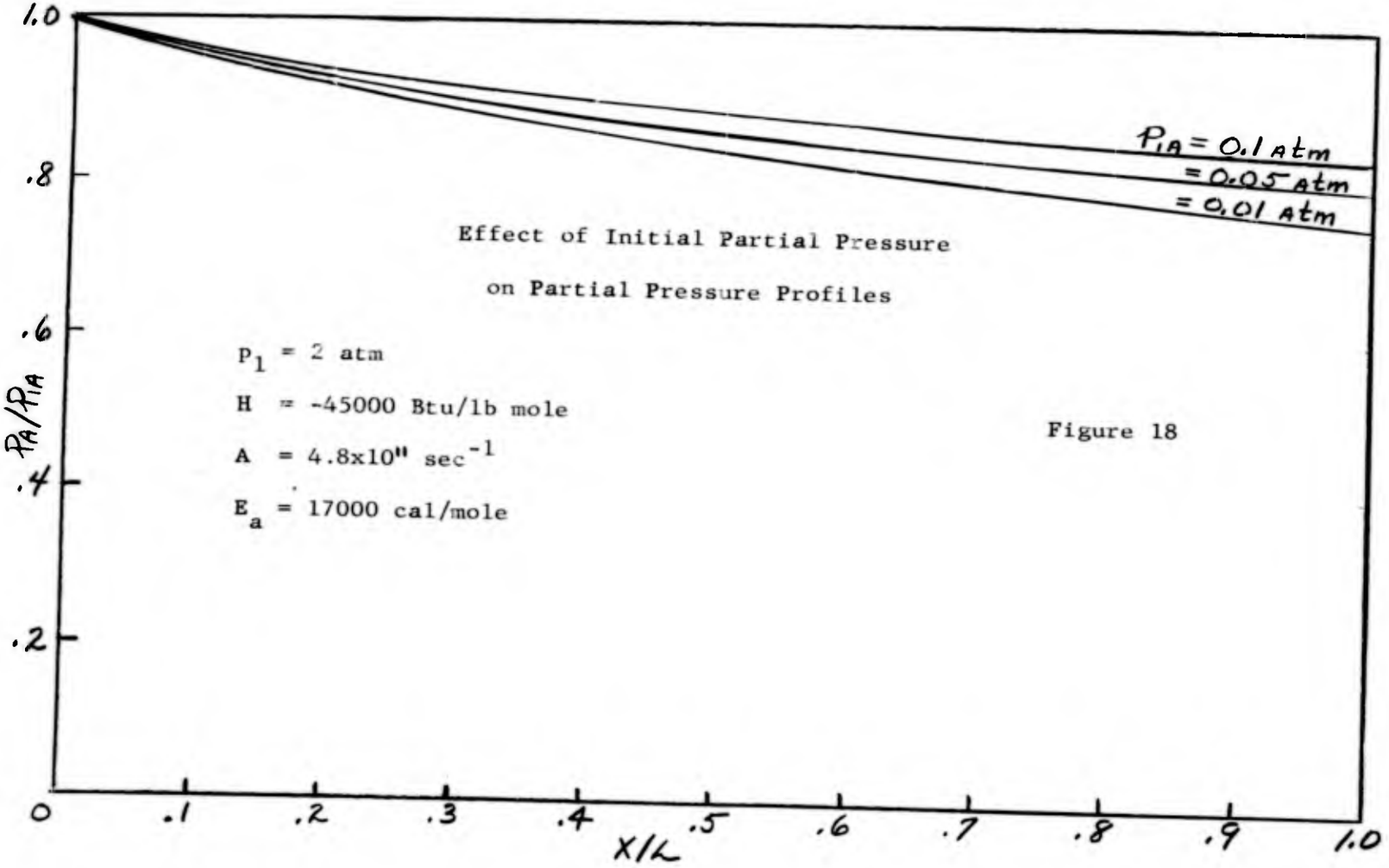

Effect of Initial Partial Pressure

on Partial Pressure Profiles

P_1 = 2 atm

H = -45000 Btu/lb mole

A = 4.8×10^{11} sec^{-1}

E_a = 17000 cal/mole

Figure 18

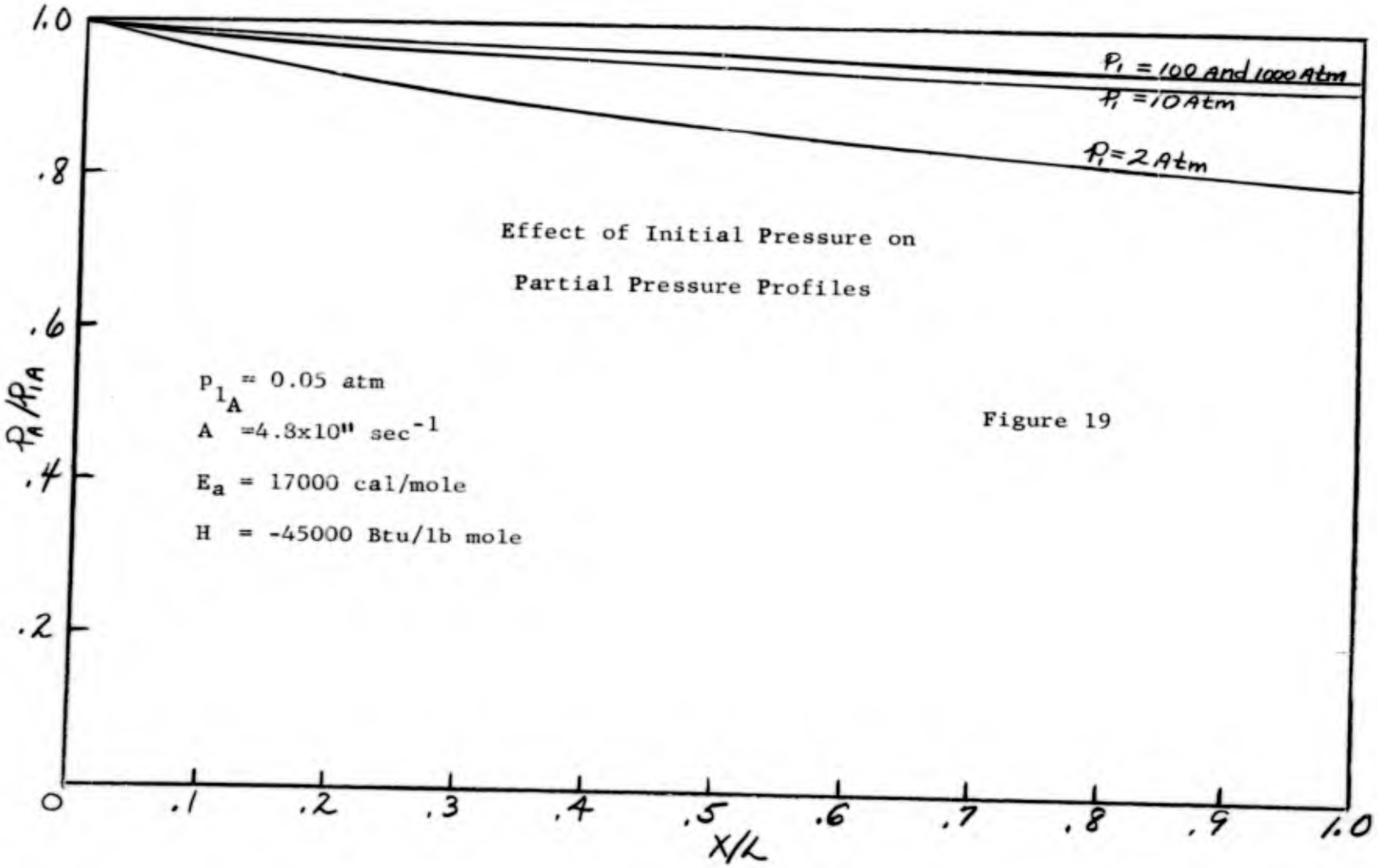

Effect of Initial Pressure on

Partial Pressure Profiles

p_{1_A} = 0.05 atm

A = 4.8×10^{11} sec^{-1}

E_a = 17000 cal/mole

H = -45000 Btu/lb mole

Figure 19

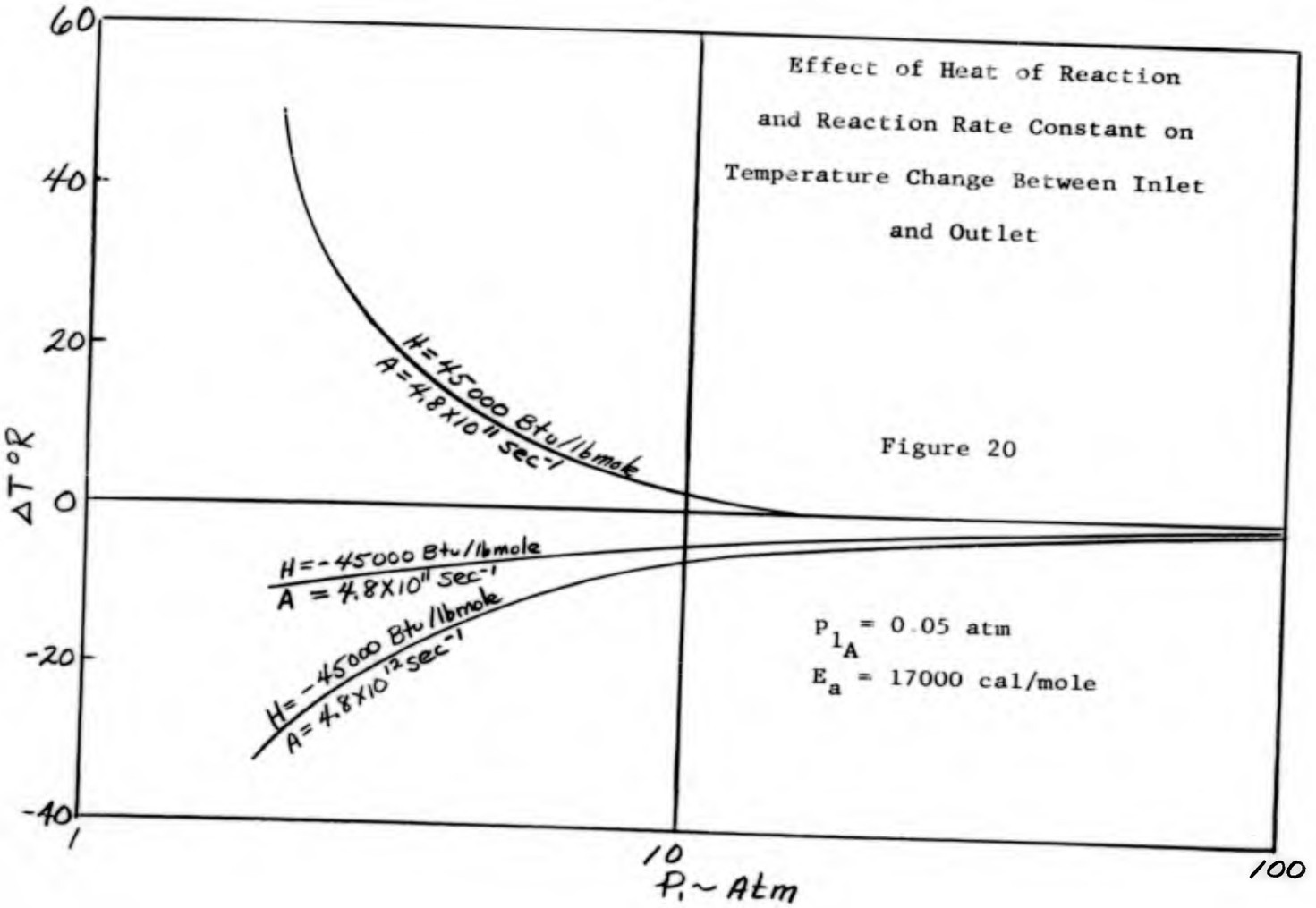
60
40
20
0
-20
-40
ΔT °R
H=45000 Btu/lbmole
A=4.8X10^11 sec^-1
H=-45000 Btu/lbmole
A=4.8X10^11 sec^-1
H=-45000 Btu/lbmole
A=4.8X10^12 sec^-1
Effect of Heat of Reaction
and Reaction Rate Constant on
Temperature Change Between Inlet
and Outlet
Figure 20
P1A = 0.05 atm
Ea = 17000 cal/mole
1
10
100
P1 ~ Atm

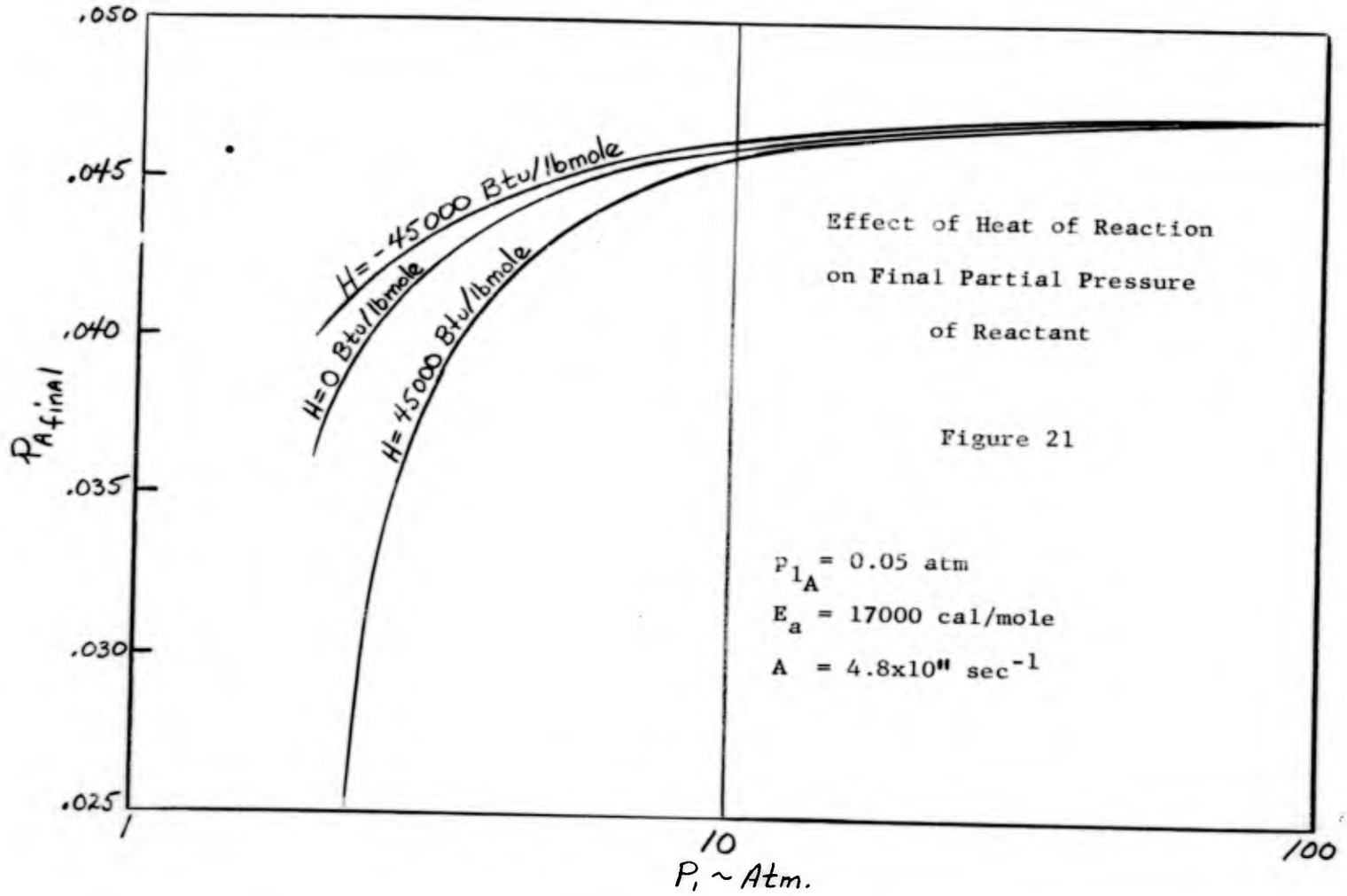

Effect of Heat of Reaction on Final Partial Pressure of Reactant

Figure 21

P_{1_A} = 0.05 atm

E_a = 17000 cal/mole

A = 4.8×10^{11} sec^{-1}

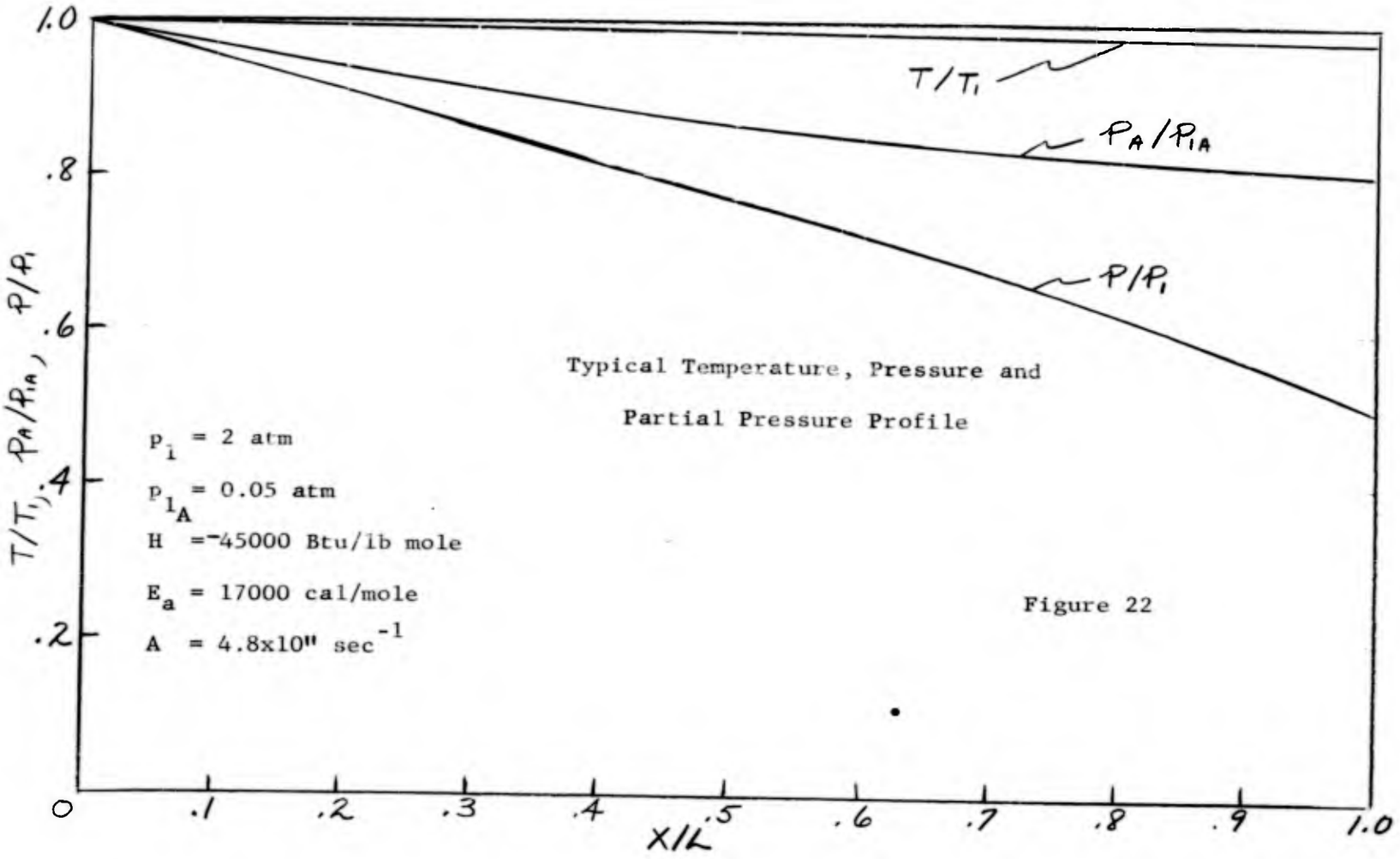

Typical Temperature, Pressure and

Partial Pressure Profile

Figure 22

this is the high initial pressures produce very fast flow rates and hence very short residence times causing very little temperature change. (See Figure 11.) For high initial pressures one might treat the temperature as a constant. The conservation of momentum equation (Equation (3.10)) can be put in the following form,

$$-\frac{dp^2}{dx} = 2(R/M)T\left[\alpha\mu G + (\beta/g_c)G^2\right] \tag{3.13}$$

Equation (3.13) can be integrated from point (1) to (2) over a length L assuming temperature is constant.

$$-\frac{(p_2^2 - p_1^2)}{L} = 2\frac{R}{M}T\alpha\mu G + 2\frac{R}{M}T\frac{\beta G^2}{g_c} \tag{3.14}$$

This is a quadratic in G and hence

$$G = \frac{-A \pm \sqrt{A^2 + 4B}}{2} \tag{3.15}$$

where

$$A = \frac{\alpha\mu g_c}{\beta} \tag{3.16}$$

$$B = \frac{(p_1^2 - p_2^2)g_c}{2\beta\frac{R}{M}TL} \tag{3.17}$$

For the present example if one works with initial pressures above 10 atmospheres then $B \gg A$

and $$G = B^{1/2} \tag{3.18}$$

or $$G = p_1\left[\frac{g_c}{2\beta\frac{R}{M}TL}\right]^{1/2} \tag{3.18a}$$

Equation (3.18) was used to calculate the mass flow for the following cases and compared with the IBM 650 data

P	(Atm)	1000	100	10
G	(Eq. 3.18) $\frac{\text{lbm}}{\text{ft}^2\ \text{sec}}$	24.96	2.496	0.2496
G	(IBM 650) $\frac{\text{lbm}}{\text{ft}^2\ \text{sec}}$	24.83	2.404	0.175

It might be noted that a mass flow of 24.96 $(\text{lbm})(\text{ft}^2\text{-sec})^{-1}$ corresponds to a local exit pore velocity of

$$u = \frac{G}{\epsilon \rho} = \frac{GRT}{\epsilon p M} = \frac{(24.96)(51.5)(530)}{(.3)(2116)} = 1090 \text{ ft/sec.}$$

This is almost equal to the speed of sound at $T = 530^{\circ}R$. Hence for the porous core in this example, $P_1 = 1000$ Atm represents the approximate upper limit beyond which Mach number effects have to be taken into account.

If X were substituted for L in Equation (3.14) then for isothermal flow the pressure squared profile through a porous core would be a straight line. This is borne out by Figures 12 through 15 where it is seen that profiles which approach a straight line are nearly isothermal. (Check Figures 8 through 11.)

Figure 8 indicates that the flow is exactly isothermal for a zero heat or reaction. This is evident when one combines Equation (3.3), (3.11) and (3.12).

$$\rho C_p u \frac{dT}{dx} = \cancel{k} \overset{0}{\cancel{H}} C_A + u \frac{dp}{dx} - u\left[\frac{dp}{dx} + \rho u \overset{\approx 0}{\cancel{\frac{du}{dx}}}\right] = 0 \qquad (3.19)$$

This is the usual assumption one makes in the "throttling" or "porous plug" process. However, from Equation (3.19) it is evident that the reason the flow is isothermal in the "porous plug" experiment is because the temperature increase due to viscous dissipation just balances out the temperature drop due to expansion of the gas. This analysis of course presupposes an ideal gas with zero Joule-Thompson effect.

Figure 16 shows the only run where essentially all of the reactant was used up. This occurred at an initial pressure of 2 AtM with a heat of reaction of 4500 Btu/lbMole.

Figure 21 shows a rather odd limiting effect of high initial total pressures on final partial pressure of reactant. There seems to be an upper bound above which the partial pressure will never exceed. This limiting partial pressure can be shown to be an explicit function of the properties of the porous media, temperature and reaction rate constant k.

Since it has been shown that at very high initial pressures the flow is essentially isothermal, then assume the temperature and reaction rate k are constant. Using the perfect gas law

$$p_A = C_A R T \tag{3.20}$$

and multiplying Equation (e.8) by density and carrying out the indicated differentiation

$$\frac{dp_A}{dx} = \frac{p_A}{T}\overbrace{\frac{dT}{dx}}^{=0} - \frac{k p_A \rho}{\frac{R}{M} T G} \tag{3.21}$$

Dividing by P_A and integrating

$$\ln \frac{p_{A_2}}{p_{A_1}} = \frac{-k}{\frac{R}{M}TG} \int_0^L p\, dx \tag{3.22}$$

However $p = [p^2]^{1/2}$ and p^2 varies linearly at high flow rates

$$p^2 = p_1^2 - x/L\,(p_1^2 - p_2^2) \tag{3.23}$$

Therefore

$$\int_0^L p\, dx = (2/3\, L) \frac{p_1^3 - p_2^3}{p_1^2 - p_2^2} \tag{3.24}$$

But $p_1 >> p_2$

Therefore

$$\int_0^L p\, dx = 2/3\, L\, p_1 \tag{3.25}$$

Now substitute Equation (3.18a) and (3.25) into Equation (3.22) and take the antilog of the equation.

$$p_{A_2} = p_{A_1} \exp\left\{-\frac{2}{3} k L \left[\frac{2\beta L}{\frac{R}{M} g_c T}\right]^{1/2}\right\} \tag{3.26}$$

As a check Equation (3.26) was compared with IBM 650 data

P_{A_1}	Atm	0.05	0.01
P_{A_1}	(Eq. (3.26))	0.04733	0.009467
P_{A_1}	(IBM 650)	0.0473	0.0094665

Conclusions

Any variables which tends to increase the gas temperature as it flows through the porous media, tends to decrease the mass flow and vice-versa. For inlet to exit pressure ratios greater than ten, the mass flow was nearly independent of reaction effects and was proportional to the inlet pressure. For this same region the flow was nearly isothermal and the square of the pressure varies linearly with distance.

CHAPTER IV

STEADY FLOW EXPERIMENTS

In order to verify some of the conclusions of the capillary-orifice model and because values of and were needed for the unsteady flow analysis, measurements were made on steady flow of nitrogen gas through two different porous cores. The experimental equipment and procedures are almost exactly that of Weger and Greenberg (12), and hence only a brief description of them will be given here.

Experimental Apparatus

The experimental apparatus consisted primarily of a hydraulic system, a gas reservoir and controlling and measuring devices. Figure 23 is a flow diagram of the equipment.

The hydraulic system was designed to maintain a constant source of high pressure gas. For very high pressures (and hence high flow rates) a dual feed Hills-McCanna type K2M-2F positive displacement pump regulates the hydraulic fluid output. This pump has a continuously varying stroke which can regulate the hydraulic fluid output up to a maximum of 4.9 gallons per hour for each feed, at 25000 p.s.i. The hydraulic system can function continuously supplying oil to the gas reservoir at a rate slightly above the gas withdrawal rate. The excess oil was bypassed back to the storage tank, thereby insuring positive control with damped pressure surges.

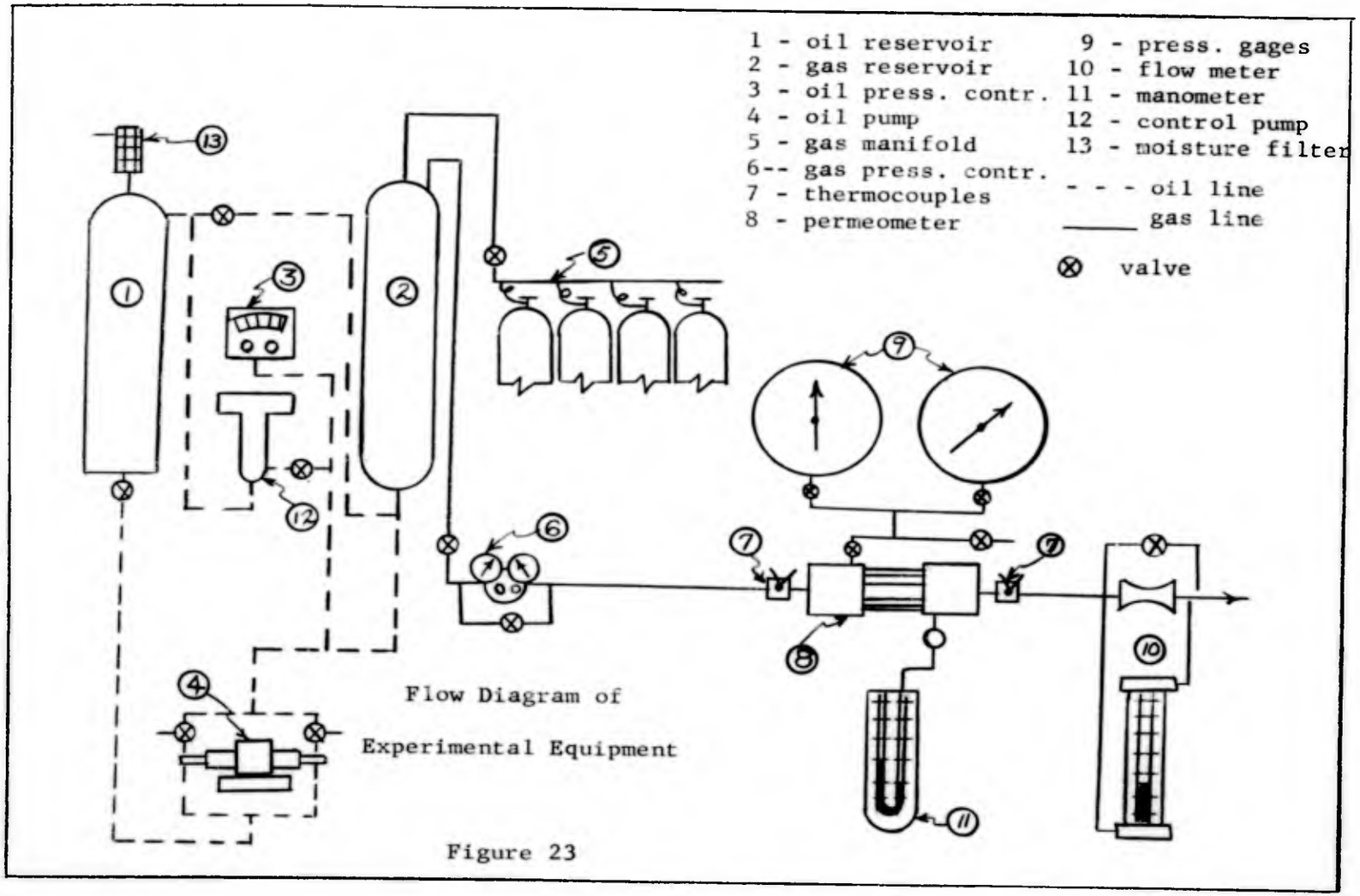

Flow Diagram of

Experimental Equipment

Figure 23

The excess hydraulic fluid was metered back to the oil storage tank by an Aminco (American Instrument Company) solenoid pneumatic piston type control value. The solenoid was controlled by a Bristol pressure-sensitive electric contact gauge.

The high pressure gas reservoir was a 38 gallon seamless steel tank with dished heads fabricated for 2500 p.s.i. working pressure in accordance with the ASME unfired boiler code standards, by the Maryland Tank Company. The tank was set in a concrete base and had a bottom connection for hydraulic oil and three top connections: a gas inlet, gas outlet, and a safety pop value set for 2500 p.s.i.

The gas flow system was controlled by a "Gas-O-Dome" gas-loaded diaphragm value manufactured by the Victor Company. This instrument consisted of a variable orifice operated by a diaphragm sensitive to the pressure differential between the upstream and downstream gas. The orifice metered gas at such a rate as to maintain a constant predetermined downstream pressure up to 1000 p.s.i. For downstream pressures above 1000 p.s.i. the "Gas-O-Dome" value could be by-passed and the pressure can be controlled by the Bristol pressure-sensitive electric contact gauge.

The porous sample imbedded in a steel sleeve is held in a holder called a permeometer. A high pressure seal was obtained by using teflon tape on the ¼ inch bearing surfaces and drawing the opposite faces of the permeometer together against the ends of the sample with four 5/8 inch bronze marine bolts.

A Heise Bourdon Tube pressure gauge measured the upstream pressure. This gauge had a 16 inch diameter face calibrated in 1 p.s.i. intervals between 0 and 1000 p.s.i. The downstream pressure was measured by a Merriam Gauge Mercury Manometer.

A "Vol-O-Flow" dual element orifice meter manufactured by the National Instrument Company was used to measure the volume rate of gas flow. The range of the instrument is from 0-100 cubic feet per hour. Accuracy obtained with this meter was better than 0.5% of the full scale reading.

A Leeds and Northrup potentiometer was used to obtain the temperature from two iron-constantin thermocouples placed three inches upstream and downstream from the ends of the porous sample. The accuracy of this system was slightly better than three degree Fahrenheit.

The high pressure equipment was housed behind a safety barricade consisting of quarter-inch steel plate with a three inch wood backing. The barricade also served as a control panel, with all values, measuring instruments, and controls mounted in the shield. The high pressure lines consisted of nominal ¼ inch stainless steel tubing and fittings manufactured by Autoclave Engineers Inc. The high pressure gas reservoir was fed from a four cylinder gas manifold. Humble Oil and Refining Company type Terrestic 43 hydraulic oil was used as the pumping medium. Oil pump bottled nitrogen gas was used as the working gas.

Porous Media

Two porous sintered metal cores imbedded in steel sleeves (see Figure 24) were selected for this investigation. The porous cores were obtained from Pitman-Dunn Laboratories of Frankfort Arsenal. The powders used consisted of spherical tincoated copper particles. The particle size range of the powder was -250+325 U.S. Mesh for one core and -100+150 for the other.

TABLE 1

PHYSICAL PROPERTIES OF POROUS CORES

Core	Particle Size Range (Microus)	Mean Pore Diameter (Microus)	Porosity (22°C)	
			From Density Measurements	From Pore Size Measurements
FC-100+150	74-104	26.6	0.486	0.424
FC-250+325	43-61	15.5	0.467	0.356

The cores were fabricated by sintering the powders in steel sleeves. The sleeves (1½" o.d. X 3/4" 1.d. X 6" long) were tapped at four positions along their wall prior to sintering process to provide positions for pressure transducers to be installed later. The ends of the sleeves were threaded and fitted with O-Ring grooves to facilitate fitting them into the permeometer assembly.

The pressure gauge taps were closed prior to sintering by means of inserted bolts. After closing off one end with a carbon disk the sleeves were filled with the graded powder and hand

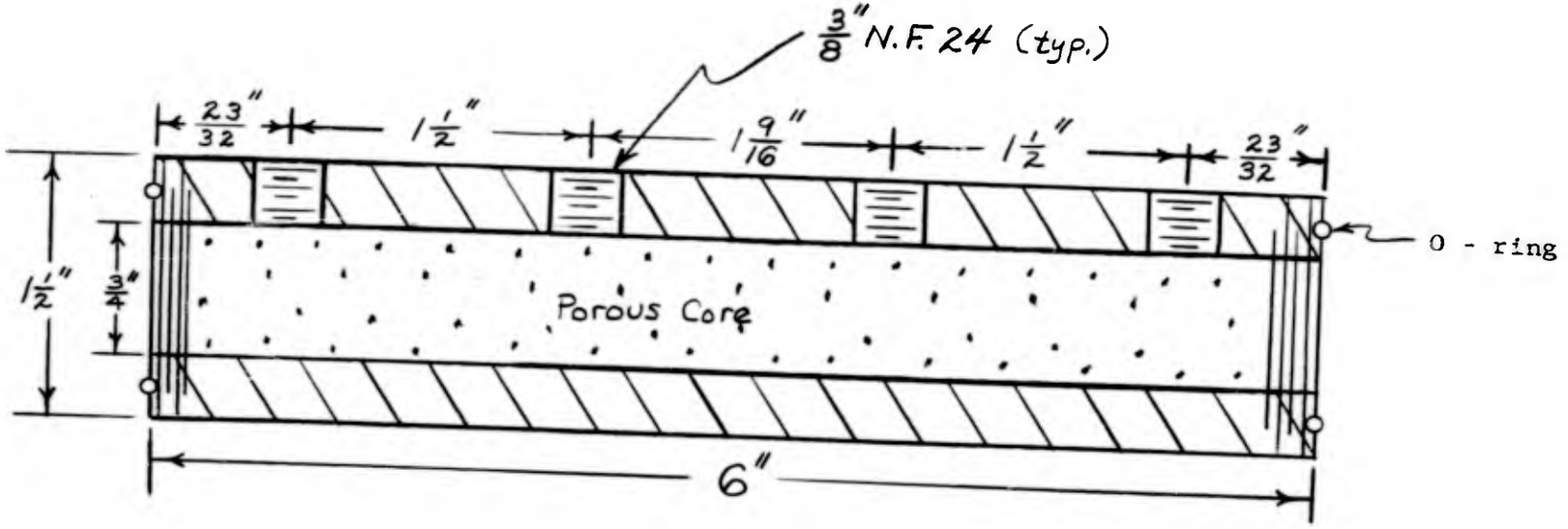

Figure 24 Porous Core Assembly

tamped with minimum of vibration to insure close packing without longitudinal classification of the particles. The samples were sintered for one hour in a dissociated ammonia atmosphere at ^{o}1650F in a vertical position.

The physical properties given in Table I were taken from Weger and Greenberg (13).

Experimental Procedure

The planned procedure was that prior to each series of runs the high pressure reservoir would be drained of oil and charged with gas, directly from commercial cylinders, to a pressure of about 1300 p.s.i. The pump would then be turned on, Bristol Controller set to the desired pressure and the run would proceed. It was discovered on both porous cores, however, that pressures above 1300 p.s.i. produced flow rates above the operating limits of the "Vol-O-Flow" flowmeter. Hence it was then necessary to by-pass the hydraulic control system and use only the "Gas-O-Dome" diaphragm value (which can regulate pressures from 0-1000 p.s.i.) to control the gas flowing from the gas manifold through high pressure tank to the permeometer.

The "Gas-O-Dome" diaphragm value was then used on all runs to set the pressure upstream of the porous core. Appropriate pressure, temperature, and flow rate measurements were recorded for each run. Runs were usually started out at low pressures and then the pressure was increased by increments until a maximum flow reading

was obtained on the flowmeter. After the maximum point was reached several runs were made at lower flow rates.

Experimental Results

The experimental results obtained for the two porous samples investigated are presented in Figures 3, 25, and 26. In Figure 3 the experimental data is compared with the "capillary-orifice" theory along with other experimental data. The experimental data compares well with the theory line as it falls slightly below the line.

The resistance coefficients for each core can be determined according to a scheme suggested by Cornell and Katz (21).

If Equations (2.9) and (2.10) were substituted into Equation (2.13) there will result,

$$\frac{M}{2ZRT}\frac{d(p^2)}{dx} = \alpha\mu G + \beta G^2 \tag{4.1}$$

For isothermal steady flow this may be integrated to give

$$\frac{(p_1^2 - p_2^2)M}{2LZRT\mu G} = \alpha + \beta \frac{G}{\mu} \tag{4.2}$$

As seen from Equation (2.9) and (2.10) α and β depend upon the skin friction and drag coefficient respectively and hence may vary with the Reynolds Number. However, over a small range of Reynolds Number they may perhaps not vary too widely and it might be possible to treat α and β as constants in Equations (4.2). With this assumption Equation (4.2) represents a linear relationship between $\frac{p_1^2 - p_2^2}{G}$ and $\frac{G}{\mu}$ whose intercept gives α and whose

slope yields β.

The data for each core sample have been plotted according to Equation (4.2) and are presented as "Cornell and Katz Plots" in Figures 25 and 26. The experimental data for α and β obtained from the Cornell and Katz Plots are compared with the "capillary-orifice" theory (Equations (2.9) and (2.10) in Table II.

TABLE 2

EXPERIMENTAL AND THEORETICAL VALUES OF α AND β

Core	$\alpha_{Exp.}$	$\alpha_{Th.}$	$\beta_{Exp.}$	$\beta_{Th.}$
FC-100+150	$5.7X10^9$	$9.5X10^9$	$6.33X10^4$	$12.8X10^4$
FC-250+325	$32.5X10^9$	$33.6X10^9$	$1.76X10^5$	$2.32X10^5$

Conclusions

As seen from Table 2 and from Figure 3 the "Capillary-Orifice" theory shows surprisingly good agreement with experimental data when the complexity of the flow situation in a porous medium is considered.

From the temperature data in Appendix C it is seen that the flow was isothermal through the porous core. This was predicted by the heat transfer analysis in Chapter IV. However, an unnoticed temperature change up to three degrees could have occurred due to the inaccuracies of the system.

It is possible that further refinements of the "Capillary-Orifice Model" can come from, (1) using pore size distributions

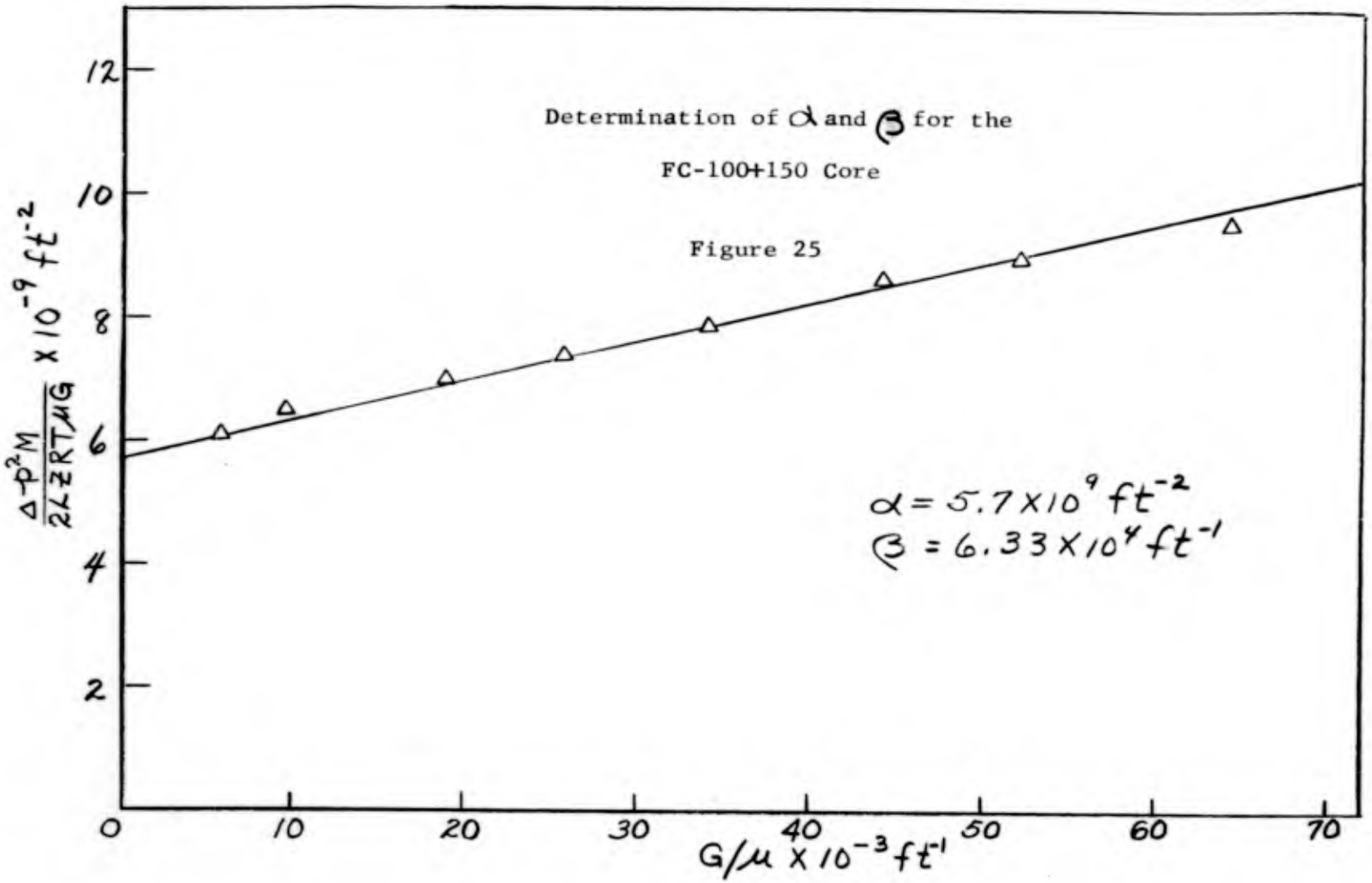
Determination of α and β for the
FC-100+150 Core
Figure 25
$\frac{\Delta p^2 M}{2LzRT\mu G} \times 10^{-9}\ ft^{-2}$
$G/\mu \times 10^{-3}\ ft^{-1}$
$\alpha = 5.7 \times 10^{9}\ ft^{-2}$
$\beta = 6.33 \times 10^{4}\ ft^{-1}$
0
10
20
30
40
50
60
70
2
4
6
8
10
12

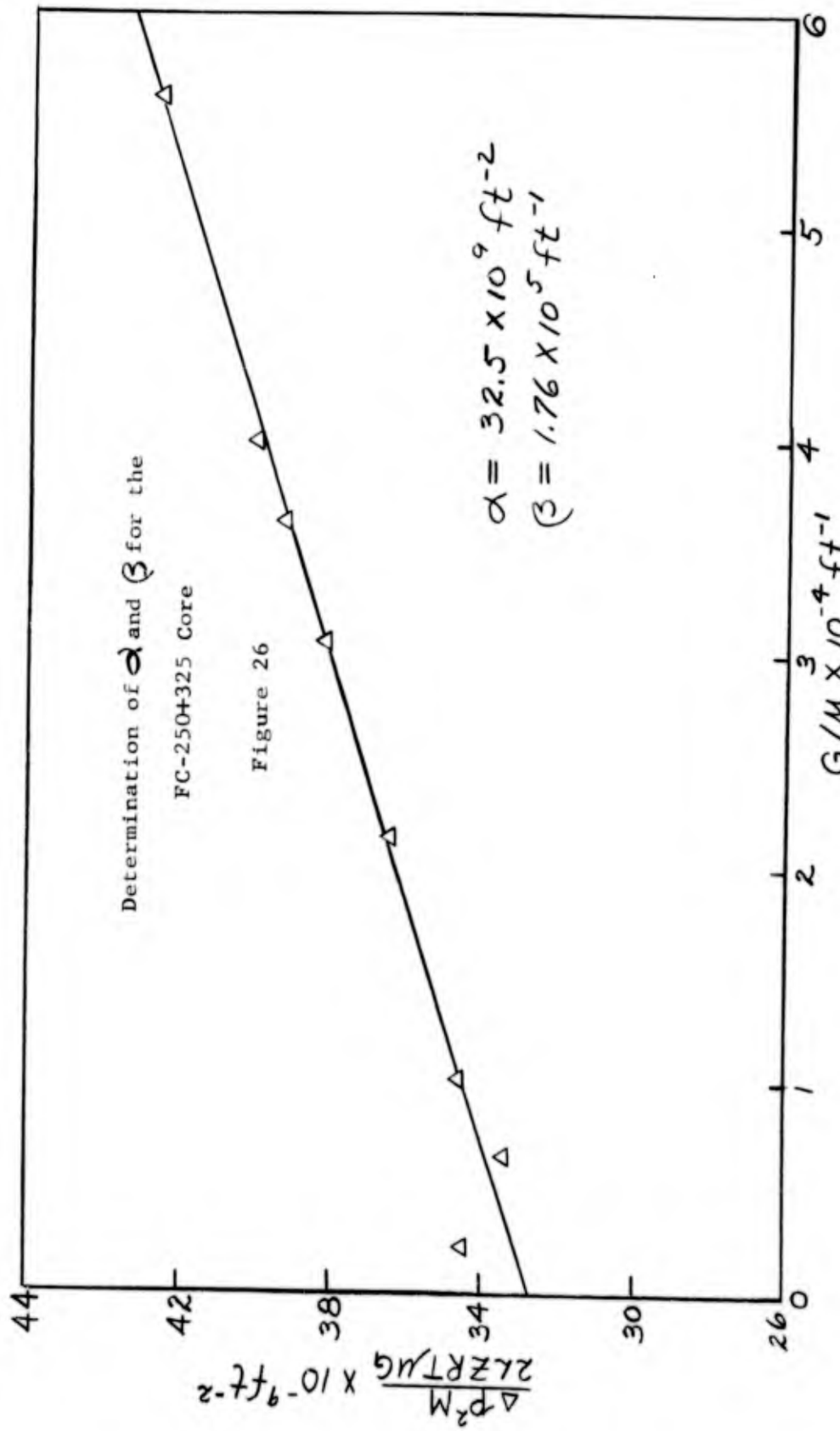

Determination of α and β for the FC-2504325 Core

Figure 26

in place of mean pore diameters (2) using a more realistic skin friction coefficient than one developed for fully developed laminar pipe flow, (3) using a drag coefficient more compatible with the "Capillary-Orifice Model."

CHAPTER V

UNSTEADY FLOW EXPERIMENTS

One of the primary goals of this work was to correlate, insofar as possible, experimental information on the behavior of gas pressure waves in consolidated porous media with results obtained on the solution of equations which represent a mathematical model of the porous medium.

Experimental Apparatus

The experimental apparatus consisted primarily of a diaphragm rupturing system, a gas reservoir and a pressure-time measuring system. Figure 27 is a flow diagram of the equipment.

The gas reservoirs consisted of two 0.915 gallon commercial steel gas bottles. The diaphragm rupturing mechanism consisted of two separate brass tubes around which many turns of wire have been wrapped to serve as a coil (see Figure 28). A steel slotted spike is placed in the far end of the tube. When the coil is connected to a 220 V.A.C. supply the steel spike is drawn into the coil, overshoots and breaks a brass diaphragm. The brass diaphragms were 1.4 inches in diameter and their thickness varied from 12 to 24 thousands of an inch. The thicker diaphragms were used on high pressure runs in order to maintain some margin of safety.

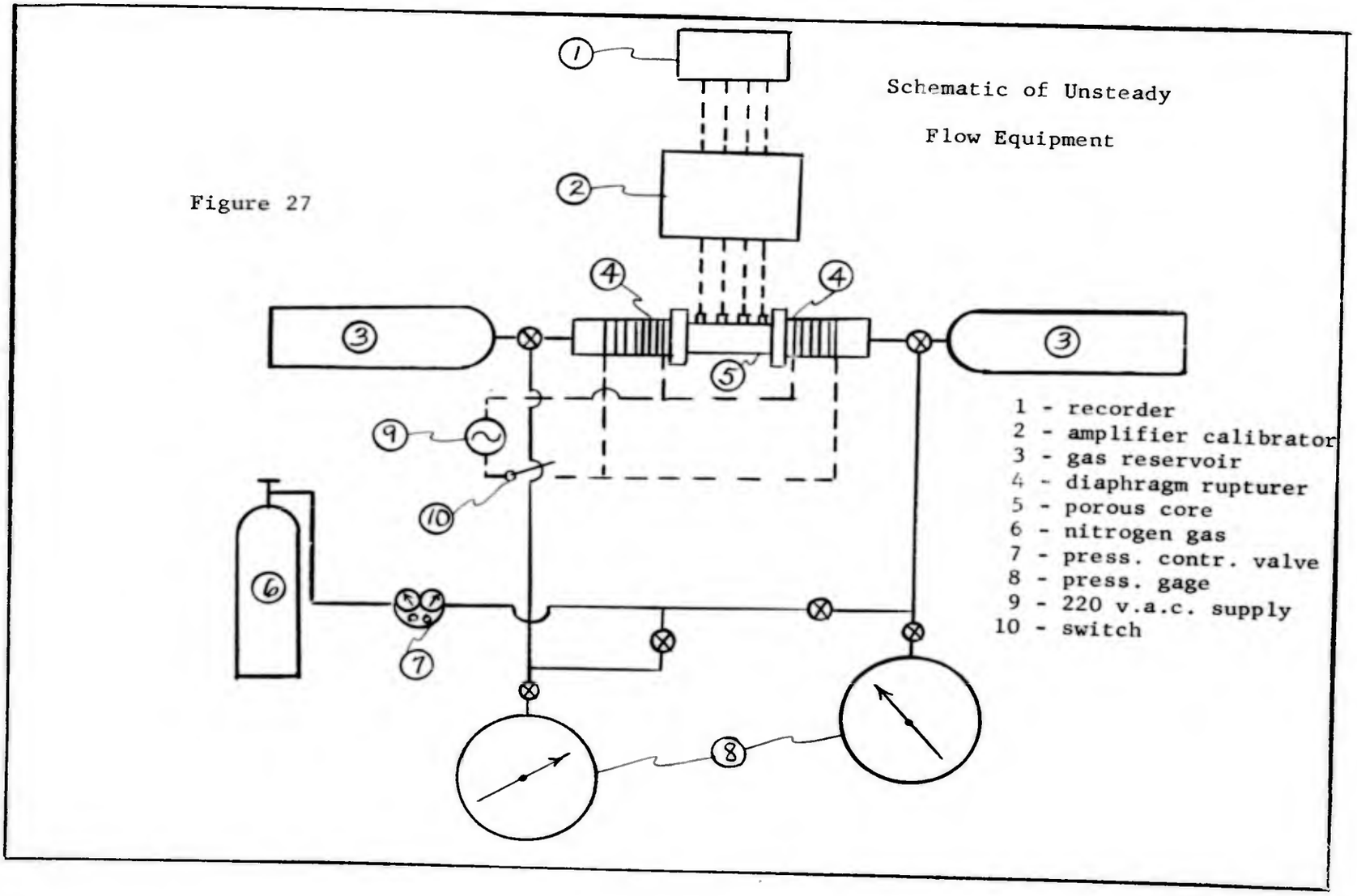
Schematic of Unsteady
Flow Equipment
1 - recorder
2 - amplifier calibrator
3 - gas reservoir
4 - diaphragm rupturer
5 - porous core
6 - nitrogen gas
7 - press. contr. valve
8 - press. gage
9 - 220 v.a.c. supply
10 - switch

Figure 27

Pressure Wave Interaction Diaphragm

Rupturing Mechanism

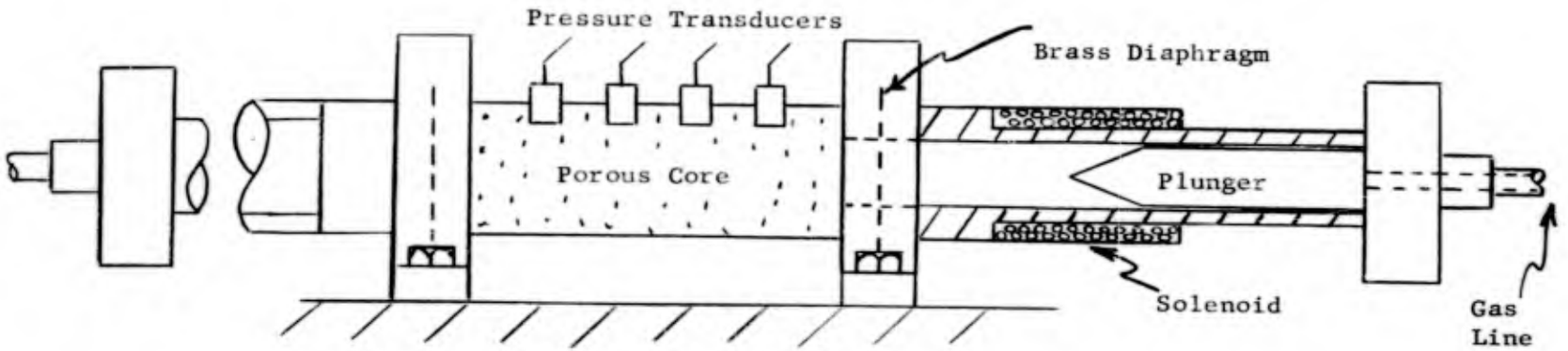

Not to Scale

Figure 28

In the steel housing surrounding the porous core were four SLM PZ-6S miniature pressure pickups manufactured by Kistler Instrument Company of N. Tonawanda N.Y. The signals from the transducers were fed to two PT-6 rack mounted two-channel amplifier-calibrators. The signals from the amplifiers were fed into a Honeywell Model 906C Visicorder oscillograph. This oscillograph is of the light beam photographic type which could write at speeds over 10,000 inches per second and its paper feed could be varied from 0.4 to 50 inches per second. A time line system is employed to provide accurately spaced lines across the width of the paper. Intervals of 0.01, 0.1 and 1.0 seconds can be selected. The records require only about 30 seconds of exposure to ordinary light before the traces were visible.

Before and after the experimental runs were made the pressure transducers were calibrated. This was done by charging the porous core with series of known pressures (read on the Heise pressure gage) and recording the response of each transducer on the oscillograph.

The porous core used in these runs was the FC-100+150 core. Experimental values of α and β are reported for this core in Chapter IV.

Experimental Procedure

The planned procedure was that prior to each run the diaphragm rupturers would be removed and two brass disks (one at each end of the porous core) would be inserted. The steel spikes would be set in the far end of the brass tube and the diaphragm rupturers would be set

back into the system. Each gas reservoir would then be charged to specified pressure. This pressure would exist right up to each diaphragm. Each coil would then be triggered simultaneously by 220 V.A.C. current. This would then accelerate the steel spikes into the diaphragms, bursting then and causing near step functions of pressure to be introduced simultaneously into opposite ends of the porous core.

Just prior to the triggering, the oscillograph would be set in motion (feeding 50 inches per second). This provided a clear and easily readable pressure time history of each transducer. It took approximately 20 minutes to set up each run.

Early in the test program a pressure transducer and its associated galvonometer (in the Visicorder) became inoperative. Neither time nor money permitted their replacement hence the bulk of the experimental runs were made with only three transducers.

Experimental Results

The experimental results obtained for the FC-100+150 core are presented in Figures 29 through 39. Runs 1, 5, 6, and 7 are not presented because they were aborted for various technical reasons.

Figure 29 is of interest in that it shows the pressure pulse on one end was triggered approximately 0.01 seconds later than the other pressure pulse on the opposite end of the core. This was due to a mismatching in the impedance of the two diaphragm rupturing coils. This was corrected after this run and the resulting time

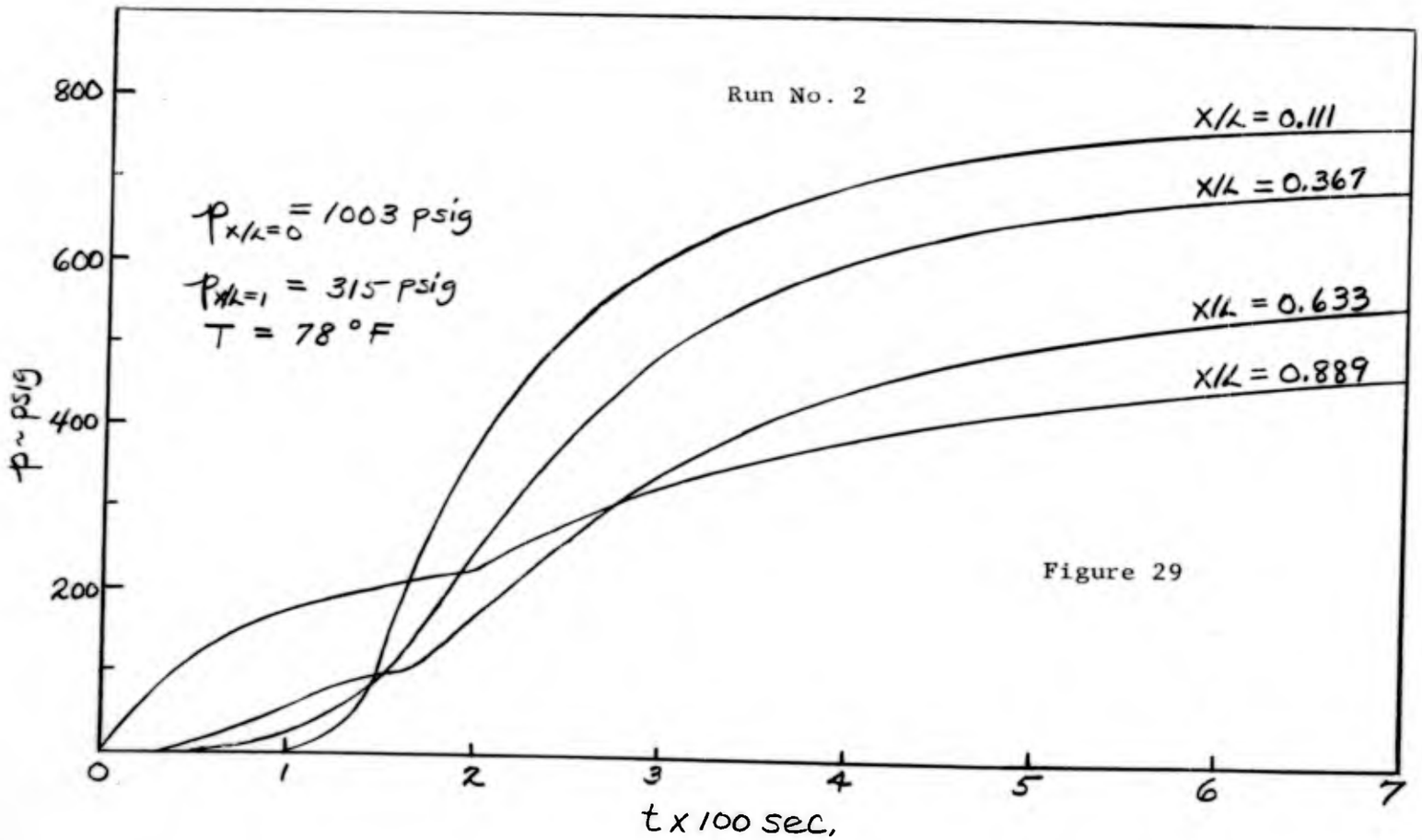
Run No. 2
$P_{x/L=0}$ = 1003 psig
$P_{x/L=1}$ = 315 psig
T = 78 °F
X/L = 0.111
X/L = 0.367
X/L = 0.633
X/L = 0.889
p ~ psig
800
600
400
200
0
1
2
3
4
5
6
7
t x 100 sec.

Figure 29

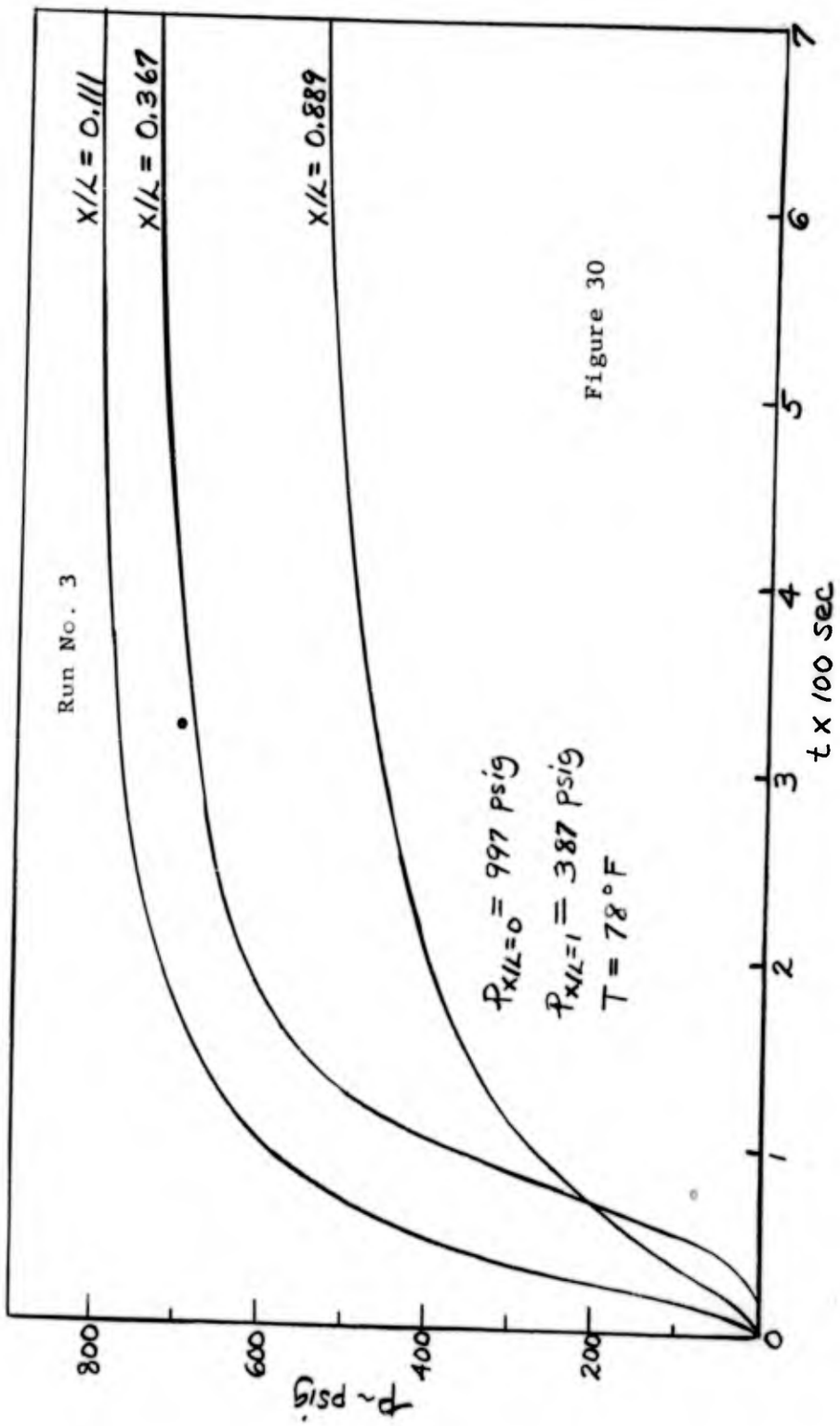
Run No. 3
X/L = 0.111
X/L = 0.367
X/L = 0.889
$P_{X/L=0}$ = 997 psig
$P_{X/L=1}$ = 387 psig
T = 78°F
P ~ psig
800
600
400
200
0
1
2
3
4
5
6
7
t x 100 sec

Figure 30

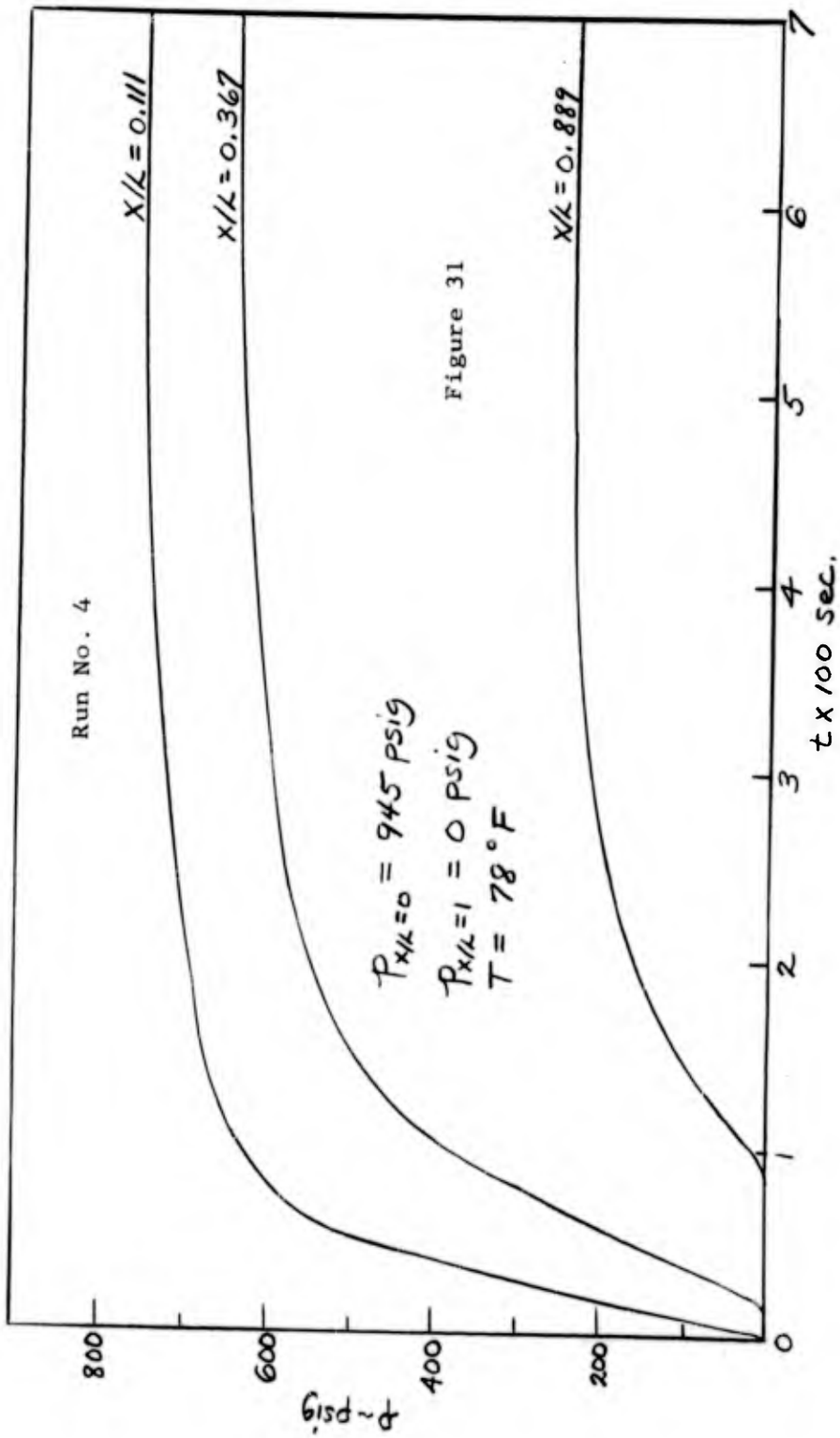
Run No. 4
X/L = 0.111
X/L = 0.367
X/L = 0.889
$P_{X/L=0}$ = 945 psig
$P_{X/L=1}$ = 0 psig
T = 78 °F
p ~ psig
800
600
400
200
0
1
2
3
4
5
6
7
t x 100 sec.

Figure 31

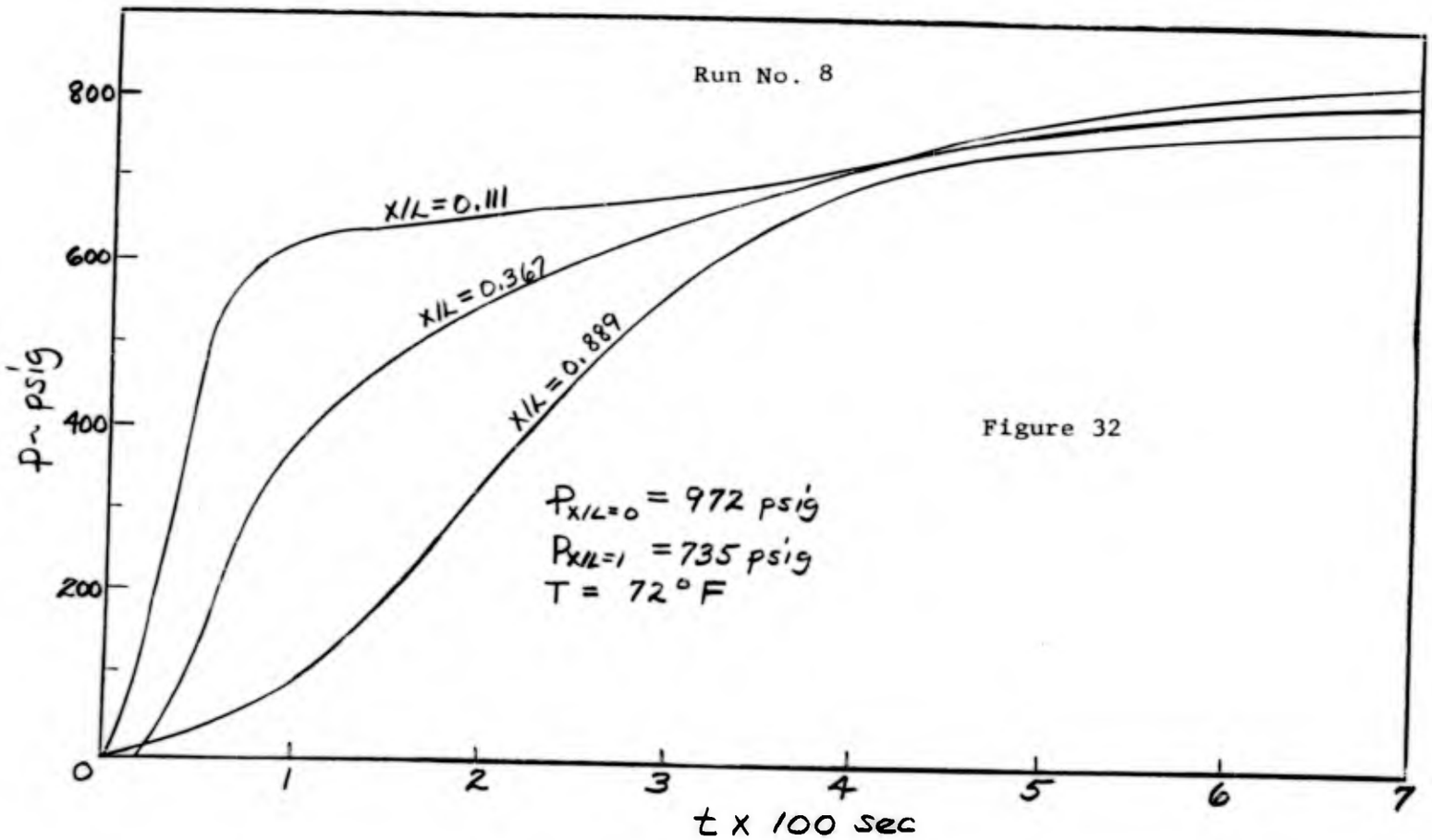
Run No. 8
800
600
400
200
0
p~ psig
x/L = 0.111
x/L = 0.367
x/L = 0.889
$P_{x/L=0}$ = 972 psig
$P_{x/L=1}$ = 735 psig
T = 72° F
1
2
3
4
5
6
7
t x 100 sec

Figure 32

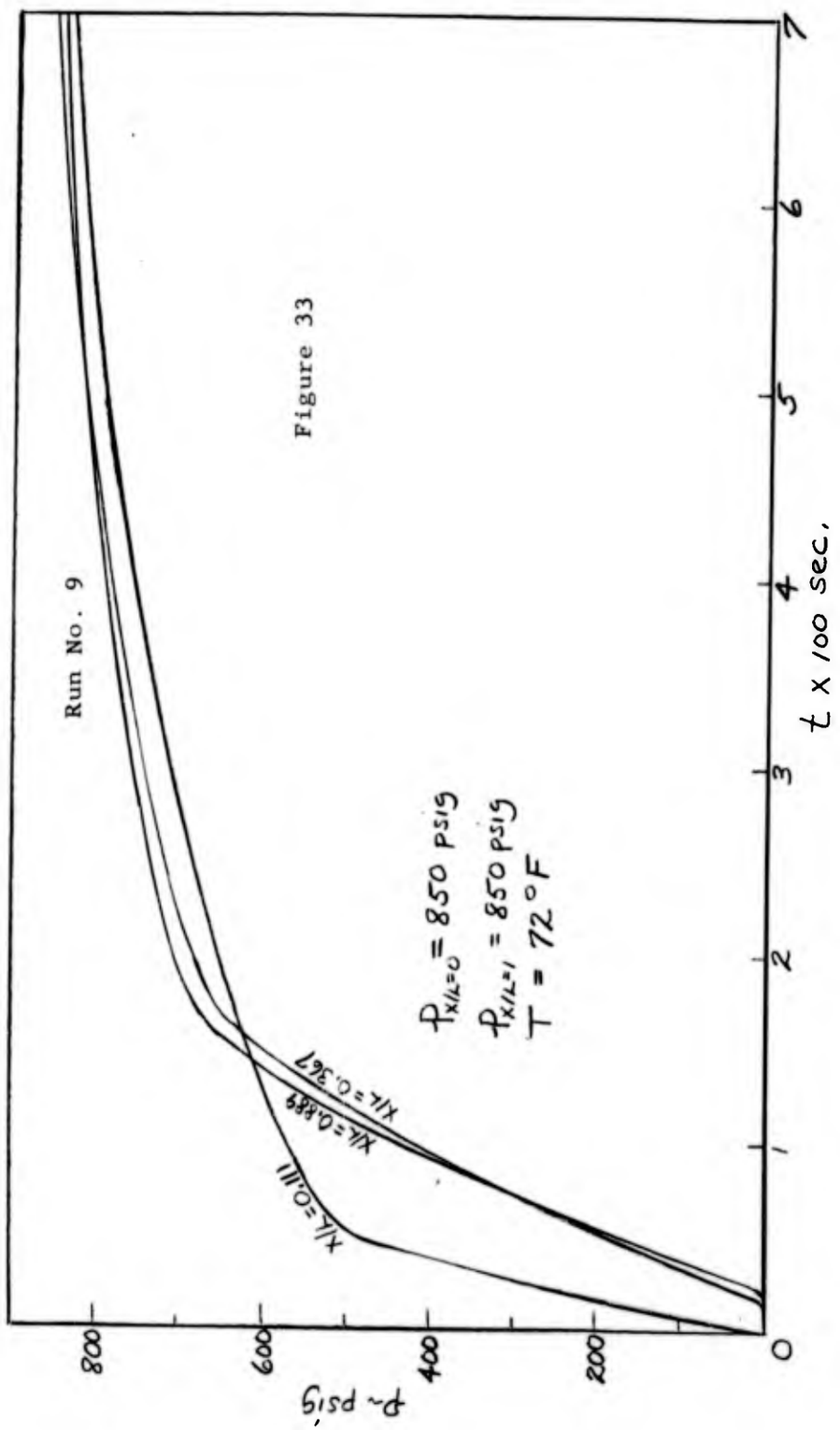
Run No. 9
$P_{x/L=0}$ = 850 psig
$P_{x/L=1}$ = 850 psig
T = 72°F
x/L = 0.111
x/L = 0.889
x/L = 0.367
P~ psig
800
600
400
200
0
1
2
3
4
5
6
7
t x 100 sec.

Figure 33

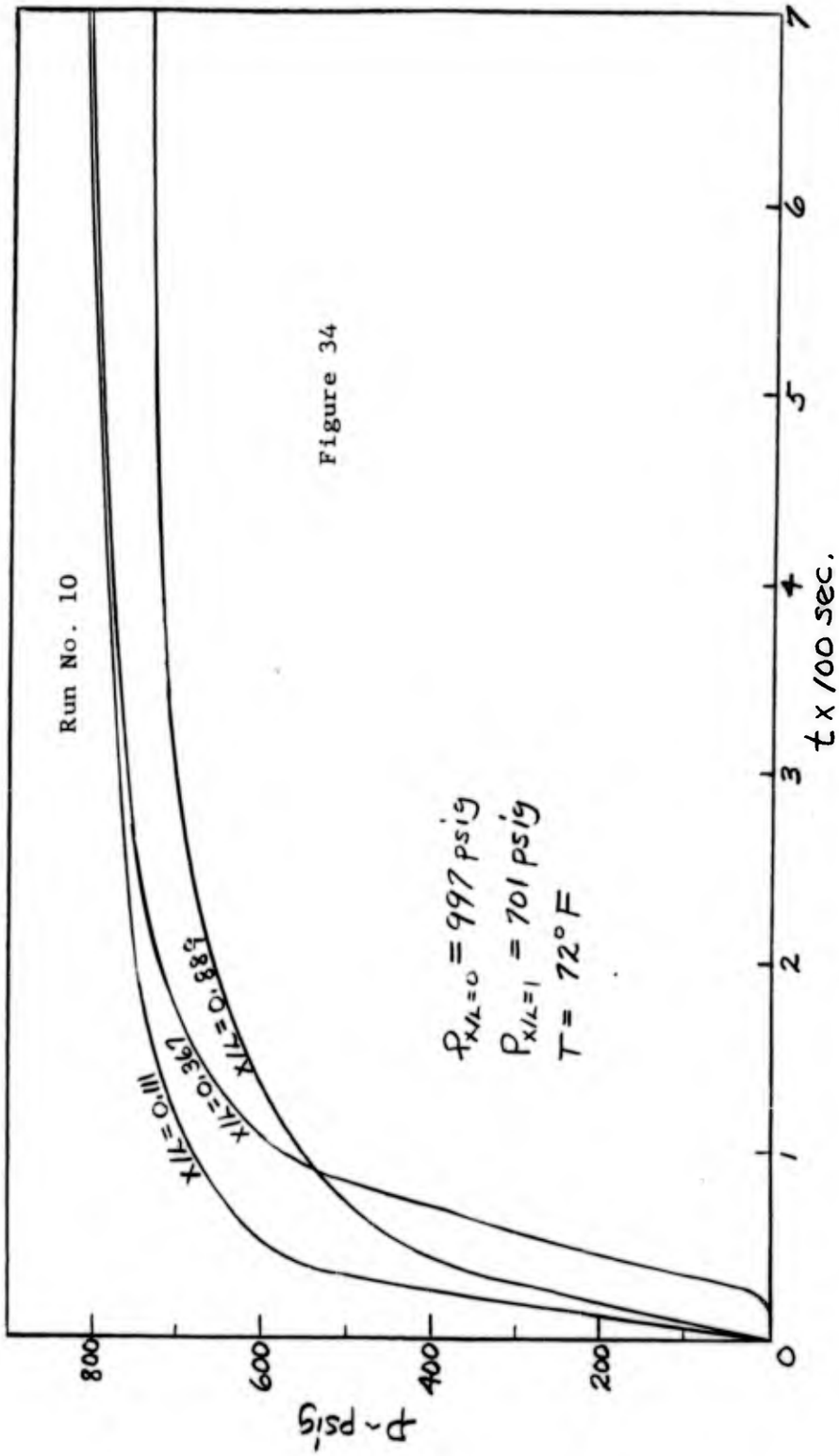
Run No. 10
$x/L=0.111$
$x/L=0.367$
$x/L=0.889$
$P_{x/L=0} = 997$ psig
$P_{x/L=1} = 701$ psig
$T = 72°F$
P - psig
800
600
400
200
0
1
2
3
4
5
6
7
t x 100 sec.

Figure 34

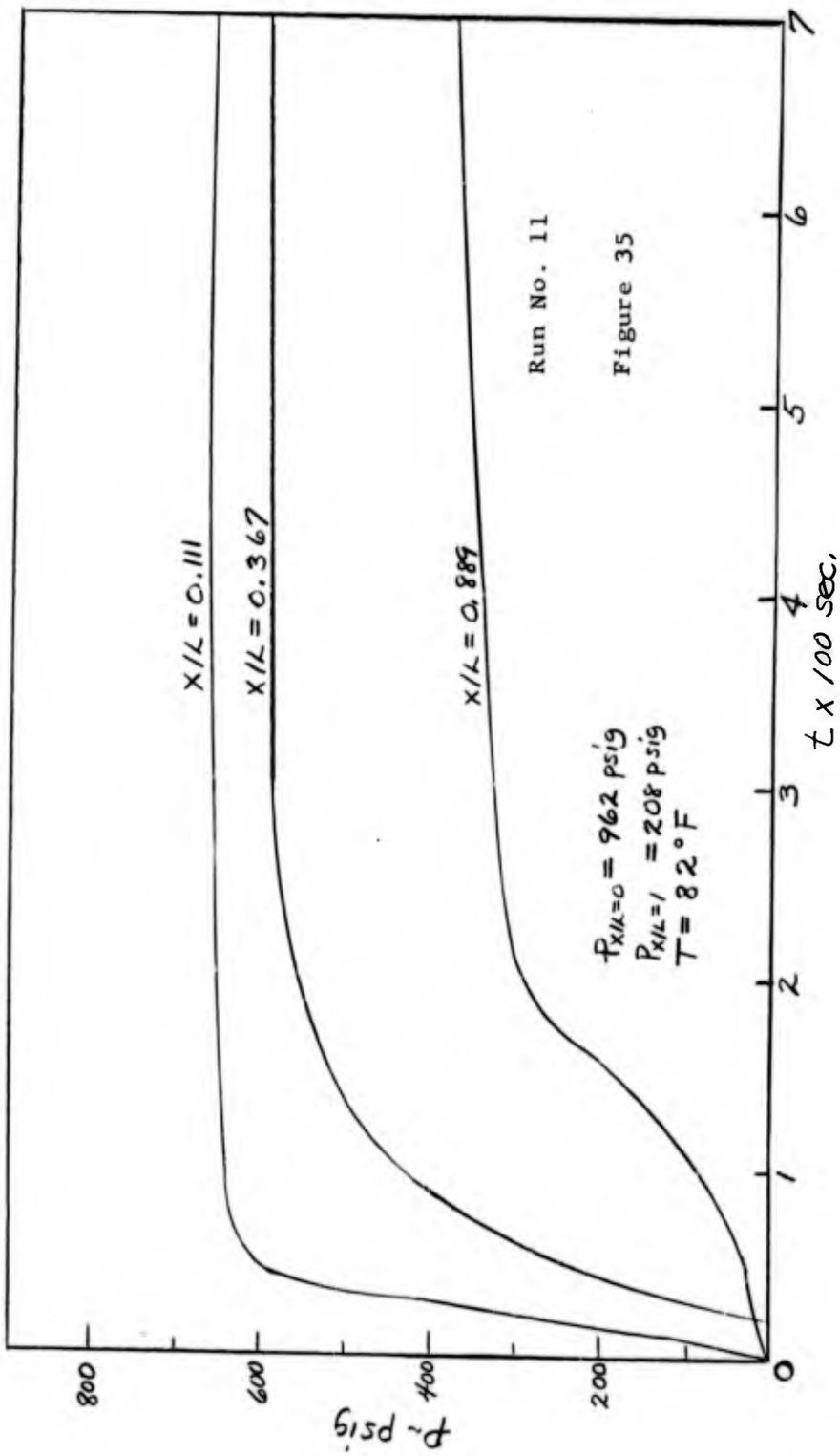
X/L = 0.111
X/L = 0.367
X/L = 0.889
$P_{X/L=0}$ = 962 psig
$P_{X/L=1}$ = 208 psig
T = 82°F
Run No. 11
Figure 35
P, psig
t x 100 sec.
800
600
400
200
0
1
2
3
4
5
6
7

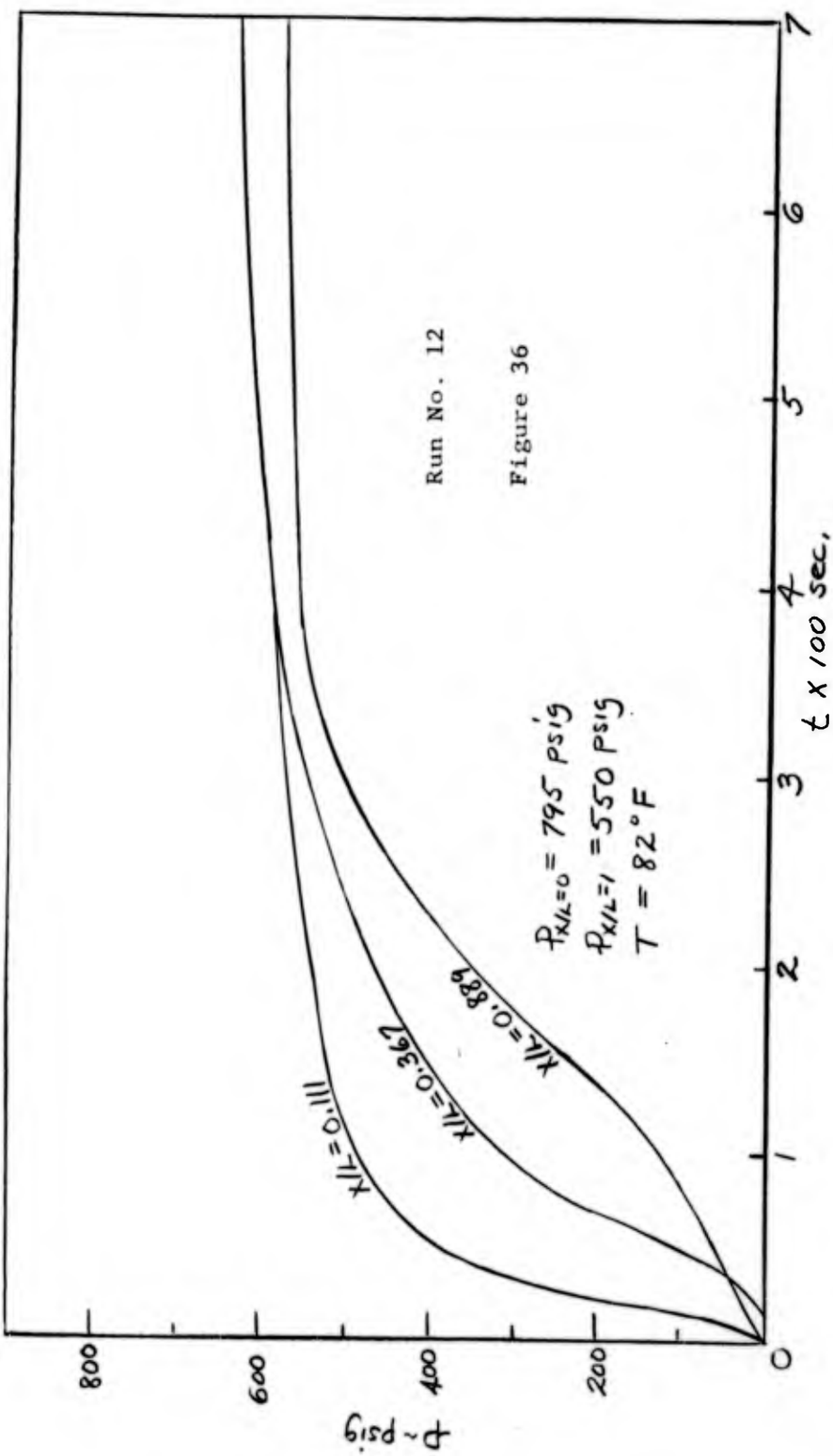
Run No. 12
Figure 36
$P_{X/L=0}$ = 795 psig
$P_{X/L=1}$ = 550 psig
T = 82°F
$x/L = 0.111$
$x/L = 0.367$
$x/L = 0.889$
P ~ psig
800
600
400
200
0
1
2
3
4
5
6
7
t x 100 sec.

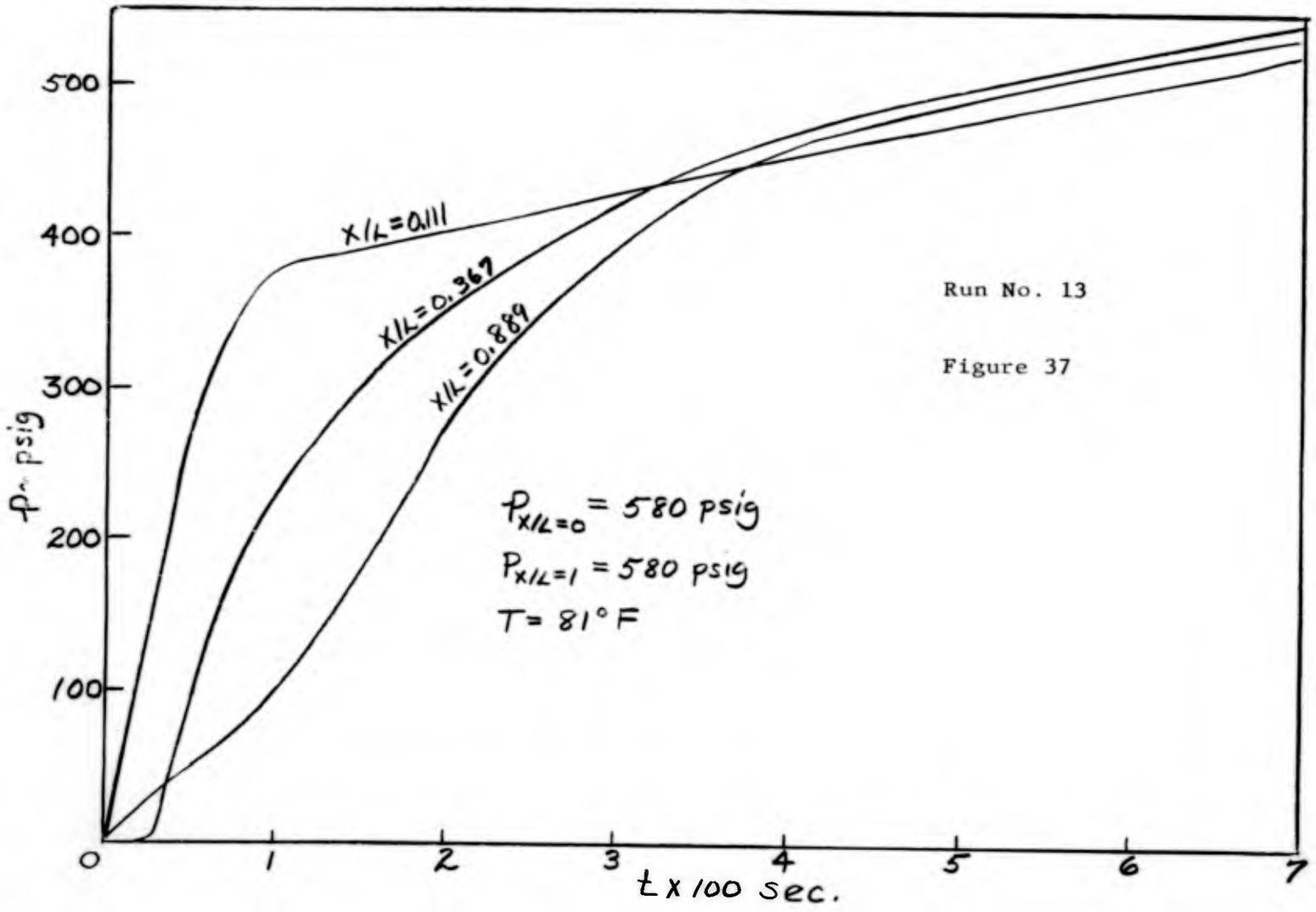

Run No. 13

Figure 37

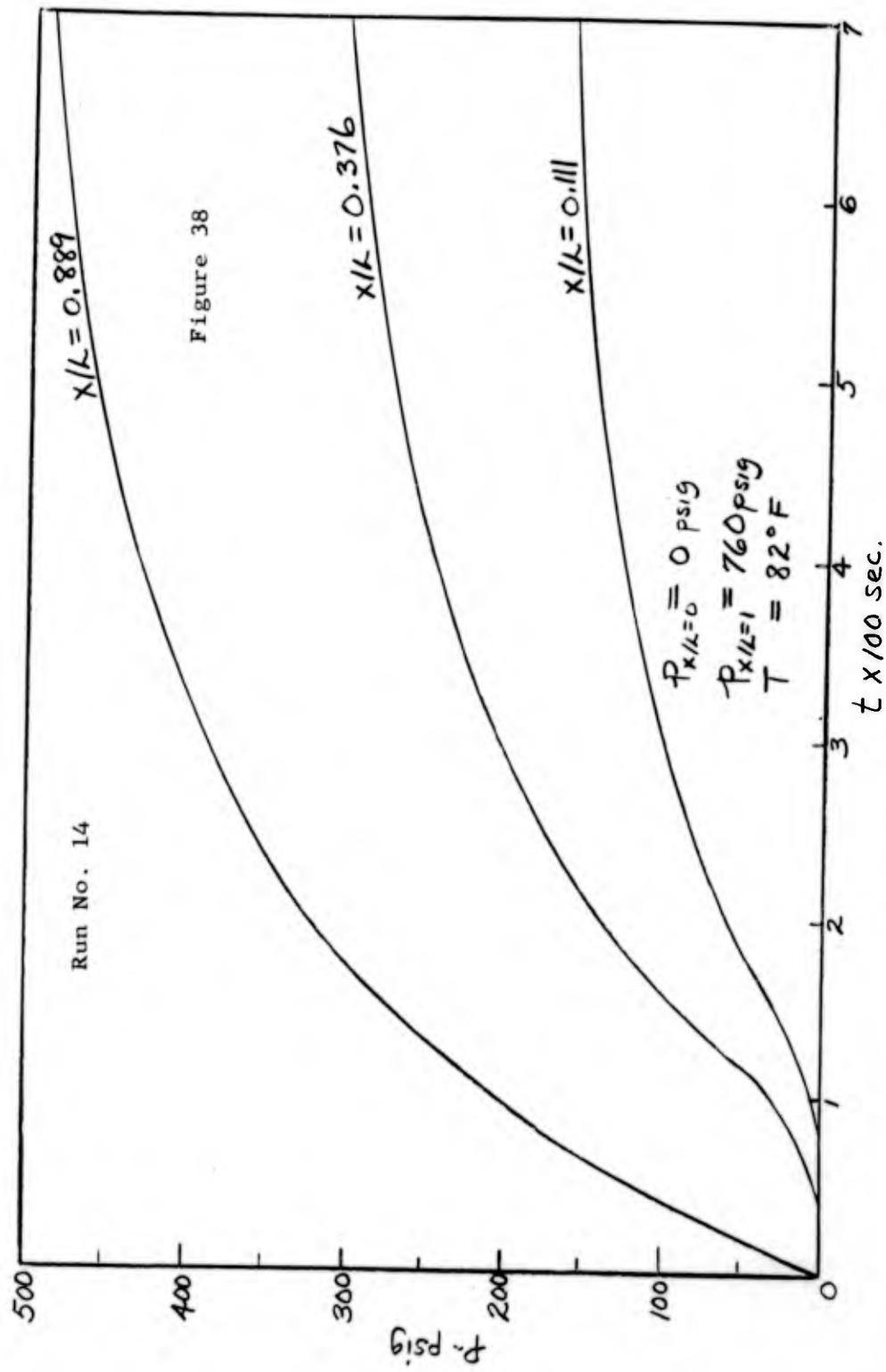
Run No. 14
Figure 38
x/L = 0.889
x/L = 0.376
x/L = 0.111
$P_{x/L=0}$ = 0 psig
$P_{x/L=1}$ = 760 psig
T = 82°F
P, psig
t x 100 sec.
500
400
300
200
100
0
1
2
3
4
5
6
7

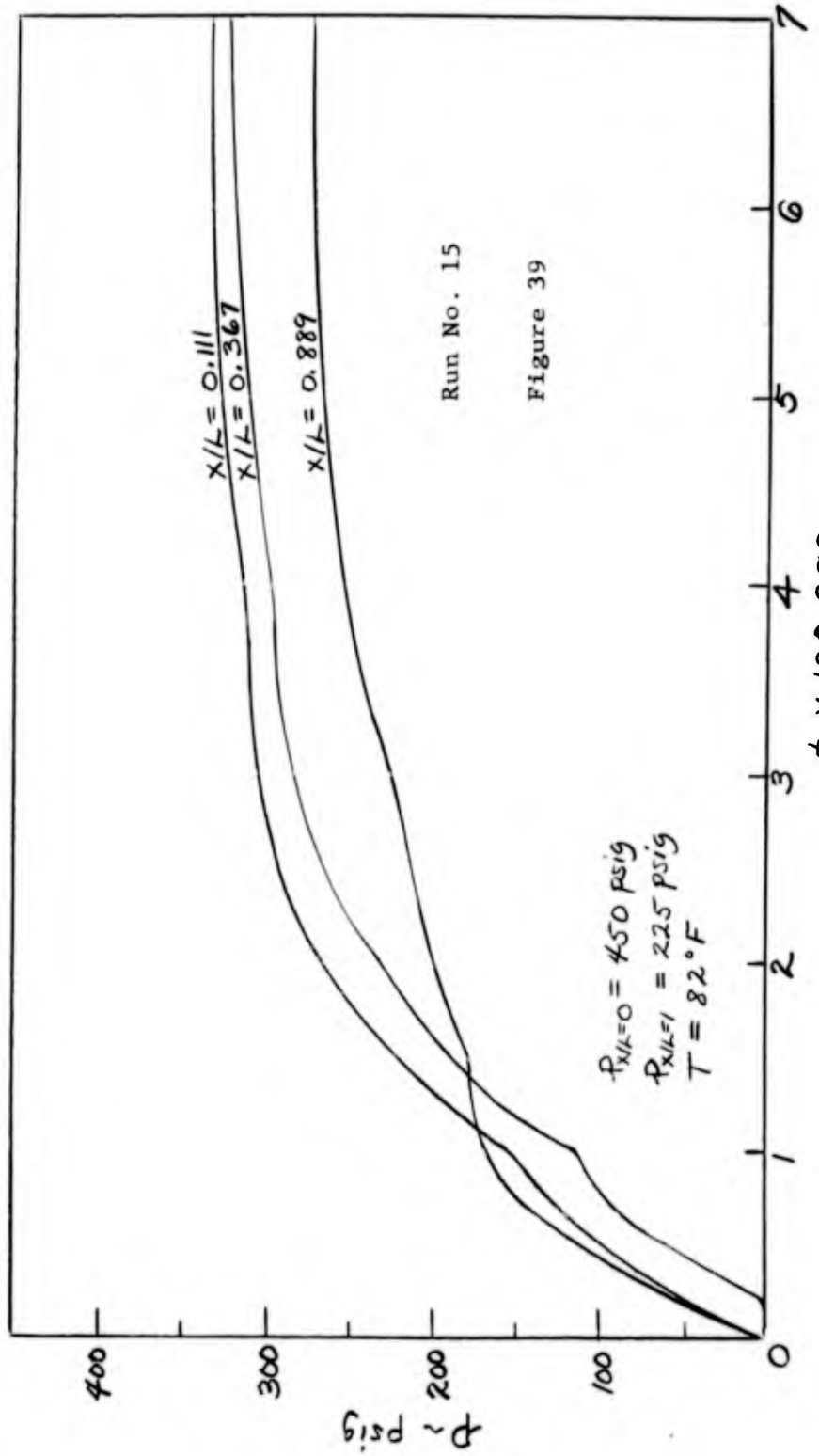

Run No. 15

Figure 39

differences between the two breaking diaphragms appeared to be less than 0.001 of a second.

Comparison of this data with theory will take place in the next chapter.

CHAPTER VI

ANALYSIS OF UNSTEADY FLOW

One objective of the project was the solution of the isothermal unsteady flow equations by numerical methods in order to compare the calculated results with the experimental work. This analysis is presented below.

Conservation of Mass

$$\frac{\partial(\rho u)}{\partial x} = -\frac{\partial \rho}{\partial t} \tag{6.1}$$

Conservation of Momentum

$$-\frac{dp}{dx} = \alpha \mu u \epsilon + \beta \rho u^2 \epsilon^2 + \frac{\partial(\rho u^2)}{\partial x} + \frac{\partial(\rho u)}{\partial t} \tag{6.2}$$

Using the experimental data of Chapter V in an order of magnitude analysis, it was found that the last two terms on the right side of Equation (6.2) were much smaller than the other terms. Hence, these two terms will be omitted in the following analysis.

Equation of State

$$p = \frac{R}{M} \rho T \tag{6.3}$$

Substituting (6.3) into (6.1) and (6.2) there results,

$$\frac{\partial \mathcal{Z}}{\partial X} + \frac{\partial \rho}{\partial t} = 0 \tag{6.4}$$

$$-\rho \frac{\partial P}{\partial X} = a\mathcal{Z} + b\mathcal{Z}^2 \tag{6.5}$$

where

$$\mathcal{Z} = \rho u$$
$$a = \alpha \mu \epsilon$$
$$b = \frac{\beta \epsilon^2}{R/M\, T}$$

At this point it is convenient to make Equations (6.4) and (6.5) dimensionless by making the following substitutions.

$$P = \frac{P}{P^*}, \quad Z = \frac{\mathcal{Z} t^*}{\rho^* L}, \quad X' = \frac{X}{L}, \quad T = \frac{t}{t^*}$$

where superscript star refers to some reference value.

Therefore,

$$\frac{\partial Z}{\partial X'} + \frac{\partial P}{\partial T} = 0 \tag{6.6}$$

$$P \frac{\partial P}{\partial X'} = a \frac{L^2 Z}{P^* t^*} + b \frac{L^3 Z^2}{t^{*2}} \tag{6.7}$$

The initial and boundary conditions are as follows:

1. $X' = 0, \; T \geq 0$: $P(0,T)$ Fixed
2. $X' = 1, \; T \geq 0$: $P(1,T)$ Fixed
3. $0 < X' < 1, \; T = 0$: $P(X',0)$ Fixed

These boundary conditions then describe the physical problem of simultaneously rupturing two diaphragms on opposite ends of a porous core.

Equations (6.6) and (6.7) are a nonlinear set of parabolic partial differential equations (20). Obviously they can only be solved by numerical methods. Hence, it was decided to use a finite-difference scheme.

It is possible to set up Equations (6.6) and (6.7) using either forward, central or backward differences or any combination thereof for each of the three derivatives. However, it was found by trial and error process that some of the combinations are not suitable in that they will not allow a solution to be stepped out along the grid with the given boundary conditions.

Limited success was obtained with the following combination called Method No. 1. (The primes have been dropped from the dimensionless distance variable.)

$$\frac{\partial P}{\partial X} = \frac{P(X+\Delta X,T)-P(X-\Delta X,T)}{2\Delta X} \qquad \text{Central Diff. (6.8)}$$

$$\frac{\partial P}{\partial T} = \frac{P(X,T+\Delta T)-P(X,T-\Delta T)}{2\Delta T} \qquad \text{Central Diff. (6.9)}$$

$$\frac{\partial Z}{\partial X} = \frac{Z(X+\Delta X,T)-Z(X,T)}{\Delta X} \qquad \text{Central Diff. (6.10)}$$

Substitute Equations (6.9) and (6.10) into (6.6) and rearrange

$$P(X,T+\Delta T) = 2(\Delta T/\Delta X)\left[Z(X,T)-Z(X+\Delta X,T)\right] + P(X,T-\Delta T) \qquad (6.11)$$

Substitute Equation (6.8) into (6.7)

$$P(X,T)\left[P(X+\Delta X,T) - P(X-\Delta X,T)\right] = \frac{2a\mathcal{L}^2\Delta X}{p^*t^*}\mathcal{Z}(X,T) + \frac{2b\mathcal{L}^3\Delta X}{t^{*2}}\mathcal{Z}^2(X,T) \tag{6.12}$$

Solving for $\mathcal{Z}(X,T)$ from Equation (6.12)

$$\mathcal{Z}(X,T) = \frac{-at^*}{2b\mathcal{L}p^*} + \left[\frac{t^{*2}}{4b\Delta X\mathcal{L}^3}\right]\left[\frac{4a^2\mathcal{L}^4\Delta X^2}{(p^*t^*)^2} + 8\frac{b\mathcal{L}^3}{t^{*2}}\Delta X\,P(X,T)\left\{P(X+\Delta X,T) - P(X-\Delta X,T)\right\}\right]^{1/2} \tag{6.13}$$

Substitute Equation (6.13) into (6.11)

$$P(X,T+\Delta T) = P(X,T-\Delta T) + \left[D + E\,P(X,T)\left\{P(X-\Delta X,T) - P(X+\Delta X,T)\right\}\right]^{1/2} - \left[D + E\,P(X+\Delta X,T)\left\{P(X,T) - P(X+2\Delta X,T)\right\}\right]^{1/2} \tag{6.14}$$

where

$$D = \left(\frac{t^*\Delta T a}{b\mathcal{L}p^*\Delta X}\right)^2 \tag{6.15}$$

$$E = -\left(\frac{2t^{*2}\Delta T^2}{b\mathcal{L}^3\Delta X^3}\right) \tag{6.16}$$

Equation (6.14) was programed for the Oklahoma University Medical School IBM 1401 digital computer (see Appendix E for the computer program).

In order to compare Equation (6.14) with experimental data, the inputs on the computer program were made to match the boundary conditions of Experimental Run # 4 (see Figure 31).

It is seen from Figure 40 that the computed (Method No. 1) pressure gradients are, in general, much greater than the experimental ones. This is due probably to the fact that the computer data, (but not the experimental data) is the pressure response to a step pressure input at X/L = 0. Because the gas storage reservoir is not infinite and because

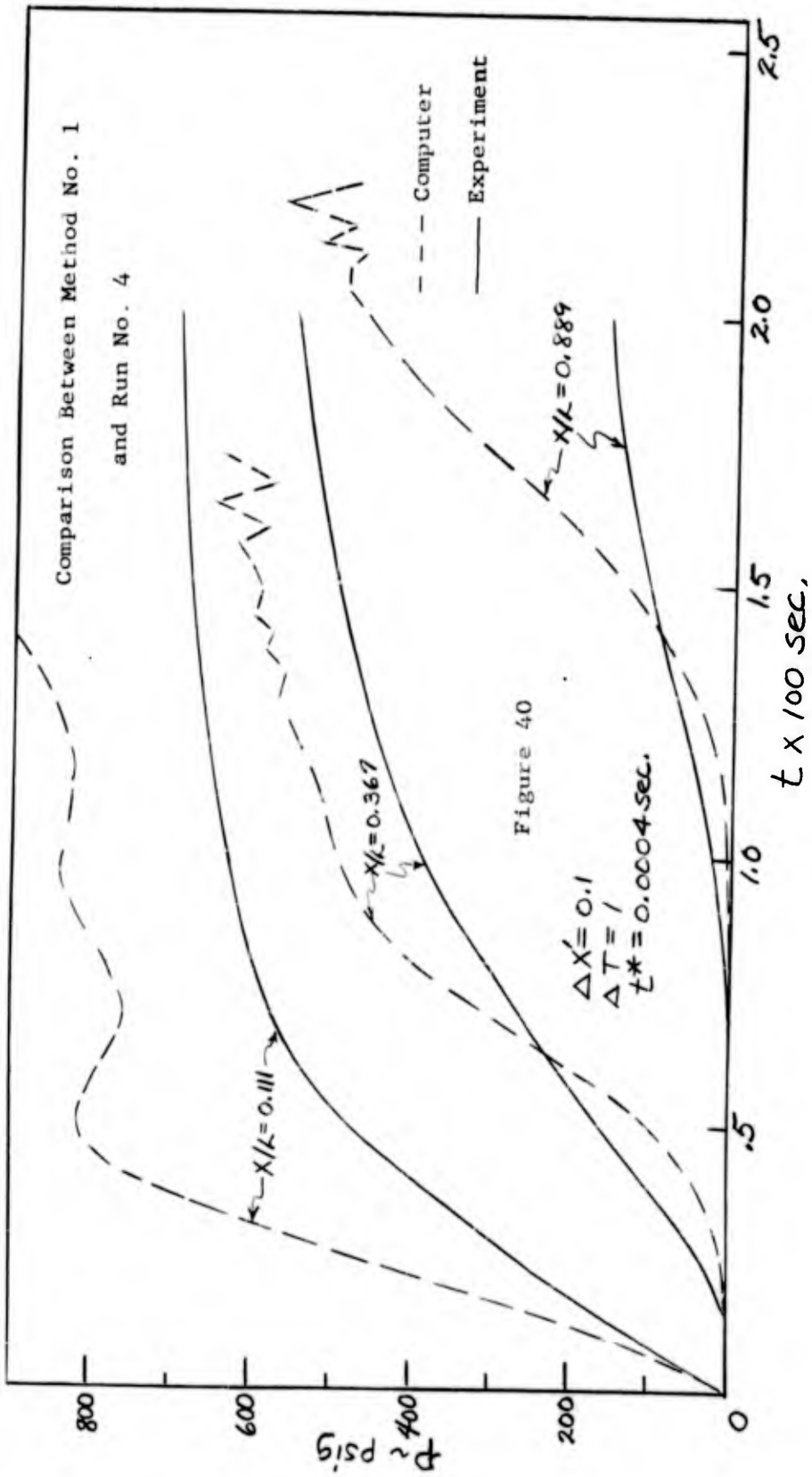
Comparison Between Method No. 1
and Run No. 4
— Experiment
- - - Computer
X/L = 0.111
X/L = 0.367
X/L = 0.889
ΔX = 0.1
ΔT = 1
t* = 0.0004 sec.
P psig
t X 100 sec.
0
200
400
600
800
.5
1.0
1.5
2.0
2.5

Figure 40

it takes a finite amount of time to break the diaphragm, the actual pressure profile input at X/L = 0 will not be a step input, but rather a rounded off approximation.

It is also noticed in Figure 40 that each computer curve becomes unstable after a certain period of time depending on the X/L value. A large amount of time was spent in trying to eliminate this stability problem, which is inherent in almost all finite difference solutions of differential equations.

The choice of the grid size ($\Delta X, \Delta t$) has a very large effect on the time at which the instability starts. The grid size ($\Delta X' = .1$, $\Delta T = 1$, $t^* = 0.0004$ sec.) chosen for the data plotted in Figure 40 represents the best size found in this respect. Below is a table which shows the time the pressure starts to oscillate for various grid sizes.

TABLE 3

STABLE COMPUTING TIME AT X/L = 0.1

GRID SIZE			STABLE COMPUTING TIME (SEC)
$\Delta X'$	ΔT	t^*(sec.)	
.05	.05	.002	0.0017
.05	.1	.002	0.002
.025	.05	.002	0.0011
.1	1	.0004	0.005

It is possible that further experimenting with grid sizes will give stable computing times greater than 0.005 sec at X/L = 0.1.

When Method No. 1 was applied to the case where two diaphragms are burst simultaneously it did not work at the end where X/L = 1. An investigation revealed that this was due to the presence of the forward difference term, Equation (6.11). However, if the forward difference is replaced by a backward difference term the resulting equation (similar to 6.14) will function at the X/L = 1 end, but will not function at the X/L = 0 end. The only choice left was to replace the forward difference equation (Equation (6.10)) by the following central difference equation

$$\frac{\partial Z}{\partial X} = \frac{Z(X+\Delta X,T) - Z(X,T)}{2\Delta X} \tag{6.17}$$

Method No. 2 consists then of using Equation (6.17) in place of (6.10). Following a procedure similar to that leading to Equation (6.14) there will result,

$$P(X,T+\Delta T) = P(X,T-\Delta T) + \left[D' + E'P(X-\Delta X,T)\{P(X-2\Delta X,T) - P(X,T)\}\right]^{1/2} - \left[D' + E'P(X+\Delta X,T)\{P(X,T) - P(X+2\Delta X,T)\}\right]^{1/2} \tag{6.18}$$

where

$$D' = 1/4\ D \tag{6.19}$$

$$E' = 1/4\ E \tag{6.20}$$

Method No. 2 was the only method found that worked at both ends of the porous core (or X-grid). However, when Equation (6.18) was programed (see Appendix E for the computer program) and run on the IBM 1401 a very undesirable characteristic was noticed. Each successive solution point oscillates and the amplitude of these oscillations increases with time. Figure 41 is a comparison of Method No. 2 with Experimental Run

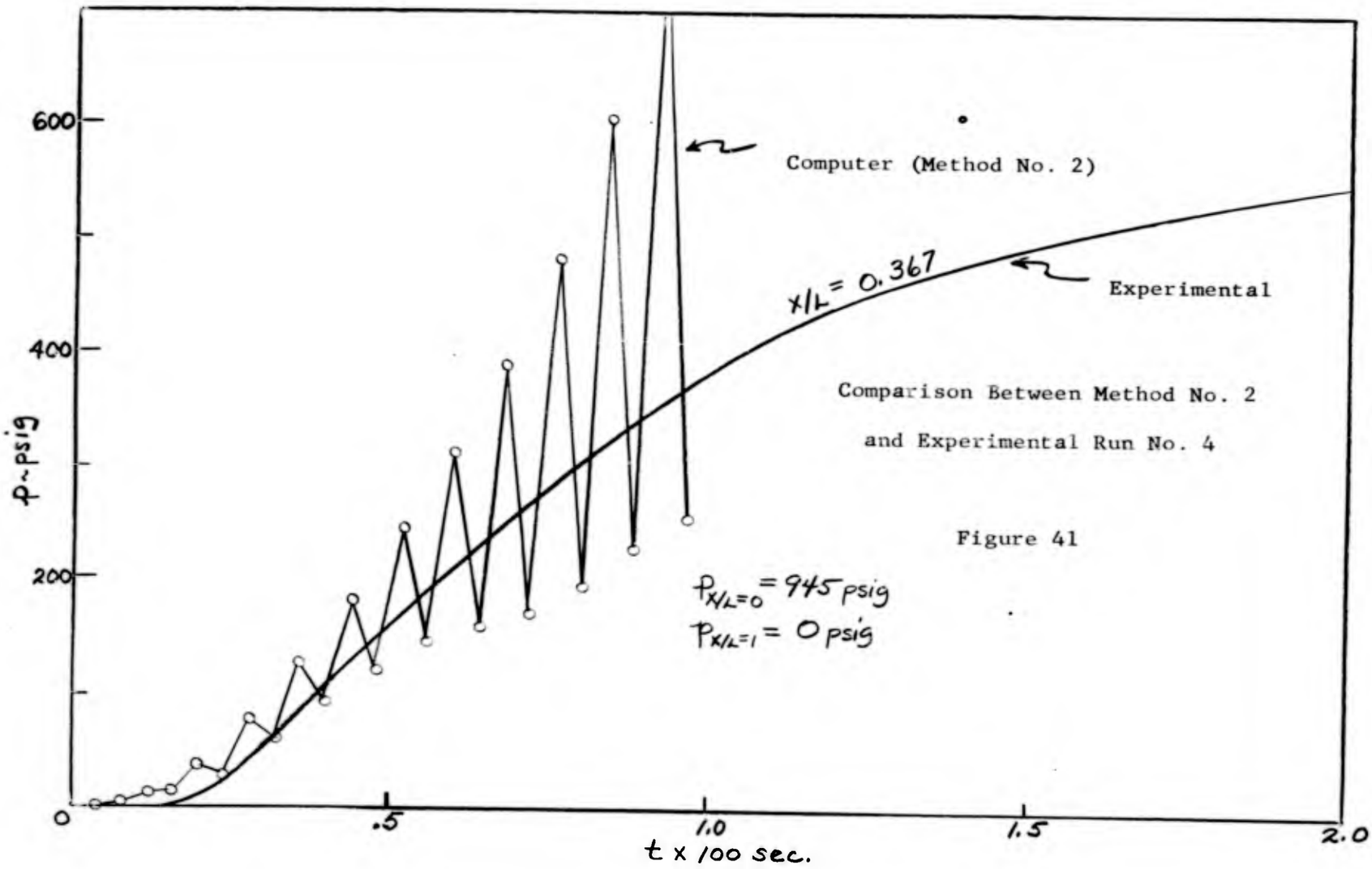

Comparison Between Method No. 2

and Experimental Run No. 4

Figure 41

No. 4 (see Figure 31). The experimental data does seem to fall approximately in the middle of the computer points, however past .005 seconds the amplitude of the oscillations are so large it would be hard to predict the pressure line accurately.

While there was not time to further investigate this problem during the period covered by the present report, the work is being continued at Washington University under the one year extension of the project which was recently granted.

BIBLIOGRAPHY

1. Scheidegger, A. E., Producers Monthly, 17, (August 1953), pp. 17-23.

2. Kawakami, M., Journal Chemical Society of Japan, 53, (1932), p. 1085.

3. Smith, W. O., Physics, 3, (1932), p. 139.

4. Rainard, L. W., Textile Research Journal, 17, (1947), p. 167.

5. Henderson, J. H., Producers Monthly, 14, (November 1949), pp. 32-39.

6. Purcell, W. R., Transactions of AIME, 186, (February 1949), pp. 39-48.

7. Burdine, N. T., et al., Transactions of AIME, 189, (1950), pp. 195-204.

8. Calhoun, J. C., Fundamentals of Reservoir Engineering, Norman, Oklahoma: University of Oklahoma Press, 1953.

9. Scheidegger, A. E., The Physics of Flow Through Porous Media, Toronto, Ontario: University of Toronto Press, 1960.

10. Bennett, C. O. and Myers, J. E., Momentum, Heat and Mass Transfer, New York, N. Y.: McGraw-Hill Book Co., Inc. (1962).

11. Rouse, H., Fluid Mechanics for Hydraulic Engineers. New York, N. Y.: McGraw-Hill Book Co., Inc. (1938).

12. Weger, E., and Greenberg, D. B., An Investigation of the Viscous and Inertial Coefficients for the Flow of Gases through Porous Sintered Metals with High Pressure Coefficients. Technical Report No. 1, Contract No. DA 36-034-ORD-2353, March 1959.

13. Weger, E. and Greenberg, D. B., Transient Gas Flow in Porous Media - The Pressure Decay Process. Final Technical Report, Contract No. DA-36-034-ORD-2353, May 1960.

14. Mach, Dechema Monographien, Vol. 6 (1934), p. 38.

15. Berl, Catalog of Messrs, Ditt and Fries, Wiesbaden.

16. Uchida, S. and Fujita, S., Journal of Society of Chemical Industry of Japan, (suppl. binding), 37, (1934), pp. 724B and 791B.

17. Brownell, L. E. and Katz, D. L., Chemical Engineering Progress, (November 1947), p. 537.

18. Blake, F. C., Transactions of American Institute of Chemical Engineers, 14, (1922), p. 415.

19. Kay, J. M., An Introduction to Fluid Mechanics and Heat Transfer, New York, N. Y.: Cambridge Press, (1957).

20. Crandall, S. H., Engineering Analysis, New York, N. Y.: McGraw-Hill Book Co., Inc. (1956).

APPENDIX A

DETERMINATION OF VISCOUS DISSIPATION BY CAPILLARY-ORIFICE MODEL

During the flow of all real fluids heat is generated internally due to the work done by the shear stresses in distorting the fluid. This irreversible generation of heat per unit volume is called the viscous dissipation Φ . In a Cartesian coordinate system the expression for Φ is (19),

$$\Phi = \mu \left\{ 2\left(\frac{\partial u}{\partial x}\right)^2 + 2\left(\frac{\partial v}{\partial y}\right)^2 + 2\left(\frac{\partial w}{\partial z}\right)^2 + \left(\frac{\partial u}{\partial y} + \frac{\partial v}{\partial x}\right)^2 + \left(\frac{\partial v}{\partial z} + \frac{\partial w}{\partial y}\right)^2 + \left(\frac{\partial w}{\partial x} + \frac{\partial u}{\partial z}\right)^2 - \frac{2}{3}\left[\frac{\partial u}{\partial x} + \frac{\partial v}{\partial y} + \frac{\partial w}{\partial z}\right]\right\} \tag{A.1}$$

This is a very formidable looking equation indeed, but fortunately for the usual state of affairs with heat transfer at low velocities of the order of sonic velocity it should not be omitted. For flows through porous media the viscous forces are very large, hence one would expect the viscous dissipation to be very large also.

Rather than attempt to solve Equation (A.1) for Φ , another line of attack is proposed. Consider the case of steady flow of a

real fluid through a tube or any system with fixed boundaries. The differential equation for mechanical energy is (See page 34 of (19)).

$$\frac{dp}{\rho} + u\,du + g\,dz = dQ_f \tag{A.2}$$

where dQ_f = Friction heat

z = Vertical coordinate

g = Acceleration of gravity

p = Pressure

ρ = Density

u = Mean velocity

If the tube is horizontal then $dz = 0$ and Equation (A.2) can be put in the following form,

$$\frac{dQ_f}{dx} = \frac{1}{\rho}\left[-\frac{dp}{dx} - \rho u \frac{du}{dx}\right] \tag{A.3}$$

If the system in question is a section of the capillary-orifice tube model then one can substitute Equations (2.7), (2.9) and (2.10) into (A.3).

$$\frac{dQ_f}{dx} = \frac{1}{\rho}\left(\alpha \mu v + \beta \rho v^2\right) \tag{A.4}$$

Equation (A.4) represents the rate of energy dissipated per unit length per mass flowing. By multiplying Equation (A.4) by the mass flow per unit tube area

$$G = \rho u = \rho v/\epsilon \tag{A.5}$$

the viscous dissipation function is obtained

$$\Phi = (v/\epsilon)(\alpha\mu v + \beta\rho v^2) \qquad \text{(A.6)}$$

APPENDIX B

HEAT TRANSFER COMPUTER PROGRAM

This program is written in the GAT language for computation on an IBM 650 computer. The program was greatly simplified by using an existing Runge-Kutta subroutine for solving a set of differential equations.

The problem is essentially this: Solve for the mass flow and temperature and pressure profiles for a fixed initial pressure and temperature and fixed exit pressure for one-dimensional steady flow through a porous media.

Rearrange Equations (3.1) - (3.3) and (3.8) - (3.12) then substitute the following non-dimensional terms.

$$P = \frac{p}{p^*}, \quad P_A = \frac{p_A}{p^*}, \quad \theta = \frac{T}{T^*}, \quad X' = \frac{X}{L}, \quad G = \frac{G}{G^*}$$

and $a = \frac{A}{A^*}$

(The superscript star refers to some reference value.)

$$\frac{dP^2}{dX'} = \frac{-2(R/M)L\eta M^* T^* G^*}{p^{*2}} \mathcal{G}\theta^2 e^{\gamma T^* \theta} - \frac{2(R/M)L G^{*2} T^* \beta}{p^{*2} g_c} \mathcal{G}^2 \theta \qquad \text{(B.1)}$$

$$\frac{d\theta}{dX'} = \frac{\mathcal{G}^2\theta^2}{\frac{C_p p^{*2}\epsilon^2}{G^{*2}R^2T^*}P^4 + \mathcal{G}^2\theta P^2}\left[\frac{1}{2}\frac{dP^2}{dX'} + \left(\frac{H\epsilon^3 p^{*3} L A^*}{G^{*3}R^3T^{*3}}\right)\cdot \left(\frac{P_A P^4 a}{\mathcal{G}^3\theta^3}\right) e^{-E_a/RT^*\theta}\right] \tag{B.2}$$

$$\frac{dP_A}{dX'} = \frac{P_A}{\theta}\frac{d\theta}{dX'} - \frac{p^* A^* L a P_A P}{(R/M) G^* \mathcal{G} T^* \theta}\, e^{-E_a/RT^*\theta} \tag{B.3}$$

Introduce the following terms,

C1 = a

C2 = G

D0 = $\Delta Y0 = 0.1$

D1 = $\frac{H\epsilon^3 p^{*3} L A^{*3}}{G^{*3}R^3T^{*3}}$

D3 = $-E_a/RT^*$

D4 = $\frac{C_p p^{*2}\epsilon^2}{G^{*2}R^2T^*}$

D6 = $\frac{p_i A^* L}{(R/M) G^* T^*}$

D8 = $\frac{2(R/M)T^*\eta_M^* G^* L}{p^{*2}}$

D9 = $\frac{2\beta(R/M)T^* L G^{*2}}{p^{*2} g_c}$

D10 = γT^*

GAT Language		Algebra
Y0	⟷	X
Y1	⟷	P^2
Y2	⟷	θ
Y3	⟷	P_A

By substituting in the above quantities, Equations (B.1) - (B.3) becomes

$$Y0' = 1 \tag{B.4}$$

$$Y1' = -(D8)(C2)(Y2)^2 \exp.\left[(D10)(Y2)\right] - (D9)(C2)^2(Y2) \tag{B.5}$$

$$Y2' = \left[\frac{(C2)^2\,(Y2)^2}{(D4)\,(Y1)^2 + (C2)^2\,(Y2)\,(Y1)}\right]\left[1/2\,(Y1') + (D1)\left(\frac{(Y3)\,(Y1)^2\,(C1)}{(C2)^3\,(Y2)^3}\right)\exp\,(D3/Y2)\right] \qquad (B.6)$$

$$Y3' = \left(\frac{Y3}{Y2}\right)\left(Y2'\right) - \left(\frac{(D6)\,(C1)\,(Y3)\,(Y1)^{1/2}}{(C2)\,(Y2)}\right)\exp\,(D3/Y2) \qquad (B.7)$$

Let,

$$Y4 = Y0' \qquad (B.8)$$

$$Y5 = Y1' \qquad (B.9)$$

$$Y6 = Y2' \qquad (B.10)$$

$$Y7 = Y3' \qquad (B.11)$$

The boundary conditions are

Y0(0) = 0 = initial value on Y0

Y1(0) = $\mathcal{Z}$1 = initial value on Y1

Y2(0) = $\mathcal{Z}$2 = initial value on Y2

Y3(0) = $\mathcal{Z}$3 = initial value on Y3

One can now substitute Equations (B.8) - (B.11) into Equations (B.4) - (B.7) and write them out in full GAT language.

```
Y4 = 1                                                          (B.12)

Y5 = -D8*C2*Y2* EXP. (D10*Y2) - D9*Y2*C2*C2                      (B.13)

Y6 = ((C2*Y2) P2/(2.*(D4*Y1P2 + C2PZ + N
     Y2*Y1)))*Y5 + 2.*D1*Y3*Y1P2*C1*N
     EXP. (D3/Y2) / (C2*Y2) P3)                                 (B.14)

Y7 = Y3/Y2*Y6 - D6*C1*Y3*Y1P.5* EXP. (D3 /Y2)/(C2*Y2)           (B.15)
```

One of the difficulties of this program is that it will not solve for the mass flow (C2) explicitly. Hence one must insert a value of C2 into the program, let the program run, then note the value of the pressure at the end of the core. If the pressure is atmospheric then a correct guess was made on C2. If the pressure at exit is not atmospheric ($Y0 \neq 1$) then another value is chosen for C2, etc. The machine can handle this easily if one assumes an initial C2 (called C6) and increments it every run by a finite amount (C7) until a final value is reached (C8).

C2	C6 (initial)	C7 (increment)	C8 (final)

Figure 42 illustrates the flow diagram for the steady flow through porous media program, and Figure 43 is the machine program.

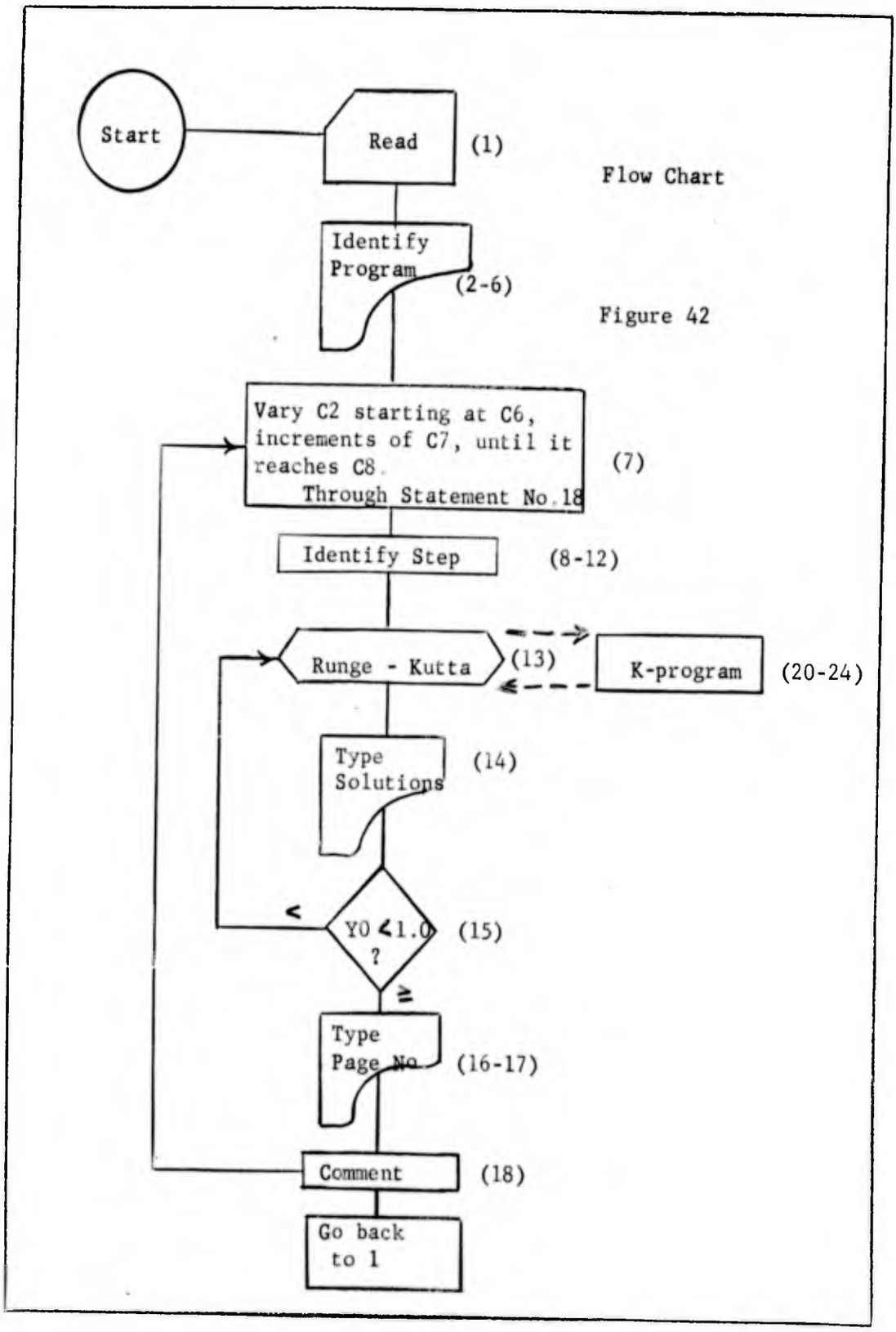

Flow Chart

Figure 42

HEAT TRANSFER COMPUTER PROGRAM

```
      25 IS HIGHEST STATEMENT NUMBER
      TEST
      750 USED IN SUBROUTINES
      DIMENSION Y (22) D(21) C(8)N
      Z(7) X(7) I(1)
 1    DO. . .D10ETC. CM READ
 2    AT$INPUT$AT$ DATA$
 3    TC1 TC2 TC6. . .C8N
      TDO. . .D1ON
      TZ1. . .Z3
 4    Y0=0 M Y1=Z1 M Y2=Z2 M Y3=Z1
 5    AT$INITI$AT$AL CO$AT$NDITI$
      AT$ONS  $
 6    TY0. . . Y3
 7    18,C2,C6,C7,C8,
 8    AT$ITERA$AT$TIV $AT$STEP $
 9    TC6 TC7 TC8 TC2
10    TO
11    Y0= 0 M Y1=Z1 M Y2=Z2 M Y3=Z3
12    AT$SOLUT$AT$IONS $
13    RKSUB.(4,LY0, D0,20
14    TY0. . .Y7
15    GO TO 13 IF Y0 Q 1.
16    I1=I1+1
17    PCHSK.(I1)
18    END OF K LOOP  C
19    GO TO 1
20    Y4=1.
21    Y5=-D8* C2* Y2* EXP.(D10* Y2 -N
      (D9* Y2* C2* C2)
22    Y6=-((C2* Y2) P2/(2.* D4* Y1N
      P2+C2P2* Y2* Y1)))*(Y2* D8* N
      C2* Y2* EXP. (D10* Y2)=D9* C2N
      P2* Y2-2.* D1* Y3* Y1P2* C1* EXP.N
      (D3/Y2)/(C2* Y2)P3)
23    Y7= Y3/Y2* Y6-D6* C1* Y3* Y1N
      P.5* EXP.(D3/Y2)/(C2* Y2)
24    GO TO 21
      END
```

Figure 43

APPENDIX C

TABLES OF DATA AND RESULTS FOR

STEADY FLOW

TABLE 4

Steady Flow Results ~ FC-250+325

CORE: FC-250+325

Length: 5.814 in.

Diameter = 0.75 in.

$$A = \left[\frac{Mg_c}{2ZRT\mu L}\right] \qquad \Psi = \frac{\Delta(P^2)M\delta\epsilon g_c}{2LG^2ZRT}$$

Run No.	P_1 (psia)	P_2 (psia)	T_1 (^oF)	T_2 (^oF)	Q_c (scfh)	Q_c/csa (scfh/in^2)	$\Delta(P^2)A/G$ (ft^{-2}) $\times 10^9$	G/μ ft^{-1} $\times 10^3$	Ψ	Re
1	26.5	14.56	84	84	4.09	9.26	34.6	2.26	99.2	.324
2	40.0	14.74	84	84	12.0	27.2	33.4	6.55	33.1	.94
3	49.5	14.88	84	84	18.68	42.25	34.7	10.3	21.9	1.476
4	71.5	14.59	84	84	38.8	88	36.5	21.5	11.1	3.085
5	101.0	14.77	84	84	71.9	163	40.1	39.8	6.53	5.71
6	122.5	14.97	84	84	100.4	227.5	42.6	55.6	4.96	7.95
7	95.5	14.74	84	84	65.5	148.5	39.3	36.3	7.01	5.2
8	86.5	14.65	84	84	55.1	125	38.2	30.5	8.13	4.38

TABLE 5

Steady Flow Results ~FC-100+150

CORE: FC-100+150

Length: 5.875 in.

Diameter: 0.75 in.

$$A = \left[\frac{Mg_c}{2ZRT\mu L}\right] \qquad \psi = \frac{\Delta(P^2)M\delta\epsilon g_c}{2LG^2ZRT}$$

Run No.	P_1 (psia)	P_2 (psia)	T_1 (^oF)	T_2 (^oF)	Q_c (scfh)	Q_c/csa (scfh/in^2)	$\Delta(P^2)A/G$ (ft^{-2}) x10^9	G/μ ft^{-1} x10^3	ψ	Re
9	21.0	14.68	78	78	10.7	24.28	6.11	5.93	16.3	1.22
10	24.6	14.80	78	78	17.18	38.9	6.52	9.5	10.8	1.96
11	37.5	14.60	78	78	46.6	105.6	7.41	25.8	4.53	5.32
12	51.0	14.76	78	78	80.0	181	8.64	44.2	3.08	9.15
13	63.5	14.97	78	78	116	263	9.52	64.2	2.34	13.22
14	56.0	14.85	78	78	94.5	214	8.97	52.1	2.71	10.74
15	43.5	14.70	78	78	61.6	139.7	7.88	34.1	3.65	7.02
16	32.3	14.59	78	78	34.25	77.6	7.0	18.95	5.84	3.91

APPENDIX D

SAMPLE CALCULATIONS FOR STEADY FLOW

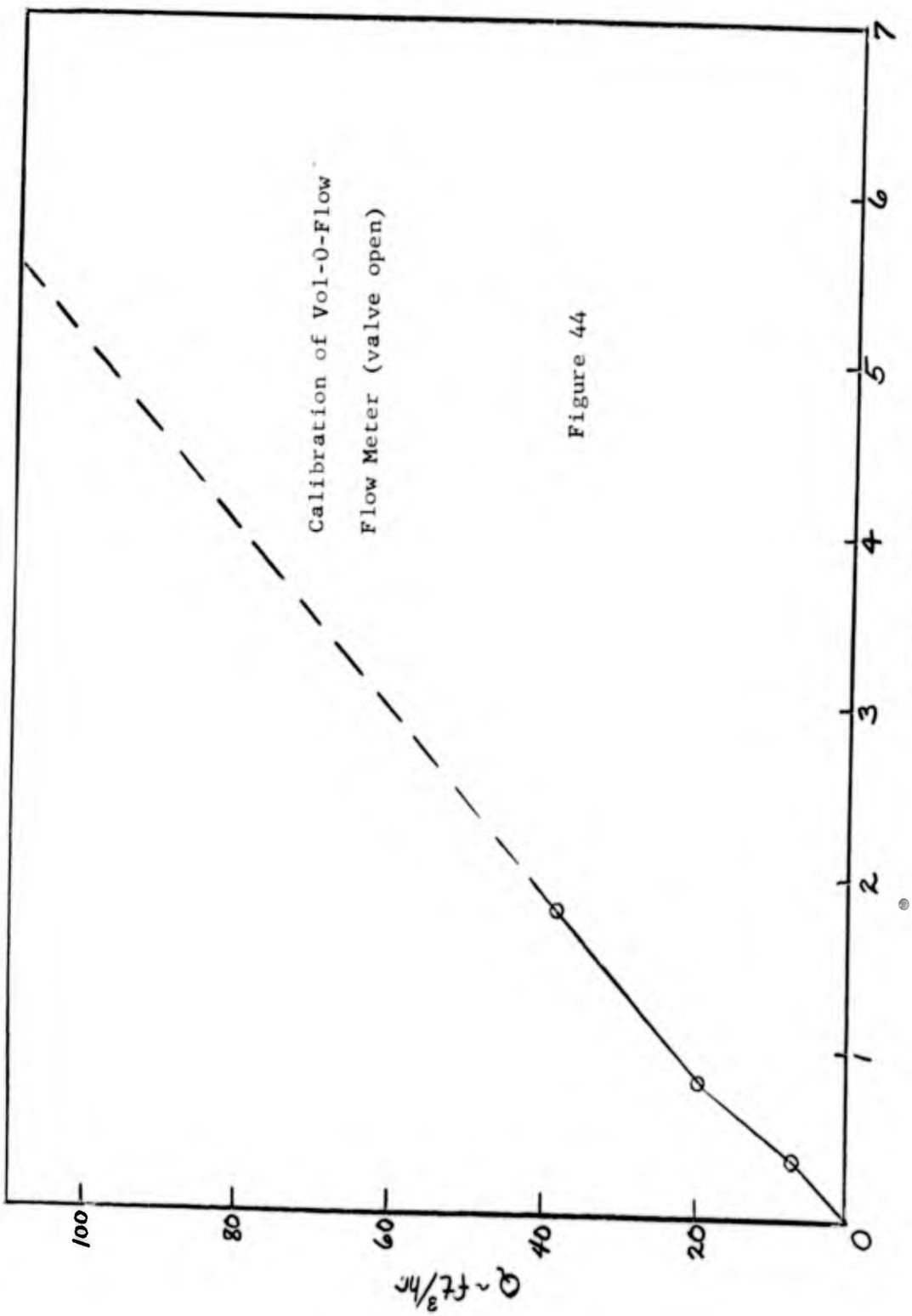
Calibration of Vol-O-Flow
Flow Meter (valve open)
Q ~ ft³/hr
0
20
40
60
80
100
1
2
3
4
5
6
7
Flow Meter Reading

Figure 44

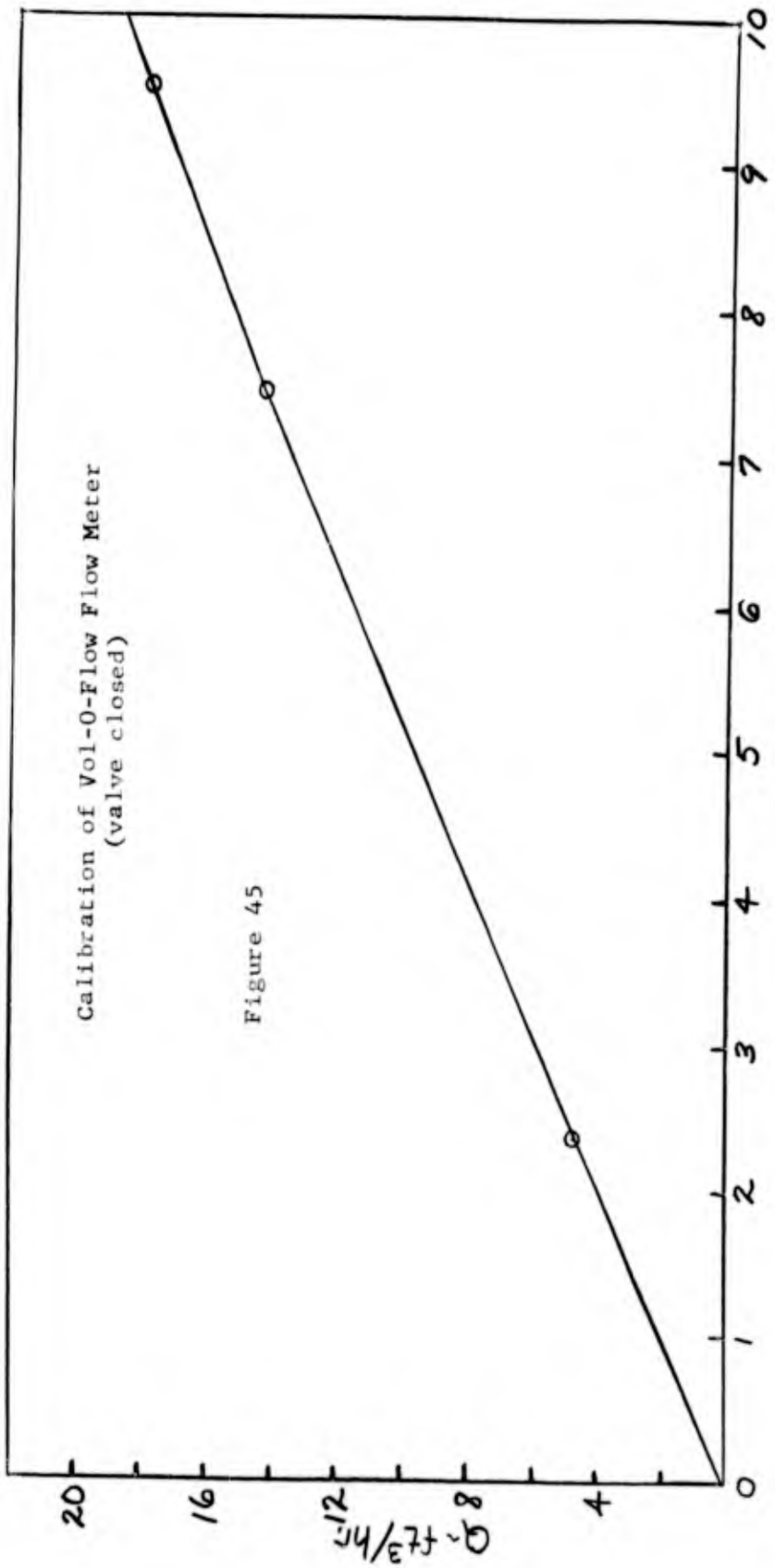
Calibration of Vol-O-Flow Flow Meter
(valve closed)
Q - ft³/hr
20
16
12
8
4
0
1
2
3
4
5
6
7
8
9
10
Flow Meter Reading

Figure 45

Run No. 6, Core FC-250+325

1. Physical Data

(a)	Length of sample	$L = 5.814$ in.
(b)	Diameter	$d = 0.75$ in.
(c)	Cross sectional area	$csa = 0.442$ in.^{2}
(d)	Porosity	$\epsilon = 0.356$
(e)	Mean pore diameter	$dp = 15.5$ Microns
(f)	Particle size range	$43 \leq d_2 \leq 61$ Microns

2. Experimental Measurements

(a)	Upstream pressure	$P_1 = 122.5$ psia
(b)	Downstream pressure	$P_2 = 14.97$ psia
(c)	Upstream gas temperature	$T_1 = 84\ ^oF$
(d)	Downstream gas temperature	$T_2 = 84\ ^oF$
(e)	Ambient room temperature	$T_a = 89\ ^oF$
(f)	Flow meter reading	$q = 5.20$

3. Corrected Flow Rate: Q_c (68^oF, 14.7 psia)

(a) Flow rate at experimental conditions (Figure 44) $Q = 103.5$ cfh

(b) Corrected flow rate

$Q_c = Q\ [1-.001834\ (T_2-68)]\ Q$ $Q_c = 100.4$ cfh

4. Tabulated Experimental Data

(a) P_1 = 122.5 psia

(b) P_2 = 14.97 psia

(c) P_{avg} = 68.7 psia

(d) P = 107.5 psi

(e) P^2 = 14772 $(psi)^2$

(f) Q = 103.5 cfh

(g) Q_c = 100.4 cfh

(h) P/L = 18.5 psi/in.

(i) Q_c/csa = 227.5 scfh/$in.^2$

(j) T_{avg} (for run) = 84°F

5. Physical Properties of Nitrogen

(a) Density (68°F, 14.7 psia) = 0.0729 $lb./ft^3$

(b) Compressibility (84°F, 68.7 psia) = 1.00

(c) Viscosity (84°F, 68.7 psia) = 0.043 lb./ft-hr.

(d) Molecular weight M = 28.02

6. Mass Flow Rate

$$G = \left(\frac{144\ in.^2}{1\ ft^2}\right) \rho_c\ Q_{c/csa} = \left(\frac{144\ in.^2}{1\ ft^2}\right)\left(\frac{0.0729\ lb.}{ft^3}\right)\left(227.5\ \frac{scfh}{in^2}\right)$$

$G = 2390\ lb/hr\text{-}ft^2$

7. Cornell and Katz Plot

(a) $$\left[\frac{Mg_c}{2(ZRT)\mu L}\right]\left[\frac{(P^2)}{G}\right] = \left[\frac{(28.02)(32.2)(3600)^2(144)^2(12)}{2(1.00)(10.71)(144)(544)(.043)(5.814)}\right] \cdot \left[\frac{14772}{2390}\right] = 42.6 \times 10^9$$

(b) $$(G/\mu) = \frac{2390}{.043} = 55.6 \times 10^3\ ft^{-1}$$

(c) α is obtained as the intercept and β as the slope in Figure 26

$\alpha = 32.5 \times 10^9\ ft^{-2}$

$\beta = 1.76 \times 10^5\ ft^{-1}$

8. Ψ Plot

(a) $$\Psi = \frac{\Delta(P^2)M\delta\epsilon^2 g_c}{2LG^2ZRT} = \left[\frac{Mg_c\,\Delta(P^2)}{2ZRT\mu LG}\right]\left[\frac{1}{G/\mu}\right]\left[\delta\epsilon^2\right]$$

$$= \left[42.6 \times 10^9\right]\left[\frac{1}{55.6 \times 10^3}\right]\left[(15.5)(3.281 \times 10^{-6})(.356)^2\right]$$

$$= 4.96$$

(b) $$Re = \frac{\rho u \delta}{\mu} = \frac{\rho v \delta}{\epsilon\mu} = \frac{G}{\mu}\,\frac{\delta}{\epsilon}$$

$$Re = (55.6 \times 10^3)\,\frac{(15.5)(3.281 \times 10^{-6})}{(.356)} = 7.95$$

APPENDIX E

UNSTEADY FLOW COMPUTER PROGRAMS

Constants for Methods No. 1 and 2

A : boundary value on left

B : boundary value on right

C : boundary value on bottom

D : see Equation (6.15)

E : see Equation (6.16)

I : Example Number

Note, in Method No. 2 computer program $D = D'$. (See Equations (6.19) and (6.20)).

METHOD NO. 1

```
SEQ     STMNT     FORTRAN STATEMENT

 1                DIMENSION P(12,5),X(12)
 2          1     FORMAT (5F10.0,I5)
 3          2     FORMAT (I4,9F14.7)
 4          3     FORMAT (IHI,17HMETHOD 1, EXAMPLE,I3)
 5        100     DO 101 I=1,12
 6                X(I)=0.0
 7                DO 101 J=1,5
 8        101     P(I,J)=0.0
 9                READ 1,A,B,C,D,E,I
10                PRINT 3,I
11                M=1
12                MM=11
13                II=12
14                DO 102 J=1,5
15                P(M,J)=A
16                P(MM,J)=B
17        102     P(II,J)=B
18                N=1
19                I=2
20                DO 103 M=2,10
21                P(M,I)=C
22        103     P(M,N)=C
23                DO 109 IX=2,100
24                N=3
25                DO 106 M=2,10
26                X=D+E*P(M,N-1)*(P(M-1,N-1)-P(M+1,N-1))
27                Y=D+E*P(M+1,N-1)*(P(M,N-1)-P(M+2,N-1))
28                IF (X) 1031,1032,1032
29       1031     X=SQRTF(-X)
30                GO TO 1033
31       1032     X=SQRTF(X)
32       1033     IF (Y) 1034,1035,1035
33       1034     Y=SQRTF(-Y)
34                GO TO 106
35       1035     Y=SQRTF(Y)
36        106     P(M,N)=P(M,N-2)+X-Y
37                PRINT 2,IX,(P(I,3),I=2,10)
38                DO 107 KX=1,4
39                DO 107 JX=1,12
40        107     P(JX,KX)=P(JX,KX+1)
41        109     CONTINUE
42                GO TO 100
43                END
```

Figure 46

METHOD NO. 2

```
SEQ     STMNT     FORTRAN STATEMENT

  1               DIMENSION P(13,3),X(13)
  2         1     FORMAT (F10.0,F10.0,F10.0,F10.0,F10.0,I5)
  3         2     FORMAT (I3,9F14.8)
  4         3     FORMAT (IHI,18HMETHOD 2A, EXAMPLE,I3)
  5       100     DO 101 I-1,13
  6               X(I)=0.0
  7               DO 101 J=1,3
  8       101     P(I,J)=0.0
  9               READ 1,A,B,C,D,E,I
 10               PRINT 3,I
 11               X(1)=A
 12               X(2)=A
 13               X(12)=B
 14               X(13)=B
 15               M=1
 16               I=2
 17               MM=12
 18               II=13
 19               DO 102 J=1,3
 20               P(M,J)=A
 21               P(I,J)=A
 22               P(MM,J)=B
 23       102     P(II,J)=B
 24               N=1
 25               I=2
 26               DO 103 M=3,11
 27               P(M,N)=C
 28       103     P(M,I)=C
 29               DO 109 IX=3,100
 30               N=2
 31               DO 106 M=3,11
 32               J=N+1
 33               X=D+E*P(M-1,N)*(P(M-2,N)-P(M,N))
 34               Y=D+E*P(M+1,N)*(P(M,N)-P(M+2,N))
 35               IF (X) 1031,1032,1032
 36      1031     X=SQRTF(-X)
 37               GO TO 1033
 38      1032     X=SQRTF(X)
 39      1033     IF (Y)1034,1035,1035
 40      1034     Y=SQRTF(-Y)
 41               GO TO 1036
 42      1035     Y=SQRTF(Y)
 43      1036     IF (X-Y) 104,105,105
 44       104     P(M,N+1)=P(M,N-1)+(Y-X)
 45               GO TO 106
 46       105     P(M,N+1)=P(M,N-1)+(X-Y)
 47       106     CONTINUE
 48               PRINT 2,IX,(P(I,3),I=3,11)
```

Figure 47

```
SEQ     STMNT       FORTRAN STATEMENT

 49                 DO 107 KX=1,2
 50                 DO 107 JX=1,13
 51       107       P(JX,KX)=P(JX,KX+1)
 52                 DO 108 JX=1,13
 53       108       P(JX,3)=X(JX)
 54       109       CONTINUE
 55                 GO TO 100
 56                 END
```

APPENDIX F

NOMENCLATURE

a = A/A^*

a = $\alpha \mu \epsilon$ ($lb_f sec/ft^4$)

A = See Equation (3.16)

A = $(Mgc)/(2\ ZRT\mu L)$ (lb_m/lb_f^2 sec)

B = See Equation (3.17)

b = $(\beta \epsilon^2)/(R/MTgc)$ (sec^2/ft^3)

C_A = Concentration of reactant A ($moles/ft^3$)

C_D = Drag coefficient

C_f = Skin Friction coefficient

D = See Equation (6.15)

E = See Equation (6.16)

E_a = Activation Energy (cal/mole)

F = Force (lb_f)

F_D = Drag Force (lb_f)

F_B = Body Force (lb_f)

g_c = Conversion Factor 32.17 $(lb_m - ft)/(lb_f - sec^2)$

G = Mass velocity of gas ($lb_m/sec\ ft^2$)

g = G/G^*

k = Reaction rate constant (sec^{-1})

k_g = Thermal Conductivity of gas (Btu/hr ft^3 ^oR)

k_s = Thermal Conductivity of solid (Btu/hr ft^3 ^oR)

L = Length of porous sample (ft)

M = Molecular Weight

p = Pressure (lb_f/ft^2)

p_A = Partial Pressure of reactant A (atm)

p^* = Reference Pressure (lb_f/ft^2)

P = Dimensionless Pressure

Q = Volume Flow (ft^3/sec)

Q_f = Friction Heat ($ft\text{-}lb_f/lb_m$)

q = Flow Meter Reading

R = Universal Gas Constant (ft lb_f/lb mole ^oR)

R_e = Reynolds Number

S = Specific Internal Area (Internal area per unit volume)

t = Body Temperature (^oR)

t = Time (sec)

t^* = Reference Time (sec)

T = Gas Temperature (^oR)

T = Dimensionless Time t/t^*

u = Flow velocity in X-direction (ft/sec)

v = Filter velocity (Volume flow per unit area)

$\vec{V}$ = Velocity of Fluid (Vector) (ft/sec)

$\check{V}$ = Volume (ft^3)

X = Length coordinate (ft)

X' = Dimensionless length coordinate, X/L

z = Vertical Corrdinate (ft)

$\mathcal{J} = \rho u$ (lb_f/ft sec)

$Z = \mathcal{J}\, t^* / \rho^* L$

Z = Compressibility Factor

α = Viscous Resistance Coefficient (ft^{-2})

β = Inertial Resistance Coefficient (ft^{-1})

γ = See Equation (3.1)

δ = Average Pore Diameter (ft)

ϵ = Porosity (Ration of void volume to total volume)

η = See Equation (3.1)

θ = Dimensionless Gas Temperature T/T_o

μ = Viscosity

ρ = Density

σ = Angle between X direction and direction of gravity

τ = Shear Stress (lb_f/ft^2)

Φ = Viscous Dissipation Function (lb_f/ft^2 sec)

Ψ = See Equation (2.15)

Ψ' = See Equation (2.18)

UNCLASSIFIED